NASA CONTRACTOR REPORT

NASA CR-2686

ANALYSIS OF DISTORTION DATA FROM TF30-P-3 MIXED COMPRESSION INLET TEST

R. W. King, J. A. Schuerman,
and R. G. Muller

1. Report No. NASA CR-2686	2. Government Accession No.	3. Recipient's Catalog No.
4. Title and Subtitle ANALYSIS OF DISTORTION DATA FROM TF30-P-3 MIXED COMPRESSION INLET TEST		5. Report Date June 1976
		6. Performing Organization Code
7. Author(s) R. W. King, J. A. Schuerman, and R. G. Muller		8. Performing Organization Report No. None
		10. Work Unit No.
9. Performing Organization Name and Address Pratt & Whitney Aircraft 400 Main Street East Hartford, Connecticut 06108		11. Contract or Grant No. NAS3-19076
		13. Type of Report and Period Covered Contractor Report
12. Sponsoring Agency Name and Address National Aeronautics and Space Administration Washington, D.C. 20546		14. Sponsoring Agency Code

15. Supplementary Notes

Final Report. Project Manager, Harvey E. Neumann, Wind Tunnel and Flight Division, NASA Lewis Research Center, Cleveland, Ohio

16. Abstract

A program was conducted to reduce and analyze inlet and engine data obtained during a recent NASA Lewis Research Center testing of a TF30-P-3 engine operating behind a mixed compression inlet. Previously developed distortion analysis techniques were applied to the data to assist in the development of a new distortion methodology. Instantaneous distortion techniques were refined as part of the distortion methodology development. A technique for estimating maximum levels of instantaneous distortion from steady state and average turbulence data was also developed as part of the program.

17. Key Words (Suggested by Author(s)) Turbofan engine; Inlet flow distortion; Engine stall characteristics; Distortion synthesis; Dynamic distortion	18. Distribution Statement Unclassified – unlimited STAR Category 02

19. Security Classif. (of this report) Unclassified	20. Security Classif. (of this page) Unclassified	21. No. of Pages 159	22. Price* $6.25

* For sale by the National Technical Information Service, Springfield, Virginia 22161

TABLE OF CONTENTS

SUMMARY

Pratt & Whitney Aircraft conducted a twelve-month program to reduce and
analyze inlet and engine data obtained during the recent NASA/Lewis
Research Center testing of a TF30-P-3 with an axisymmetric Mach 2.5
mixed compression inlet. As part of the test, the propulsion system was
intentionally mismatched to generate combinations of steady state distortion
and turbulence that allowed the engine to drift into surge. During these
"drift stall" test runs, inlet and engine pressure data was recorded with
high response instrumentation. This data was evaluated to develop methods
of correlating inlet pressure distortion data to loss in engine surge margin.
Both analog and digital data reduction techniques were used in the evaluation
of the distortion analysis techniques. Results of previous TF30 engine tests
were used in the development of the distortion analysis methods. In addi-
tion to the development of data analysis methods, an evaluation and refine-
ment of a synthesis technique for the estimation of peak instantaneous
distortions was conducted.

The program was divided into two tasks. Task I consisted of extensive
analysis of ten "drift stall" points. The objective of Task I was to define a
set of procedures for the analysis of inlet pressure distortion. This task
included analog reduction of inlet and engine parameters, digital analysis of
inlet data, and analysis of engine response to stall propagation. Task II
consisted of the verification of the procedures defined in Task I and the
evaluation of the peak distortion estimating synthesis methods. Task II was
conducted by the analysis of an additional twelve "drift stall" points.

A distortion methodology that successfully indicated surge inducing inlet
distortion was developed. Analysis of the engine data showed that vir-
tually all of the instabilities were initiated in the low pressure spool com-
pressor, suggesting that a core flow distortion factor should be used for
inlet data analysis. It was found that by using a core flow distortion
factor, K_θ splitter, stall inducing distortion could best be detected when
the inlet pressure data is preconditioned by a filter with a cut-off fre-
quency equal to the low compressor rotor speed. A destabilizing influence
of full face in-phase pressure fluctuations was observed.

A method of estimating maximum instantaneous distortion factor levels
from steady state total pressure measurements and turbulent RMS measure-
ments was defined. Application of this distortion synthesis method re-
sulted in a reasonably good correlation of estimated to actual stall inducing
values of instantaneous distortion.

1

INTRODUCTION

Inlet/engine compatibility is a subject that has grown in importance and complexity during the past decade. This trend is directly related to the development of advanced aircraft with increased performance requirements over a broad maneuvering envelope. The continued striving to obtain higher performance has led to the point where a trade between performance and stability must be made; since increased performance usually leads to decreased stability.

Much work during the past decade has been directed toward better definition of inlet/engine destabilizing phenomena. Initial studies were concerned with the correlation of engine surge with steady state inlet total pressure distortion. Later studies found that the level of inlet turbulence has a strong influence on the stability of an inlet/engine combination. It was then observed that the effect of turbulence on the engine was dependent upon the inlet type; thus, the concept of instantaneous distortion was adopted to represent the destabilizing phenomena.

Current efforts have been directed toward quantifying the effects of instantaneous distortion. The origins of the total pressure fluctuations that create the instantaneous distortion are not completely understood; thus, analytical prediction of distortion is not obtainable. Likewise, the effect of instantaneous distortion on engines is not yet analytically determinable. It is apparent then that empirical techniques must be employed to define instantaneous distortion and its effect on engine stability.

A full scale supersonic mixed compression inlet was tested with a TF30-P-3 turbofan engine as part of an engine/inlet compatibility program at NASA-Lewis Research Center. The inlet tested was an axisymmetric, mixed compression inlet designed for Mach 2.5 operation with a TF30 engine. The test was conducted in the NASA-Lewis 10 x 10 foot Supersonic Wind Tunnel. The inlet was equipped with flow bypass doors which allowed supercritical inlet conditions to be obtained for study of pressure distortion. Part of the test program consisted of obtaining data, both inlet and engine, for "drift stall" events. A "drift stall" is an engine surge induced by the combination of steady state and turbulent inlet distortion during steady state engine/inlet operation. Such an event was obtained by setting both the inlet and engine at a steady state operating condition and then waiting for the engine to surge. Not all operating conditions result in instabilities; therefore, most of the "drift stall" events that were recorded were a result of severe inlet operating conditions.

The data obtained in the above mentioned test was reduced and analyzed to define an empirical methodology for the analysis of distortion data. Previous Pratt & Whitney Aircraft experience with the TF30-P-3 turbofan engine was used as a guide for the development of the methodology. Two approaches were examined. One was an extension of the instantaneous distortion technique of representing stall inducing inlet flow. The other was a technique of combining steady state and turbulence data to obtain synthetic instantaneous distortion information. Development of the methodology required a thorough analysis of the engine data as well as the inlet data.

Both analog and digital analysis was conducted on ten "drift stall" data points selected mutually by Pratt & Whitney Aircraft and NASA/Lewis Research Center. The time of surge and the critical component were determined from analog traces of engine parameters. Indication of the peak distortion were obtained by reducing the dynamic inlet pressure data with an analog distortion factor calculator. Definition of the effect of data preconditioning on engine surge correlation was obtained through digital manipulation of the inlet dynamic data near the surge event. Information on the effect of data sample length was obtained by digital reduction of three 3-second intervals of data. Evaluation of the results of these studies was used to define the required procedure of distortion data analysis.

The verification of the previously defined distortion analysis procedure was conducted by application of the selected methods to additional "drift stall" data points. Twelve additional "drift stall" points were evaluated using the digital and analog techniques developed. A tabulation of the twenty-two "drift stall" points analyzed is presented in Table I.

The surge levels of distortion were compared to levels of in-house tests (distortion valve and turbulence generator testing) and flight test experience. Analysis consisted of comparing instantaneous K_{D2} surge levels to the predicted steady state and steady state plus turbulence levels estimated for the TF30-P-3 engine.

Synthesis procedures suitable for the estimation of maximum levels of instantaneous inlet distortion were used to analyze data from the twelve selected "drift stall" points. The results of the application of synthesis techniques were compared with the results of the digital analysis to evaluate the accuracy of the synthesis method. Refinements required to improve the correlation between synthesized values of distortion and measured values were made.

3

RESULTS AND DISCUSSION

Analysis of Engine Data

The surges which occur in propulsion systems are dynamic events. Significant events leading to and including the surge occur during periods of time measured in terms of milliseconds. Identification and analysis of these short duration events requires installation of high response instrumentation at locations which are close coupled to the engine compression system. High response pressure instrumentation was installed in this manner during NASA-Lewis testing of the TF30-P-3 engine/mixed compression inlet configuration. The data acquired from the compression system was analyzed in support of the inlet distortion data analysis for the purposes of 1) determining which compression system component was critical to system stability and 2) to attempt to identify the origin and propagation of instabilities through the system.

Definition of Terms

The stability limits of a compression system are sometimes referred to in terms used interchangeably as "surge" or "stall" limits. Use of the terms in this manner does not give insight into the actual events occurring during a system instability. For this reason, Pratt & Whitney Aircraft defined a glossary of terms for analyses of the type performed on the NASA/TF30 data. The definitions are given below to facilitate understanding of the TF30 analysis.

Stall

The term stall or flow separation refers to the local deviation of the airflow from contours of the airfoils or walls. A stall may be either abrupt - the flow rapidly transists from being attached to being separated over a large area, or gradual - the extent of the surface which is separated varies smoothly with compressor pressure ratio. A stall region may remain fixed in relation to hardware, or may propagate, as in the case of rotating stall. A compression system may operate stably with some stalled regions present on some airfoils or walls; however, local stalls can induce a system instability.

4

- Rotating Stall

  Rotating stall occurs when a localized stall propagates circumferentially. It usually begins as a "cell" of stalled flow covering a fraction of the circumference and span, but may grow to cover the whole span and over half the circumference. A local reduction in flow accompanies the rotating stall cell. The growth of the stall cell is a compression system instability which generally leads to system surge.

- Surge

  Surge is a system instability which originates as a major flow breakdown at some axial location in the compressor that stops or retards the flow around essentially the whole circumference. The flow breakdown in a multispool compressor system may occur in any of the individual compressors and the compressor in which it occurs may be different for various operating conditions.

  Surge may develop into a system of multiple stall cells. The surge process includes a flow breakdown, ensuing surge wave, depressurization, and eventual reflowing and repressurizing of the compressor and associated duct volumes. In some cases, such as when conditions which drove the compressor beyond its stability boundary are not removed, the system surge can be cyclic in nature.

  The surge wave is a pressure pulse, generated by the flow breakdown, which travels forward as a compression wave (overpressure) and travels rearward as an expansion wave from the origin of the surge. The identification of the origin of the surge wave therefore is sufficient for defining the compressor which caused the major flow breakdown.

5

Detection and Classification of Instabilities

Pressure-time histories of the data acquired from the high response instrumentation serve as the basis for analysis of the instabilities. A single history provides a record of the pressures fluctuations as a function of time at one spatial location in the compression system. Comparison of the time histories recorded at different locations in the system reveals the time of initial instability and events leading to surge, as well as the surge itself. Rotating stall and surge were the two kinds of instability identified in the TF30 data.

Because of the localized extent and the rotational nature of the rotating stall cell, its presence is indicated by a periodic fluctuation in the pressure time history. As shown in Figure 1, the direction of the fluctuation is dependent on the location of the pressure probe in relation to the cell. A downstream probe shows a reduction in pressure due to the stalled condition of the flow, while the probe upstream of the cell shows a pressure increase due to the back pressure (flow blockage) effect of the cell on the incoming flow. The positions of the upstream and downstream probes define the axial location of the cell within the compression system. The rotational frequency of the cell, used to identify stall type, can be determined by plotting the circumferential location of the probe versus the time of the pressure fluctuation as shown in Figure 2. This method is particularly useful if the duration of the cell is less than one cell revolution, which in turn requires that probes at more than one circumferential location be included on the plot.

The surge characteristics exhibited in the pressure time histories are generated by a major flow breakdown at some axial location in the compression system. Probes downstream of the breakdown point show a rapid decrease in pressure; the upstream probes show a rapid pressure increase. These characteristics, shown in Figure 3, differ from rotating stall characteristics primarily in magnitude of the pressure variations, the surge pressure variations being substantially larger.

Previous Pratt & Whitney Aircraft analyses of TF30 compressor instabilities have shown that the origin of compression system instabilities as well as the occurrence and order of events leading to surge vary on a case to case basis. It has therefore been found useful to classify each case according to the origin and types of instability leading to surge. This practice was continued in the analysis of the NASA/TF30 data and definitions of the surge event classifications are given below to clarify results of the analysis.

- Initial Instability in Fan

    Type 1 - Rotating stall initiating in fan root followed by rotating stall in the low pressure compressor (LPC), followed by a surge wave emanating from the high pressure compressor (HPC).

Type 2 - Rotating stall initiating in fan tip (coupling with fan duct resonant frequency) followed by depressurization of the core.

*Type 3 - Rotating stall initiating in the fan root followed by rotating stall in LPC, followed by rotating stall in HPC, followed by a surge wave emanating from HPC.

- Initial Instability in LPC

Type 1 - Rotating stall initiating in LPC followed by a surge wave emanating from the HPC.

Type 2 - Rotating stall initiating in LPC followed by a surge wave emanating from the LPC.

Type 3 - Rotating stall initiating in LPC followed by HPC rotating stall and followed by a surge wave emanating from HPC.

- Initial Instability in HPC

Type 1 - Rotating stall initiating in HPC followed by surge wave emanating from HPC.

Type 2 - Surve wave emanating from HPC.

Instrumentation

Figure 4 shows the five axial high response instrumentation stations that were installed for the NASA/TF30 test. Coverage of the entire fan face was provided by the inlet pressure rakes used in the inlet distortion analysis. Instrumentation internal to the compression system was located in the core flow path which in turn permitted positive identification of instabilities occurring in this region. The core path was instrumented such that the low pressure compressor was isolated into three blade row groups while the high pressure compressor was isolated as a complete unit. The groups in the low compressor were inlet guide vane (IGV) through rotor 3 (fan roots), stator 3 through rotor 6, and stator 6 through rotor 9.

*Note - New classification based on NASA test results.

7

The internal instrumentation was circumferentially spaced in the manner shown in Figure 5. The operating probes provided data for at least one circumferential location at each axial station and were adequate for identification of rotating stall cells and determination of rotating frequency.

Interpretation of Engine Data

Two methods of generating the pressure-time histories for analysis were explored. Initially, the histories were generated by analog tracing of unfiltered playback of the dynamic pressure components. Subsequently, the histories were generated by analog to digital conversion of filtered playback of the dynamic pressures. The latter method proved to be more desirable because the filtering provided better resolution of the compression system instabilities through attenuation of higher frequency activity. In addition, the digital output format permitted machine plotting of the pressure-time coordinates on grid paper, making reading of the time scale easier than on the analog traces. A real time filter cut-off frequency of 320 Hz and an effective cut rate of 1024 cuts/sec. were selected for the analog to digital process and produced the time histories shown on Pages 86 through 109 of Appendix D. These histories were used in the final analysis of the instabilities.

The time history plots were interpreted by initially identifying the system surge. From this point in time, preceding periods were examined to determine the time of initial instability as well as the location and types of instabilities preceding surge. In general, time histories of P_{t2} showed only overpressure resulting from surge; therefore, the analysis was centered around the time histories of the internal engine pressures shown on Pages 86 through 109. The significant events occurring in each case were identified on each plot.

Rotating stall cell frequencies were determined from the plots shown on Pages 110 through 130 of Appendix D where probe position was plotted versus time of cell indication. In some cases it appeared that the rotating cells were superimposed on top of the surge waves. When this occurred and cell duration prior to surge was short (less than one rotation) the post surge indication was used to improve resolution of the rotating frequency. This type of rotating stall can be observed in the pressure data for case 408 (Pages 91 and 92), where the presence of the low compressor rotating stall cell is indicated after the time of surge.

The 22 surge cases which were analyzed spanned a low rotor corrected speed range of 6000 to 7050 rpm. Within this range, various configurations of bleed position and exhaust area settings were tested as shown in Table I.

Table I shows that the surge events were not identical on a case to case basis. Results which can be derived are as follows:

1. Positive identification of instabilities in the core flow path were made in all surge events.

2. Five different sequences of events leading to and including surge were found.

3. In all cases except 519, instabilities were identified in the core low spool compressor prior to surge. Those initial instabilities were identified as rotating stall.

4. High compressor surge was the only instability positively identified in case 519. This case was the only one analyzed for operation with both 7th and 12th bleeds open.

5. In five cases, high compressor rotating stall was identified prior to surge. These five cases occurred at corrected low rotor speeds of 6500 rpm and lower as shown in Figure 6.

6. In the majority of cases (16 of 22) the initial instability was identified in the Stator 3 through Rotor 6 (Sta. 2.3 - 2.6) row group. These cases covered the full range of low rotor speeds; see Figure 6.

7. The initial instability was identified in the IGV through Rotor 3 (Sta. 2.0 - 2.3) fan root row group in four cases. These occurred at corrected low rotor speeds of 6180 rpm and below; see Figure 6.

8. In case 438 the initial instability was first identified in the Rotor 6 through Rotor 9 (Sta. 2.6 - 3.0) group at a corrected low rotor speed of 6970 rpm; see Figure 6.

The surge classification system defined from previous TF30 testing provided the key to interpreting the NASA data. The instabilities noted in the data were easily linked to events described in the surge classification system to identify the origin and type of instability. Case 497 was the only one which presented any problem because previous Pratt & Whitney Aircraft experience did not show high compressor rotating stall subsequent to a rotating stall initiated in the fan root. No reason was seen to rule out the possibility of this occurrence and a new classification was defined (Fan/Type 3) on the basis of the NASA data.

9

Case 519 also stood out as different from the other surge cases because no instability in the low spool was clearly evident prior to surge. This case was unique in that it was the only one analyzed for operation with both 7th and 12th stage bleeds open. Although it was not evident in the data, it was felt that an undetected short duration rotating stall in the low spool compressor should not be completely ruled out as a cause of the surge.

The next area of interest in this analysis was the location of initial instability. The matrix shown in Figure 6 was used to identify trends of results for cases where instability initiated in the low compressor. The matrix included the major engine variables which were exercised during the test and in turn affected the compression system matching.

A significant majority of the instabilities (16 of 21) initiated in the Stator 3 through Rotor 6 group; instabilities originated at this location over the full range of tested rotor speeds. In contrast, instabilities which initiated in the fan roots were concentrated in a speed range of 6000 to 6180 $N_1/\sqrt{\theta_{t2}}$ while the one instability that initiated in the Stator 6 through Rotor 9 row group occurred at 6970 $N_1/\sqrt{\theta_{t2}}$. The cases where instability initiated outside the Stator 3 through Rotor 6 group qualitatively displayed the expected movement of stalled operation from the front to the rear of the compressor with increasing speed; however, the trend was not felt to be conclusive. In contrast, consideration of all 21 cases led to the conclusion that the location of initial instability was somewhat random and therefore unpredictable. It did appear that the most probable location for initial instability was the Stator 3 through Rotor 6 group.

Compressor Row Matching

The test results showed the low compressor to be critical to engine stability. For purposes of augmenting analysis of the engine test data, a computer model of the fan/low compressor was exercised to determine which blade row in the core compressor might be critical to its stability.

The model was composed of average ϕ -ψ characteristics defined for each blade row of the fan and core compressor. The characteristics were derived from data acquired during rig testing of a Bill of Material TF30-P-3 fan/low compressor. The model was operated by input of the corrected low rotor speed, corrected total airflow and corrected core flow at the fan inlet station; output from the model included both the overall and row operating conditions.

The operating conditions investigated with the model were limited to corrected low rotor speeds of 7000 rpm and above due to the range of definition of the row characteristics; in addition, the fan match was restricted to conditions encountered during static operation because testing of the rig was performed at ambient inlet and discharge conditions. With these limitations in mind, the row operating conditions were examined for operation of the low compressor near the rig surge line with the fan operating on a line near the level experienced during static operation of the engine. A range of rotor speeds of 7000-9000 rpm was investigated as shown in Figures 7 and 8 so that the trend of shifts in row operating points could be qualitatively extrapolated to the 6000 to 7050 rpm corrected speed range covered by the NASA engine test.

Assessment of the low compressor row operating conditions was made by evaluating the position of each rotor and stator row operating point relative to the peak pressure rise of its characteristic. As illustrated in Figure 9, the point was identified as operating on either the choked or stalled side of the ϕ -ψ characteristic and the percentage deviation from peak pressure rise ($\%\Delta\psi$) was calculated. The results were plotted as a function of the row location and inlet corrected rotor speed, as shown in Figure 10, to give an overview of the predicted operating conditions within the compressor.

The results of this analysis showed that operation of the low compressor 3rd stator was predicted to progress toward a relatively highly stalled condition as rotor speed was reduced from 9000 to 7000 rpm (see Figure 10); qualitative extrapolation of these results therefore predicted the 3rd stator to be the predominantly stalled row in the 6000 to 7050 rpm speed range tested.

Interpretation of these results required consideration of the findings made from the internal compression system data taken during the test. The data showed that in the majority of cases, the instabilities initiated in the Stator 3 through Rotor 6 blade row group. This, coupled with the model predictions, left the 3rd stator as a row suspected of frequently

11

influencing the stability limit of the compressor; in contrast, it could not be said that instability universally initiated at this location because of the exceptions demonstrated in the test data, namely the instabilities which initiated in the fan roots and in the rear stages. In addition, Pratt & Whitney Aircraft testing of the TF30 compression system has also shown that instabilities initiate at different locations (stages) in the compressor under apparently similar operating conditions.

Application of Previously Developed Methodology

Early testing of the TF30/F111 installation led to development of a factor which evaluated the severity of the predominantly 180° distortion generated by the aircraft inlet. The factor, K_{D2} (see Appendix A) was initially implemented in both the engine development and flight test programs and evaluated the engine stability limits on the basis of low response data. This approach correlated the development test and flight test results separately, but indicated the stability limits of the engine to be lower in the aircraft than in the test cell.

As the aircraft flight testing progressed, it became apparent that the inlet flow environment contained significant nonsteady, high frequency characteristics. These were known to degrade the apparent stability limits of the engine indicated by the K_{D2} level calculated from low response data. It was necessary to establish a method of accounting for the high frequency activity (turbulence) and the K_{D2} - turbulence approach was developed. A sample surge limit curve is illustrated in Figure 11. The approach correlated the stability limits of the engine at constant airflow in terms of the low response K_{D2} and turbulence level $\Delta \bar{P}_t$ rms$/\bar{P}_t$ 0-150 Hz). The cutoff frequency of 150 Hz for turbulence was confirmed by testing of a fan/low compressor rig.

The stability limits of the engine in terms of K_{D2} and turbulence were derived from cell testing of the engine behind a distortion valve and turbulence generator which are shown in Figure 12. The distortion valve defined stability limits at conditions of low turbulence and the turbulence generator at conditions of relatively high turbulence. During this testing the distortion patterns were maintained at one per revolution conditions so that the aircraft environment could be simulated as closely as possible. (See Figure 13.)

Implementation of the K_{D2} - turbulence method was found to provide much improved agreement between the stability limits of the engine as measured in the test cell and in the aircraft. In the vast majority of cases, surge events occurring in the aircraft could be predicted by the concurrent levels of K_{D2} and turbulence. In a few cases, this approach did not work and another method was employed - instantaneous K_{D2}.

The instantaneous K_{D2} method calculated the factor from high response measurements of inlet data filtered to 150 Hz. As illustrated by Figure 14, this method was found to predict engine surges that could not be confirmed by the K_{D2} - turbulence method.

Under this contract, the data acquired from the NASA testing was investigated in terms of K_{D2} - turbulence and instantaneous K_{D2} to evaluate these approaches as methodologies for correlating the engine stability limits.

Instrumentation

The distortion data for the test was acquired with the instrumentation illustrated in Figure 15. Twelve rakes were installed at the compressor face and provide a total of 72 sampling locations. All locations provided low response data; high response data was acquired at three points on each rake for a total of 36 locations. As a result, K_{D2} low response was based on 72 measurements and turbulence levels based on 36 in the K_{D2} - turbulence analysis. Instantaneous K_{D2} was derived by merging the low response with corresponding 36 high response pressure readings.

Analysis of the verge of surge pressure profiles indicated the patterns fell within two extreme types, a four per revolution and a one per revolution pressure defect pattern. The four per revolution pattern was generated with the inlet at zero or low angle of attack and high levels of bypass airflow. The four per revolution distortion pattern was caused by a combination of the four center body support struts and the position of the bypass doors; see Figure 16A. The second type, a one per revolution pattern, occurred at high inlet angles of attack and low bypass airflow; see Figure 16 B and Appendix D for the profiles of all the test points analyzed.

Figure 17 presents typical turbulent energy distributions that were measured with the inlet instrumentation. The data is presented in the form of a normalized power spectral density plot. Compared to previous experience, denoted by the TF30 Spec. limits, the turbulent energy measured for the axisymmetric mixed compression

inlet was concentrated at high frequencies. The distribution of high frequency pressure fluctuations specified by the TF30 Spec. is consistent with F111/PWA inlet characteristics and the in-house turbulent distortion generating devices that were used to define compressor surge margin.

K_{D2}-Turbulence

The K_{D2} levels were calculated from the 72 steady state inlet probes for each of the 22 data points considered. The turbulence levels associated with these points were based on an average of the 36 high response probes low pass filtered to 150 Hz. These data are shown on Figure 18a compared to the estimated distortion tolerance limits based on previous TF30-P-3 experience. Different symbols are used to delineate airflow level and bleed configuration. Close examination of the 150 pps airflow points shows reasonable agreement between this test and previous tests at low turbulence levels (see Figure 18b). For the low turbulence points the steady state K_{D2} level is comparable to previous TF30-P-3 K_{D2} levels. At high turbulence levels, however, the agreement is not as good. Figure 18b presents the observed turbulence effect through new curves of K_{D2} versus turbulence.

Opening 7th bleed considerably increases engine distortion tolerance and this improvement is consistent with previous experience. Addition of 12th bleed improved distortion tolerance only slightly. Previous experience has been with either 7th or 12th bleeds open, not with both bleeds. The results obtained, therefore, indicate that the improvement due to either 7th or 12th bleeds should not be added to predict an improvement with both bleeds open. Reducing nozzle area, while not changing engine distortion tolerance at low turbulence, does have a detrimental effect on the engine tolerance to increasing turbulence, see Figure 19. Previous experience did not indicate that engine response to turbulence was a function of nozzle area (fan match).

Of the 22 points analyzed, 3 points showed a lower stall K_{D2} versus turbulence relationship than the rest. The 3 points, the flagged symbols plotted on Figure 19, have been shown to have nonstationary inlet activity in another analysis performed by NASA.

The primary difference between previous Pratt & Whitney Aircraft experience and the inlet test is the response of the engine to increasing amounts of turbulence. The data indicates that the engine is more tolerant of four per revolution distortion at high turbulence than previous experience would predict. Previous testing at Pratt & Whitney Aircraft has indicated that a 4 per revolution pattern should cause stall at K_{D2} level approximately 80% of that of 1 per revolution pattern. Adjustment of the high turbulence four per revolution data

points would not significantly change the results. Since the PSD characteristic between Pratt & Whitney Aircraft experience and the inlet tests are considerably different, this difference is suspected to be the cause of the increased tolerance to turbulence.

K_{D2} Instantaneous

The concept of instantaneous distortion is based on the premise that a total pressure distortion existing for a short time period causes the engine to surge. Such a distortion pattern must exist for a sufficient time to allow the engine to sense it; thus, the distortion must be averaged over some finite time interval which is characteristic to the engine. An effective means of achieving the required averaging is the filtering of the pressure data. The resulting instantaneous distortion can then be compared to low turbulence or steady state surge limit data to define engine/inlet compatibility.

The instantaneous distortion approach was applied to the K_{D2} index system by calculating K_{D2} using total pressure readings low pass filtered to 150 Hz for the ten Task I data points. Using this approach to defining K_{D2}, it is expected that the K_{D2} (steady state) levels associated with low turbulence, as shown on Figures 18 and 19, would represent the expected distortion tolerance limits for K_{D2} instantaneous. Figure 20 summarizes the results of this analysis. Two levels of distortion tolerance limits are shown, one for 7th bleed open (highest level line) and one for 7th bleed closed.

Analysis of the data shows that the two bleeds closed points, denoted by solid symbols in Figure 20, correlate with the predicted distortion tolerance limit. The surge inducing distortion is larger than the prior peak distortion and it exceeds the limit line. The remaining eight data points, 7th bleed open points, require consideration of the distortion pattern type for proper interpretation. Four of the points, cases 421, 438, 445 and 457, are nearly one per revolution type patterns and closely correlate with the predicted limit line. The remaining four points were nearly four per revolution patterns and do not present as good a correlation with predicted surge levels of K_{D2}. This limitation of the K_{D2} instantaneous system is attributed to the development of K_{D2} to define the severity of F111 inlet distortion, a predominantly one per revolution distortion.

Development of Methodology

Analog Data Reduction

The primary requirement of a distortion methodology is that the selected distortion factor maximizes for the stall inducing inlet distortion. Definition of such a factor from high response data of

an inlet/engine test requires examination of the engine data sample to insure that the factor does indeed maximize for the stall inducing distortion. There are two data reduction methods that can be used to analyze high response data; digital and analog. Each method has its own advantages which make it more suited to a particular application. Examination of long time samples is usually conducted through the use of analog analysis because of its low cost and online data reduction capability.

Since the current data was lengthy, up to five minutes per data point, analog techniques were used to provide economical analysis of all the data. An analog computer was used to determine the time and level of each distortion peak and to determine if the maximum distortion factor occurred immediately prior to rotating stall or surge.

The analog distortion factor calculator used for the reduction of the TF30-P-3 mixed compression inlet test distortion data is presented schematically in Figure 21. This unit, the only analog distortion factor calculator available for in-house use, is currently located at the Florida Research and Development Center Facilities of Pratt & Whitney Aircraft. The calculator is a hardwired computer designed specifically for the determination of F100 distortion indices. These factors are referred to as K_{A2}, K_{C2}, K_θ, and K_{RA2} and are defined in Appendix A. The computer is also hardwired to handle a maximum of eight equally spaced rakes with six probes per rake and to condition each input channel with a 170 Hz linear phase filter.

To check the validity of the assumptions made in the use of the analog calculator, the analog output of one case was compared to digitally reduced data for the same case. Figure 22 presents the results of the comparison made for case 457. Each symbol on the plot represents a specific time on the data trace. The results of the comparison indicate that the assumptions cause the computer to calculate slightly lower levels of distortion than corresponding digital calculations.

Figure 23 presents a sample visicorder trace for case 457. The particular trace that is presented includes the time of stall and the indication of hammershock at the compressor face. Four distortion factors are recorded along with respective peak detection signals and time code. The factors calculated are K_{A2}, K_{C2}, K_{RA2}, and K_θ. A flag, such as the one occurring for K_{A2} just prior to hammershock, is recorded for each successively higher peak distortion. These flags provided the means for searching the analog output for the maximum level of distortion.

16

The results of the analog data reduction indicated that maximum levels of the F100 distortion factors occurred for inlet distortion that did not cause the engine to surge. Engine data analysis indicated that a core flow type factor, such as K_{C2}, should provide the best indication of surge inducing distortion. Table II presents a comparison between the time of maximum K_{C2} and the time of initial instability within the engine. The smallest interval between time of initial instability and time of maximum K_{C2} is about one second which is too long to permit data correlation. The same results were found for the other distortion factors that were calculated.

These results indicated that use of a different distortion factor may be required to provide better correlation of the data. The significance of this finding was tempered by two additional considerations. One was that relative peak levels of distortion factors were observed just prior to stall. These distortion levels were within a few percent of the maximum distortion levels. The other was that the data reduced by the analog calculation was preconditioned by a filter with a relatively high cut-off frequency, thus not adequately representing the response of the engine to distortion. Both of these considerations indicated that refinement of the data filter characteristics would improve the correlation.

Study to Determine Effect of Data Filtering

The desired result of the use of filters in high response distortion data reduction is to eliminate the calculation of nonsurge inducing peak distortions. In addition, proper filter selection should provide a direct correlation between instantaneous inlet data and steady state compressor rig data.

The work reported by Plourde and Brimelow, Reference 1, indicated that filtering of the data does reduce extraneous peak distortions below that of the surge inducing distortion. Figure 24 presents a sample of that data. Figures 24a and 24d, 1050 Hz and 45 Hz filtering, respectively, demonstrate that use of extremes in preconditioning the data does not aid in the correlating of inlet data. However, the peak distortion trends for 400 Hz and 160 Hz filtered data, Figures 24b and 24c, are similar, and are useful for the correlating of inlet distortion data. Only a qualitative effect of filtering was obtained from the referenced work since the four filters that were examined covered such a wide variation of filter characteristics.

A study to better define the effects of filtering on high response distortion data was conducted as part of Task I of this contract. To allow more flexibility in the selection of filter characteristics to be used in the analysis of the data, digital filtering was chosen as the method of preconditioning the data. The effect of three filter characteristics

17

(cut-off frequency, roll-off rate and phase shift) were examined as part of the study. First, the effect of cut-off frequency was examined for a given roll-off rate and phase shift. The effects of roll-off rate and phase shift were then defined by reanalyzing some of the Task I data points with different filter designs.

The digital system used to conduct the study was first devised at Pratt & Whitney Aircraft to analyze the stability of the F111/TF30-P-3 aircraft/engine combination. Flight and rig tests were run comparing the steady state value of distortion to the instantaneous or high response value. Since that time, the system has evolved to its present state through experience in additional programs. Figure 25 illustrates the flow of data through the various components of this system and shows its two major parts, data preparation and data analysis.

Data preparation encompasses the demultiplexing, digitizing, and converting of all inlet pressure parameters to engineering units in a single pass operation for each data point being analyzed. The maximum required sampling rate is established at this point. In part two, data analysis, the inlet pressures are first preconditioned. Digital filters are designed in a periphery deck, the output of which is applied to the data in the preconditioning deck. Also, in the preconditioning deck is a phase shift option and a variable sampling rate option. Distortion indices are then calculated at the sampling rate selected.

High response pressure data recorded on analog, multiplexed, magnetic tapes during NASA LeRC TF30-P-3 inlet distortion tests were played back and digitized to a form suitable for analysis. A total of 8 passes of the data through the system was required to read all 36 inlet total pressures. Data playback was 30 ips. The data was passed through a 500 Hz, linear phase, 3 pole low pass filter which, since playback speed is half record speed, provides an effective cut-off frequency (i.e., signal is attenuated 3 db at cut-off frequency) of 1000 Hz. The data was digitized at 4000 samples per second, at half speed, for an effective rate of 8000 samples per second.

The output of the digitizing process was a magnetic tape which was then processed with a computer program that merged the passes, converted the data to physical units and added steady state pressures to the dynamic signals. Statistical properties of the data for each channel were also calculated with this program. The maximum effective error that is expected between passes is equal to 12 microseconds.

In the data analysis part of the system, the data was passed through a preconditioning routine for filtering studies. A large portion of the analysis of the NASA LeRC distortion data involved evaluating the influence of filter cut-off frequency and roll-off characteristics on distortion factor. Input signals in digital form were filtered by numerical techniques such as weighted averaging of a succession of digital values. The design of the digital filters involved determination of the number of terms to be averaged and a calculation of the values of the weighting parameters.

The first part of the study, that of determining the effect of cut-off frequency, was conducted using phaseless (zero phase shift) digital filters to precondition the pressure data. Design procedures for the filters used are outlined in Appendix B. The cut-off frequencies selected were 50 Hz, 100 Hz, 150 Hz and 200 Hz. The filters were designed to have a roll-off rate of 18 db per octave. Figure 26 is a nondimensionalized plot of the gain versus frequency characteristics of the filters used.

Input from the engine data analysis indicated that a factor defining the quality of flow entering the engine core (splitter type factor) should be used to indicate the stall inducing distortion. This conclusion was derived from the result that the low compressor was virtually always the first component to lapse into rotating stall just prior to engine surge. Several splitter type distortion factors, in addition to K_{C2}, were examined to determine the factor that would provide the best correlation of the data. The result was that K_θ splitter provided the best correlation.

Figure 27 presents plots of K_θ splitter versus time for the reduction of one "drift stall" point with the four different filters. As expected, the lower cut-off frequency filters smooth the distortion traces and lowered the peak levels of distortion. For the particular case examined, there is some variation in the relative levels of local peaks. The most significant point in this particular case is the complete disappearance of the deep trough just prior to the maximum distortion peak. Thus, qualitatively the filtering performed as expected.

19

The expected quantitative effect of data filtering is illustrated in Figure 28. The value of the distortion factor for the surge inducing distortion is compared to the engine distortion limit (K_{crit}) and to the maximum value of distortion observed. The minimum effective cut-off frequency is defined as the frequency at which the surge inducing distortion factor is equal to the engine distortion limit. The upper or maximum cut-off frequency occurs when the surge inducing distortion becomes equal to the maximum observed distortion. Since engine limits in terms of $K_{\theta\,splitter}$ were not available, only the second comparison was made to define the quantitative effects of filtering.

No clear cut quantitative effect of filter cut-off frequency on the relative levels of peak distortions was found. Table III is a tabulation of the results of analyzing the data with the filters selected. The data indicates that if the cut-off frequency is too low, the stall inducing distortion becomes lower than nonstalling distortion peaks for the predominately four per revolution patterns. On the other hand, the opposite appears to be true for the predominately one per revolution patterns. That is, as the cut-off frequency decreases, the stall inducing peak distortion becomes larger than nonstalling peaks. This phenomena has also been observed in J85 tests (Reference 2).

The effect of cut-off frequency was not definitive enough to positively identify the filter that best represents engine response to distortion. However, examination of the table of results indicates that the best correlation of the data is obtained when the pressure data is preconditioned with the 100 Hz cut-off frequency filter. Since this frequency is close to the low compressor rotor speed for all of the data examined, it was concluded that N_1 should be used as the filter cut-off frequency in any preconditioning of pressure data.

The second part of the study, that of defining the effects of phase shift and roll-off rate, was conducted using recursive or feedback type digital filters. The particular designs used, described in detail in Appendix B, were of the multipole Sine-Butterworth type. Figures 29 through 32 present the gain and phase shift characteristics for the four filters used in the study. A cut-off frequency of 100 Hz was used for all of the filters. The effective roll-off rates vary from 9 db per octave for the two pole filter to 27 db per octave for the five pole filter. The phase shift for all of the filters is linear for all practical purposes since the phase angle relation becomes nonlinear after a frequency of 150 Hz where the maximum gain is .4 for the filter with the shallowest roll-off rate.

Change in roll-off rate and phase shift did not appreciably change the levels of distortion calculated. Figure 33 presents sample K_θ splitter traces of data filtered with the four selected filters. As might be expected, use of the filter with the lowest roll-off rate resulted in a more jagged trace of the distortion data. However, no substantial change in the level of the peak distortions, or change in the wave form was apparent from the data examined.

Analysis of Longer Time Samples of Data

The existence of potential stall inducing distortion peaks occurring at times long before stall was investigated digitally as well as with analog techniques. Digital investigation, although not as extensive as the analog examination of the data, allowed the use of the findings of the filter study. Three data points of three second duration were examined for this study. The three points selected were cases 405, 438, and 457. A two pole Sine-Butterworth recursive filter with a cut-off frequency of 100 Hz was used for the preconditioning of the data.

Larger peak values of instantaneous distortion than the stall inducing distortion were found for all of the three points examined. Although larger distortion peaks were observed that did not stall the engine, local peaks did indicate the occurrence of the stall inducing distortion. Figure 34 presents sample traces for two time segments that were reduced for case 438. Both K_θ splitter and face average total pressure are plotted versus time. One of the intervals contains the stall inducing distortion, the other contains the maximum observed distortion. Examination of the trace containing the stall inducing distortion shows that the face average total pressure is decreasing as the peak value of K_θ splitter occurs. On the other hand, the pressure is on the rise when the maximum value of K_θ splitter is observed. Since decrease in pressure at the compressor face has a destabilizing effect on the compressor system, the combined effect of full face pressure variation and instantaneous spatial distortion is more severe for the stalling distortion than for the time that the maximum value of K_θ splitter occurred. Not enough data was available to quantify the effect of the combined distortion; however, the 2% difference in K_θ splitter between the maximum value and the stall inducing value can easily be attributed to the effect of the in-phase pressure fluctuations. This indicates the importance of including the effects of in-phase pressure fluctuations in the analysis of inlet distortion data.

21

Recommended Methodology

A distortion methodology based upon the concept of instantaneous distortion was developed from the interpretation of Task I data. Since eight of the ten points examined were for the 7th open/12th closed bleed condition, the interpretation of data was concentrated on this one bleed configuration. The data was examined on a surge/no surge basis. It was assumed that the data examined were for conditions where the engine/inlet combination was operating at the verge of surge. Thus the surge inducing levels of distortion were used to estimate the engine distortion limits.

During the analysis of the data, it was observed that the full face average pressure varied considerably for the high turbulence data points. These pressure fluctuations were found to be cyclic in nature with a period which was of the order of one rotor revolution. The peak to trough pressure difference for the cycle just prior to the surge inducing distortion divided by the steady state average pressure ($\Delta \bar{P}_t / \bar{P}_t$) was used to quantify this characteristic. The in-phase pressure data, as well as the instantaneous distortion data, was required to interpret the results.

Figure 35 presents a summary of the results of the data analysis. The figure presents estimated engine $K_{\theta \text{ splitter}}$ limit lines as a function of corrected airflow. The symbols indicate the surge inducing distortion data that were used to derive the engine limit lines. The data scatter is considerable until the in-phase pressure data is included. Then the data can be correlated, as the lines of constant pulse strength ($\Delta \bar{P}_t / \bar{P}_t$) indicate. The three test points that show less correlation were data for which one of the high response pressure probes was bad.

The following is a summary of the elements of the recommended distortion methodology:

1. The data should be preconditioned with a digital filter designed to simulate a two pole low pass (e. g., Sine-Butterworth) filter with a cut-off frequency equal to the rotor speed of the low compressor.

2. A splitter distortion factor, $K_{\theta \text{ splitter}}$, should be used as an indicator of surge inducing spatial distortion.

3. Planar pulse data should be bookkept along with instantaneous spatial distortion to provide the best indication of surge inducing distortion.

Selection of K_θ splitter to define instantaneous distortion was based on the findings of the engine data analysis as well as examination of the distortion data. Since analysis of the engine data indicated that the low compressor was always the component in which stall was initiated, the correlating flow distortion should be of the core or splitter variety. Thus, a splitter type factor should be used as an indicator. Analysis of the inlet data resulted in K_θ splitter being selected as the best indicator of surge inducing distortion.

The selection of the filter design for data preconditioning was based on the results of the study which indicated that a cut-off frequency equal to the low compressor rotor speed provided the best correlation of the data. In addition, it was found that variation of roll-off rate and phase shift characteristics of filters had only secondary effects on the calculated levels of distortion. Since the two pole Sine-Butterworth filter is the simplest design to use, it was selected as the recommended filter.

Verification of Recommended Methodology

A test of the recommended methodology was conducted under Task II of the contract. This verification test was conducted through the application of the recommended procedures for the analysis of twelve additional drift stall points. The points that were analyzed were cases 441, 461, 467, 471, 497, 519, 528, 537, 540, 502 and 561. Eight of these points were 7th open/12th closed bleed configurations; three were 7th closed/12th closed configurations, and the remaining point was a 7th open/12th open bleed configuration.

Each data point was reduced using the recommended methodology. Pressure data for each point was preconditioned using a digital filter designed to simulate a two pole Sine-Butterworth filter with a cut-off frequency approximately equal to the low compressor rotor speed. Values of K_θ splitter were then calculated for an interval of time starting about 10 rotor revolutions prior to engine surge. This interval of data was then searched to locate the maximum peak distortion that occurred prior to the onset of hammershock. The times that these peaks occurred were then compared to the times of initial indication of rotating stall determined from the engine data. The levels of the peak distortions were then compared to the estimated critical levels of distortion defined in Task I.

Table IV presents a summary of the results of the data reduction. Included in the table are the engine corrected airflow, the peak value of K_θ splitter, the interval of time between the occurrence of the peak distortion and the first indication of rotating stall, the amplitude of the in-phase compressor face average pressure fluctuation and the root mean square of the in-phase pressure fluctuation. Excellent correlation of occurrence of peak distortion with onset of rotating stall is observed for ten of the "drift stall" points analyzed, indicating that the splitter type distortion factor does recognize stall inducing distortion for the TF30-P-3 engine.

Figure 36 presents a comparison of peak distortion levels with the levels of critical distortion derived during Task I. Only the 7th open/12th closed bleed configuration points are plotted, since the curves of critical level of distortion apply only to that bleed configuration. The flagged symbols represent the surge inducing peak distortions. Case 502 was a condition that should not have induced stall; however, the engine did surge. With the exception of case 502, the data correlates well with the curves of critical engine distortion limits. The results tend to verify the dependence of engine distortion limits on the magnitude of in-phase pressure fluctuations.

Distortion Synthesis Study

Several approaches to the improvement of high response data reduction techniques have been pursued in the industry (3, 4, 5). Two of the approaches of current interest have been the use of analog computers for online distortion calculation and the use of data screening methods prior to the detailed search for the peak instantaneous distortion levels. This phase of study has been concerned with the latter approach, that of screening the data. In particular, this work has been concerned with the further development of procedures that use steady state and root mean square measurements to synthesize patterns that are representative of the peak instantaneous distortion levels.

Procedures were formulated for the synthesis of maximum expected instantaneous distortion from steady state and root mean square measurements. These synthesis methods were developed by Pratt & Whitney Aircraft in an independent research and development program with the aid of existing in-house scale model inlet high response data. The methods had not been verified with application to different data and, therefore, these techniques were applied to the TF30-P-3 mixed compression inlet test data for verification.

24

The synthesis procedures for the estimation of maximum levels of inlet distortion were used to analyze data from the twelve Task II "drift stall" points. The results of the application of synthesis techniques were compared with the results of the digital analysis to evaluate the accuracy of the synthesis method. The procedures were also used to analyze the three 3-second data samples that were analyzed in Task I. Refinements required to improve the correlation between synthesized values of distortion and measured values were made.

Synthesis Method

Part of the problem in the synthesis of distortion data is that an observed maximum distortion level is not a reliable indicator of inlet performance. That is, no probability of occurrence is associated with the observed maximum; and thus, it seems reasonable that there should be a great deal of scatter when comparing synthesized distortions with observed maximum instantaneous distortions. It was decided that, in order to reduce the inadequacies of distortion synthesis, it would be necessary to change the definition of the value to be synthesized. The new parameter chosen was the statistically obtained maximum expected value of distortion.

Jacocks[6] had shown that applying extreme value statistics to inlet time variant distortion data provides a dependable indicator of inlet performance. This method of data reduction provides a procedure for calculating an expected value of peak distortion as a function of inlet operation time at the flight conditions of interest. This distortion parameter, the expected value of peak distortion, is then the parameter that distortion factor synthesis methods were designed to predict.

The distortion factor that was recommended for the indicator of stall inducing distortion was K_θ splitter and, therefore, work was concentrated on the synthesis method for the maximization of K_θ. The method that was developed is a procedure for the generation of synthetic instantaneous distortion patterns that can be analyzed as actual distortion. Levels of distortion factors are obtained by application of standard factor calculation procedures.

A method used for distortion synthesis is defined by the specification of a set of steps required for the generation of a synthetic distortion pattern. A procedure that provides spatial orientation, referred to as definition of the reference probes, is the first step in pattern synthesis. Definition of a spatial orientation is followed by the determination of the procedure necessary to intensify the steady state

distortion for which the synthesis method is being tailored. This procedure of intensification is referred to as sign selection. Definition of the increment of pressure to be added or subtracted from the steady state pressures completes the definition of the steps required to generate a synthetic instantaneous distortion pattern.

Once the method of synthesis is defined, individual pressures for the synthesized distortion pattern are generated by the following equation:

$$P_{tj \text{ synthesis}} = P_{tj \text{ ss}} \pm A \Delta P_{tj} \tag{1}$$

where:

$P_{tj \text{ synthesis}}$ = the synthetic instantaneous probe total pressure

$P_{tj \text{ ss}}$ = the steady state probe total pressure

ΔP_{tj} = the probe total pressure increment defined by the synthesis method

A = multiplication coefficient for the synthesis method

Of the three terms on the right hand side of the equation, only the multiplication coefficient A is independent of probe location. This coefficient is dependent only on the type of synthesis method and the distortion factor being synthesized. Thus, complete definition of a synthesis method requires the value or values of the multiplication factor as well as definition of the procedural steps.

Since the data being synthesized is a function of the data acquisition time, the synthesis methods must provide a means of including time in the prediction technique. The most plausible way of doing this is to use multiplication coefficients that are a function of the time of inlet operation. If it can be reasoned that the coefficients are independent of both type of inlet and flight conditions, then it follows that the coefficients can be defined by an equation similar to the extreme value extrapolation equation.

The method for the synthesis of $K_{\theta \text{ splitter}}$ is defined as follows:

1. A reference 180° segment is determined for each ring and defined as the segment with the minimum steady state total pressure average.

2. Sign selection is negative for probes within the reference 180° segment and positive for the remaining segment.

26

3. The pressure increment,

$$\Delta P_{tj} = \Delta P_{t \text{ rms } j} + 1.5 \, \Delta \overline{P}_{t \text{ rms}_{180}} \tag{2}$$

where

$\Delta P_{t \text{ rms } j}$ = root mean square total pressure fluctuations at probe j

$\Delta \overline{P}_{t \text{ rms}_{180}}$ = average of the root mean square pressure fluctuations over the associated 180° ring segment

4. $A = .0635 \, \ln R + .346$ $\tag{3}$

$\sigma = .0104 \, \ln R + .0963$ $\tag{4}$

where

$$R = \frac{T}{.75} \tag{5}$$

T = time of inlet operation in seconds

The σ is the normalized standard deviation of the difference between the actual and the synthesized level of distortion. During the development of the synthesis method, comparison of synthesis distortion factor values with maximum observed values demonstrated data scatter. Thus, a level of uncertainty has been attached to the synthesized values. The error analysis assumes a normal distribution of the error between synthesis and observed distortion. This means that, for any inlet operation time, an estimate of the maximum expected distortion level can be made along with an associated level of certainty. Thus, for a given T, there is a 68% probability that the true expected maximum distortion is within $\pm\sigma$ of the synthesized value and about a 95% probability that it is within $\pm 2\sigma$ of the synthesized value and so on.

Application of Synthesis Method

This distortion synthesis method was applied to the test data in the following manner:

A. The length of operation of the engine at steady conditions prior to surge was determined from the recorded data.

B. This time interval was then used to calculate a multiplication coefficient with equations (3) and (5).

C. Filtered values of local probe $\Delta P_{t \text{ rms}}$ levels were used to calculate pressure increments as determined by equation (2).

D. The reference 180° ring segments were determined from the steady state pressures and then a synthetic instantaneous pattern was generated for the 36 probe arrangement using equation (1).

Figure 37 presents the results of the comparison between the synthesized distortion for the Task II data. The plot indicates that the original synthesis method consistently overestimates peak distortion

27

levels. Two probable reasons for this overestimation of peak values exist. First, high levels of in-phase full face pressure fluctuations were included in the local levels of ΔP_t $_{rms}$. Such in-phase fluctuations do not influence spatial distortion, thus should be removed for synthesis procedures; second, the method extreme value extrapolation used to develop the original synthesis methods is too severe for long ($\sim$ 5 seconds) time samples of data.

The K_θ synthesis method was refined to incorporate the method of extreme value extrapolation reported by Jacocks and Kneile in Reference 7. The work reported in this reference shows that a "third asymptote" fit of extreme value data should be used in the analysis of instantaneous inlet distortion data. The form of this extreme value estimation procedure, as applied to the synthesis multiplication coefficient, is:

$$A = \alpha + \beta R^{\nu}$$

where α, β and ν are coefficients derived from the fit of data and A and R are as previously defined.

To incorporate this refinement into the synthesis method, it was necessary to refer back to the original data set and rederive expressions for the multiplying factor (A) and the standard deviation (σ). The resultant equations are:

$$A = .9233 - .5773 \, R^{-.11} \tag{6}$$

$$\sigma = .1908 - .0945 \, R^{-.11} \tag{7}$$

The altered synthesis method was applied to the Task II data and the Task I data to define its validity. The synthesis was applied to the data in the manner previously described, with the exception that the in-phase full face pressure fluctuation rms level was subtracted from each probe ΔP_t $_{rms}$ and equation (6) was used for the calculation of A. Simple subtraction of the rms levels was selected since it provided the best correlation of data.

Figure 38 presents the comparison of synthesized distortion versus stall inducing distortion. The symbols represent individual data points. The agreement between synthesized values of K_θ $_{splitter}$ and the stall inducing values of K_θ $_{splitter}$ is surprisingly good for a majority of the points analyzed. There still appears to be a tendency to overpredict the surge inducing distortion; however, the correlation of data is much better than for the unrefined synthesis method. A tabulation of the data plotted in Figure 38 is presented in Table V.

28

CONCLUSIONS

A program to reduce and analyze inlet and engine data obtained during a recent NASA/Lewis Research Center testing of a TF30-P-3 engine operating behind a mixed compression inlet has been conducted. Previously developed distortion analysis techniques were applied to the data to assist in the development of a new distortion methodology. Instantaneous distortion techniques were refined as part of the distortion methodology development. A technique for estimating maximum levels of instantaneous distortion from steady state and average turbulence data was also developed as part of the program.

Analysis of Engine Data

The following conclusions were reached from analysis of the compression system data:

1. The instabilities experienced during the engine testing initiated in the core flow path; therefore, a core stream distortion factor should be employed in analysis of the inlet distortion data.

2. For these tests, virtually all of the instabilities initiated in the low pressure spool compressor and it was therefore the critical compression system component. This is consistent with Pratt & Whitney Aircraft experience.

3. The stator 3 through rotor 6 row group was the most probable region for instabilities to initiate at the tested conditions; however, the location was unpredictable on a case to case basis.

In consideration of the results of both analytical compressor model predictions and the engine test results, the following conclusions were reached:

1. The 3rd stator of the TF30 is suspected of often being influential in setting the stability limits of the compressor. This row should, therefore, be instrumented during future test programs oriented toward investigation of surge to determine if, in fact, it is a frequent source of instability.

2. Realizing that instabilities do not always originate at the same compressor location, continued tracking of critical regions in the compressor against variables affecting row, stage, or stage group matching remains desirable. Future engine surge investigations, therefore, should also include instrumentation to isolate other regions of the compressor.

Application of Previously Developed Techniques

The K_{D2} versus turbulence system of predicting engine distortion tolerance was developed by Pratt & Whitney Aircraft to handle a one per revolution distortion pattern with the particular high frequency pressure versus frequency characteristic. Testing of the TF30-P-3 engine behind a mixed compressor inlet subjected the engine to spatial and high frequency pressure distortion characteristics considerably different than in-house Pratt & Whitney Aircraft flight test experience.

These engine tests demonstrated higher levels of distortion tolerance than would have been predicted from previous testing. While good agreement with predicted K_{D2} steady state levels was demonstrated at conditions of low turbulence and a one per revolution pattern, the high turbulence stall points with a 4 per revolution pattern showed considerably less engine sensitivity to turbulence than predicted. Differences in the turbulent energy/frequency characteristics between the test inlet and Pratt & Whitney Aircraft experience is believed to be the primary reason for the change in engine response to turbulence.

The K_{D2} instantaneous (0-150 Hz) analysis generally showed levels of K_{D2} at surge to be above the critical level, however, levels of K_{D2} above the surge level did occur without causing surge. Based on these results it is concluded that K_{D2} (0-150 Hz) is not a useful method of predicting engine stall for this propulsion system combination.

Distortion Analysis Methodology

A distortion methodology based on the concept of instantaneous distortion was developed from interpretation of the inlet and engine data. Analysis of the results of the methodology development and verification has led to the following conclusions:

1. The data should be preconditioned by a filter with a cut-off frequency equal to the rotor speed of the low compressor. Roll-off rate and phase shift characteristics of the filter are not important, since it was found that they have only a secondary effect on the levels of distortion calculated from the data.

2. Application of a core flow distortion factor, $K_{\theta \, splitter}$, to preconditioned data provides a good indication of the stall inducing distortion.

3. Planar pulse data should be bookkept along with spatial distortion to provide the best indication of the level of instantantous distortion factor required to stall the engine.

30

Distortion Synthesis

A previously developed method of generating synthetic instantaneous distortion patterns from steady state and turbulence data was applied to the data. When the method did not result in correlation of the data, refinements to the synthesis techniques were made. Application of the refined method to the data resulted in a reasonably good correlation between the synthesized levels of distortion and the stall inducing levels of distortion.

PRATT & WHITNEY AIRCRAFT

NASA-LEWIS TF30-P-3 60/40 MIXED COMPRESSION INLET TEST
STALL SUMMARY

Steady State Case Number	7th Bleed*	12th Bleed**	Area-%	N1-RPM	N2-RPM	Event Summary	Initial Location Of Rotating Stall Engine Stations	Low Spool Rot. Stall Freq. % N1	HPC Rot. Stall Freq. %N2	Surge Signature Classification
384	Open	Closed	100	6287	11237	'LPC Rot. Stall/HPC Surge	2.3-2.6	52.0	----	LPC/Type 1
389			100	6806	11769			52.5	----	
405			140	7031	11351			56.0	----	
408			83	6346	11719	↓		63.6	----	↓
421			100	6670	11867	LPC Rot. Stall/HPC Rot. Stall/HPC Surge	↓	50.8	40.1	LPC/Type 3
438			140	7103	11557	LPC Rot. Stall/HPC Surge	2.6-3.0	44.7	----	LPC/Type 1
441			140	7115	11559	↓	2.3-2.6	61.6	----	↓
445			83	6306	11839	Fan Rot. Stall/LPC Rot. Stall/HPC Surge	2.0-2.3	49.1	----	Fan/Type 1
457			100	6136	11303	LPC Rot. Stall/HPC Rot. Stall/HPC Surge	2.3-2.6	54.9	48.3	LPC/Type 3
464			100	6661	11863	↓	↓	44.2	56.2	↓
467			100	6647	11849	LPC Rot. Stall/HPC Surge	↓	47.5	----	LPC/Type 1
502			83	6308	11471	Fan Rot. Stall/LPC Rot. Stall/HPC Surge	2.0-2.3	63.6	----	Fan/Type 1
528			120	7255	11603	LPC Rot. Stall/HPC Surge	2.3-2.6	43.1	----	LPC/Type 1
537			100	6354	11521			57.2	----	
561	↓	↓	83	6326	11895	↓	↓	51.0	----	↓
519		Open	100	6542	11819	HPC Surge	-------	----	----	HPC/Type 2
451	Closed	Closed	100	6159	11247	LPC Rot. Stall/HPC Surge	2.3-2.6	53.8	----	LPC/Type 1
461			100	6180	11241	Fan Rot Stall/LPC Rot. Stall/HPC Surge	2.0-2.3	60.7	----	Fan/Type 1
471			100	6646	11711	'LPC Rot. Stall/HPC Rot. Stall/HPC Surge	2.3-2.6	49.9	42.7	LPC/Type 3
497			83	6288	11751	Fan Rot. Stall/LPC Rot. Stall/HPC Rot. Stall/HPC Surge	2.0-2.3	38.0	41.2	Fan/Type 3
515			100	6289	11363	LPC Rot. Stall/HPC Surge	2.3-2.6	49.4	----	LPC/Type 1
540	↓	↓	100	6317	11433	↓	↓	53.1	----	↓

* Located at the 7th stage of the 9 stage low compressor.
** Located at the 3rd stage of the 7 stage high compressor.

TABLE I

32

TABLE II

ANALOG RESULTS

Case #	TIME OF PEAK K_{C_2}	TIME OF STALL
384	01:31:10.823	01:32:53.531
389	02:17:50.429	02:19:33.136
405	00:57:53.488	00:58:58.285
408	02:01:26.322	02:02:08.495
421	02:03:32.927	02:04:12.535
438	01:27:23.767	01:27:25.535
445	00:53:09.244	00:54:13.648
457	00:55:01.273	00:56:27.049
515	01:28:09.942	01:28:17.773
451	02:13:40.055	02:13:41.088

TABLE III

TABULATION OF THE RESULTS OF
FILTER CUT-OFF FREQUENCY STUDY

Case #	Fc	K_θ splitter		$K_{\theta\,stall}/$
		Stall	Peak	$K_{\theta\,peak}$
384	50	.462	.528	.892
	100	.708	-	1.0
	150	.846	-	1.0
	200	1.017	-	1.0
389	50	.411	.429	.959
	100	.671	-	1.0
	150	.895	-	1.0
	200	1.082	-	1.0
405	50	.486	.520	.934
	100	.718	.768	.934
	150	.786	-	-
	200			
408	50	.462	.523	.883
	100	.848	-	1.0
	150	.979	-	1.0
	200	1.072	-	1.0
421	50	.613	.794	.772
	100	.92	1.146	.803
	150	1.125	1.300	.865
	200	1.310	1.423	.921
438	50	.838	.892	.939
	100	1.046	-	1.0
	150	1.137	-	1.0
	200	1.191	-	1.0
445	50	.998	1.180	.846
	100	1.080	1.447	.742
	150	1.118	1.600	.699
	200	1.159	1.667	.695
457	50	1.042	-	1.00
	100	1.167	-	1.00
	150	1.166	1.259	.927
	200	1.190	1.356	.877
515	50	.636		1.0
	100	.797		1.0
	150	.902		1.0
	200	.973		1.0
451	50	.665		1.0
	100	.731		1.0
	150	.772		1.0
	200	.798		1.0

TABLE IV

TABULATION OF RESULTS OF METHODOLOGY VERIFICATION

Case #	W_{at2}	Max. $K_{\theta \text{ splitter}}$	$\Delta P_{t2}/P_{t2}$	tK_{max}	t_{stall}	Δt (Sec)
441	171.8	1.021	.0133	8.47598	8.48319	.0072
464	159.9	.889	.011	42.73524	42.7359	.0007
467	159.4	.854	.0135	26.29169	26.29238	.0007
528	171.4	.985	.0123	21.24962	21.25458	.0049
537	152.9	1.173	.018	33.6703	33.67236	.0021
561	145.8	1.253	.0142	54.8347	54.83539	.0007
502	151.0	.611	.010	20.06537	20.06582	.0004
461	145.9	.332	-	32.82976	32.8308	.0010
471	155.1	.579	-	31.17754	31.18572	.0082
497	142.6	1.016	-	27.01199	27.08690	.07491
540	149.4	1.256	-	19.53906	19.59179	.05273
519	147.9	.831	-	40.24377	40.27201	.02824

TABLE V

SUMMARY OF DISTORTION SYNTHESIS
STUDY - REFINED SYNTHESIS METHOD

Case #	ΔT	K_θ splitter		$\Delta K/K$
		Synthesized	Stall	
441	84.4	1.17	1.021	.146
464	26.8	.565	.889	-.364
467	256.1	.83	.854	-.028
528	39.3	1.09	.985	.107
537	36.7	1.26	1.173	.074
561	324.9	1.40	1.253	.117
502	196.	.46	.611	-.247
461	44.8	.50	.332	.506
471	12.2	.55	.579	-.05
497	53.1	.9	1.016	-.114
540	76.6	1.67	1.256	.330
519	33.3	1.29	.881	.464
405	78.2	.89	.924	-.037
408	90.9	.92	.848	.085
421	44.4	.92	.92	0
438	13.4	.99	1.046	-.053
445	188.5	1.51	1.08	.398
457	106.9	1.03	1.167	-.117
515	22.7	.78	.797	-.021
451	71.	.785	.731	.074
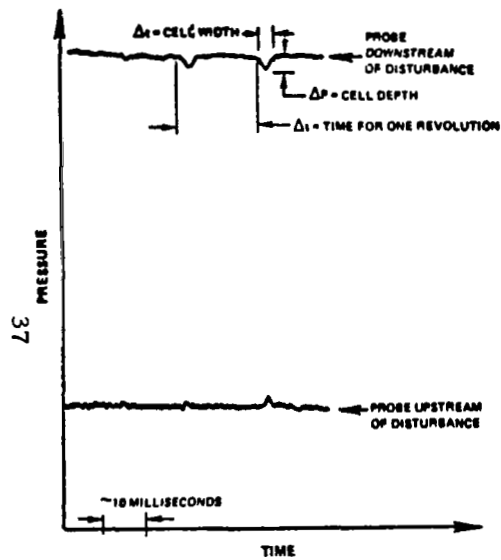
Figure 1. - Rotating stall location.
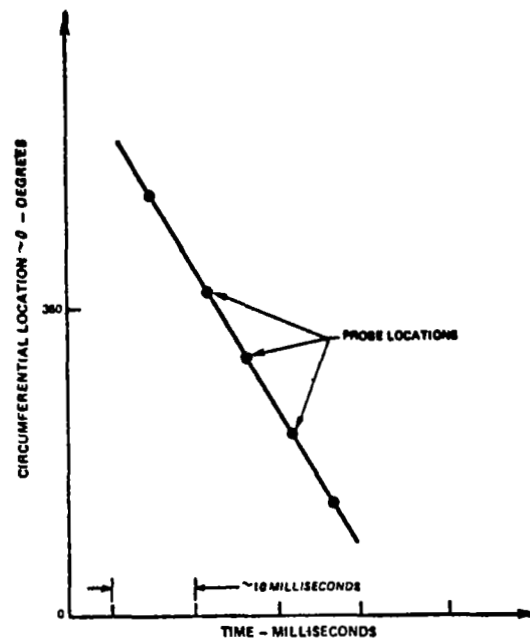
Figure 2. - Rotating stall propagation rate.
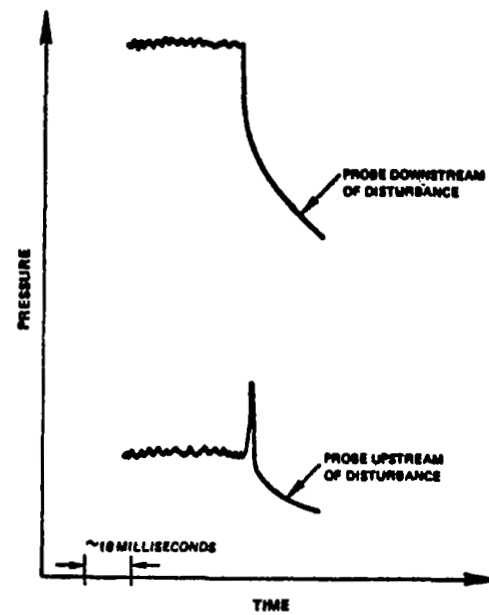
Figure 3. - Surge pressure wave identification.

Station 2.0   2.3   2.6   3.0   4.0
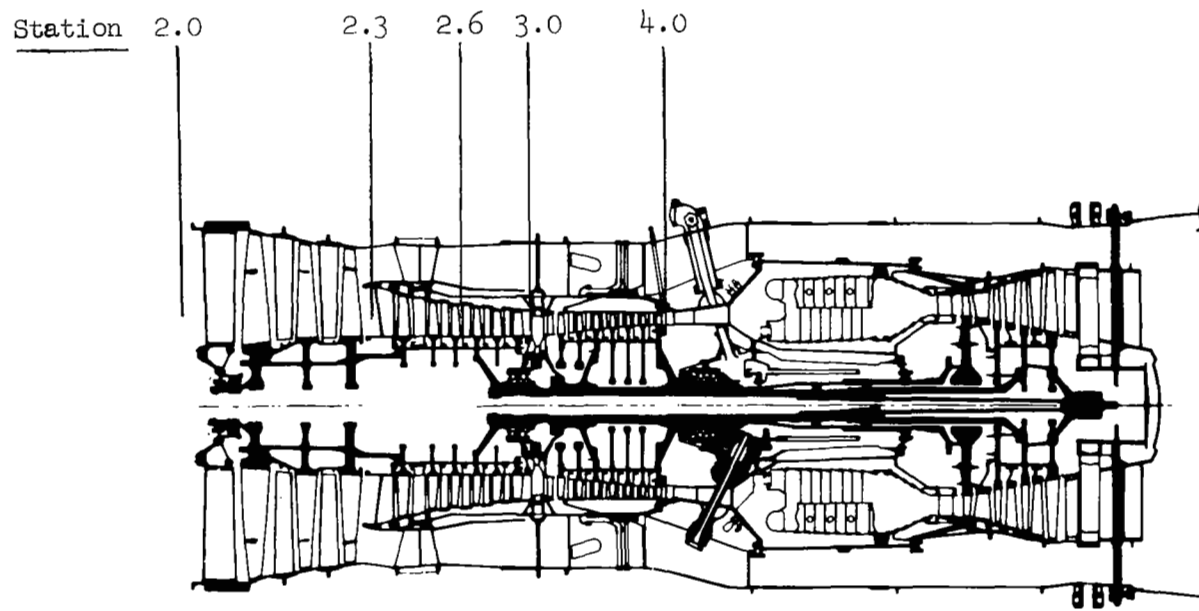
Figure 4. - Axial locations of high response instrumentation.

STA. 2.3

2.6

3.0

4.0

69°

295°

292°

89°

269°

268°

249°

117°

226°

○ PT

△ PS

FILLED SYMBOLS DENOTE OPERATIVE INSTRUMENTATION
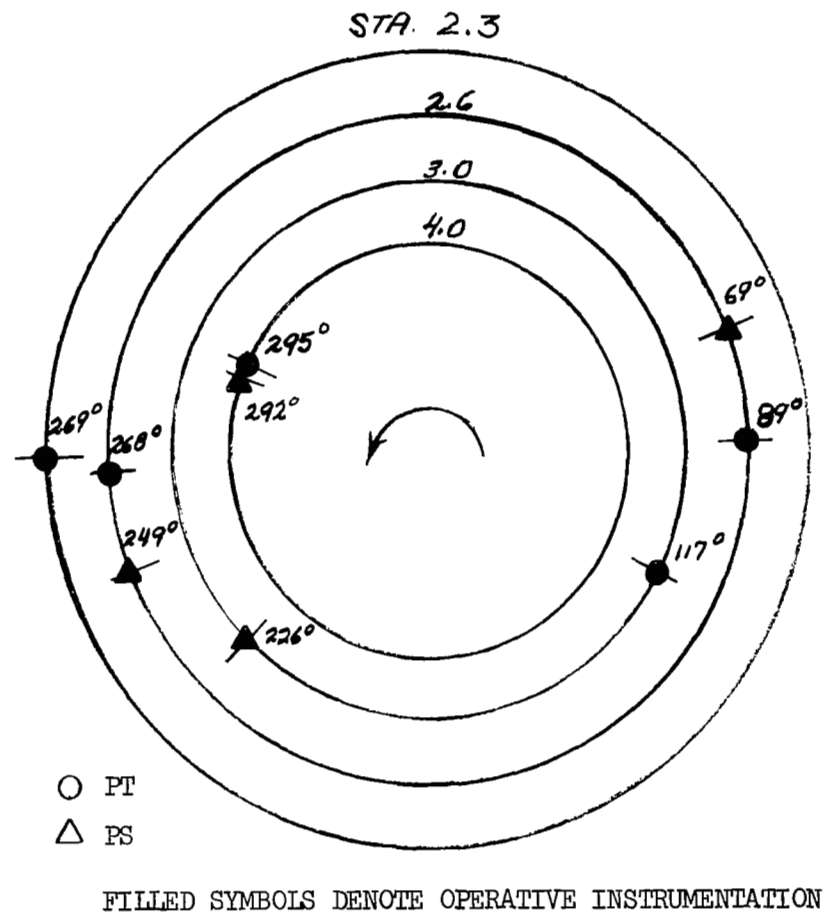
Figure 5. - NASA/Lewis TF30-P-3 mixed compression
inlet test; internal instrumentation summary looking
into front of engine.
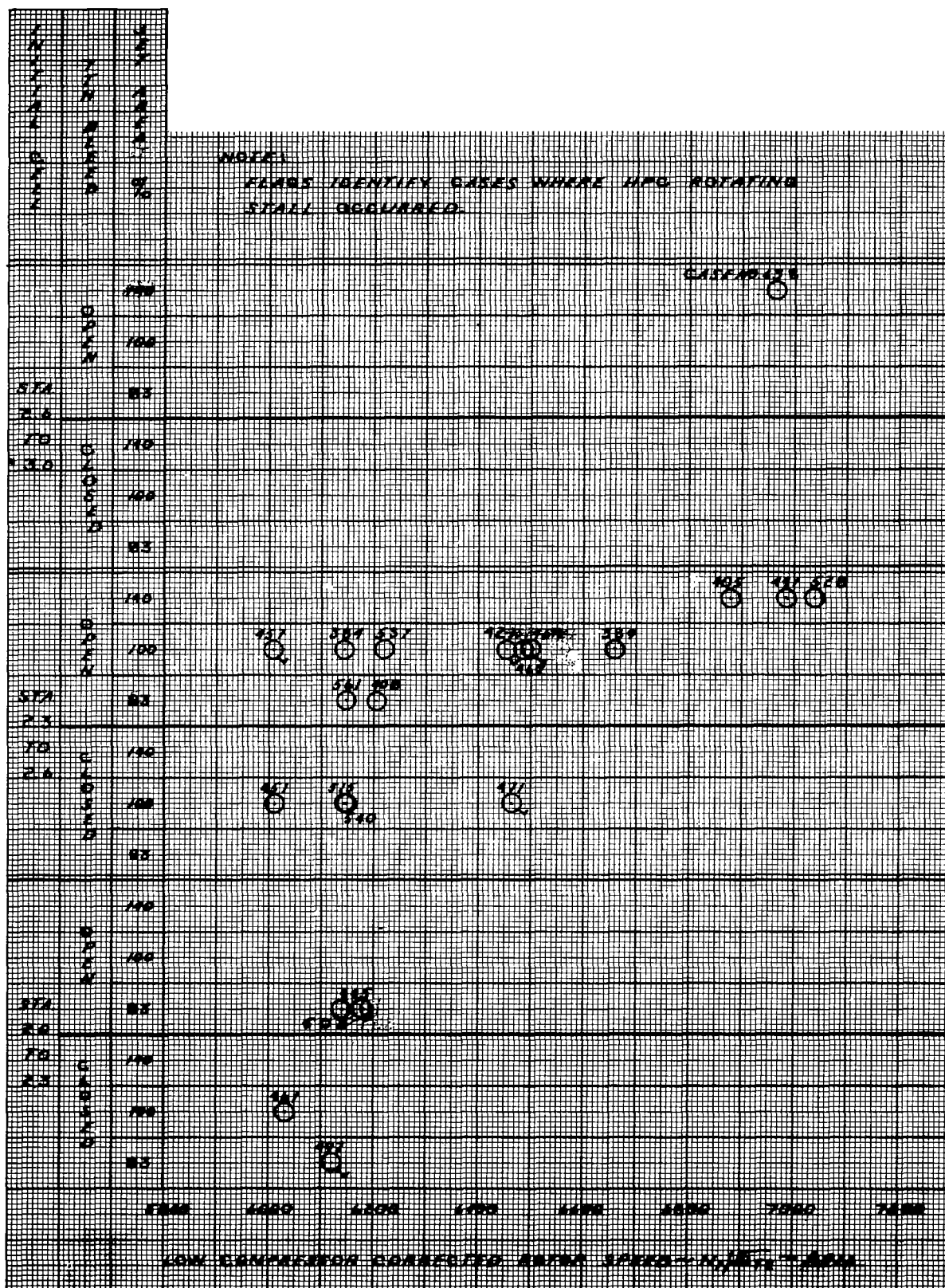
Figure 6. – Result matrix; instabilities initiated in low compressor.
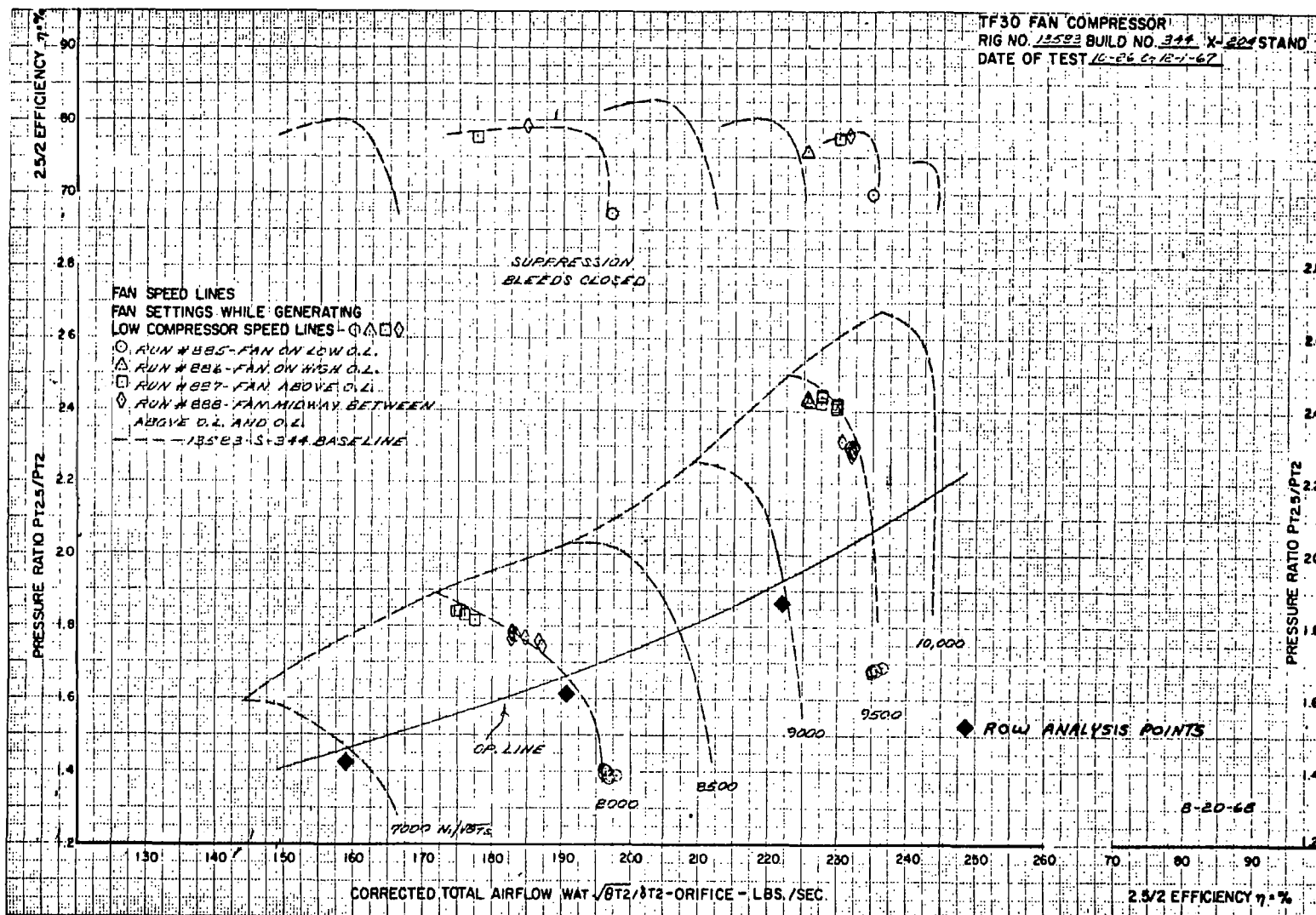
Figure 7. - Row by row analysis, fan match points.
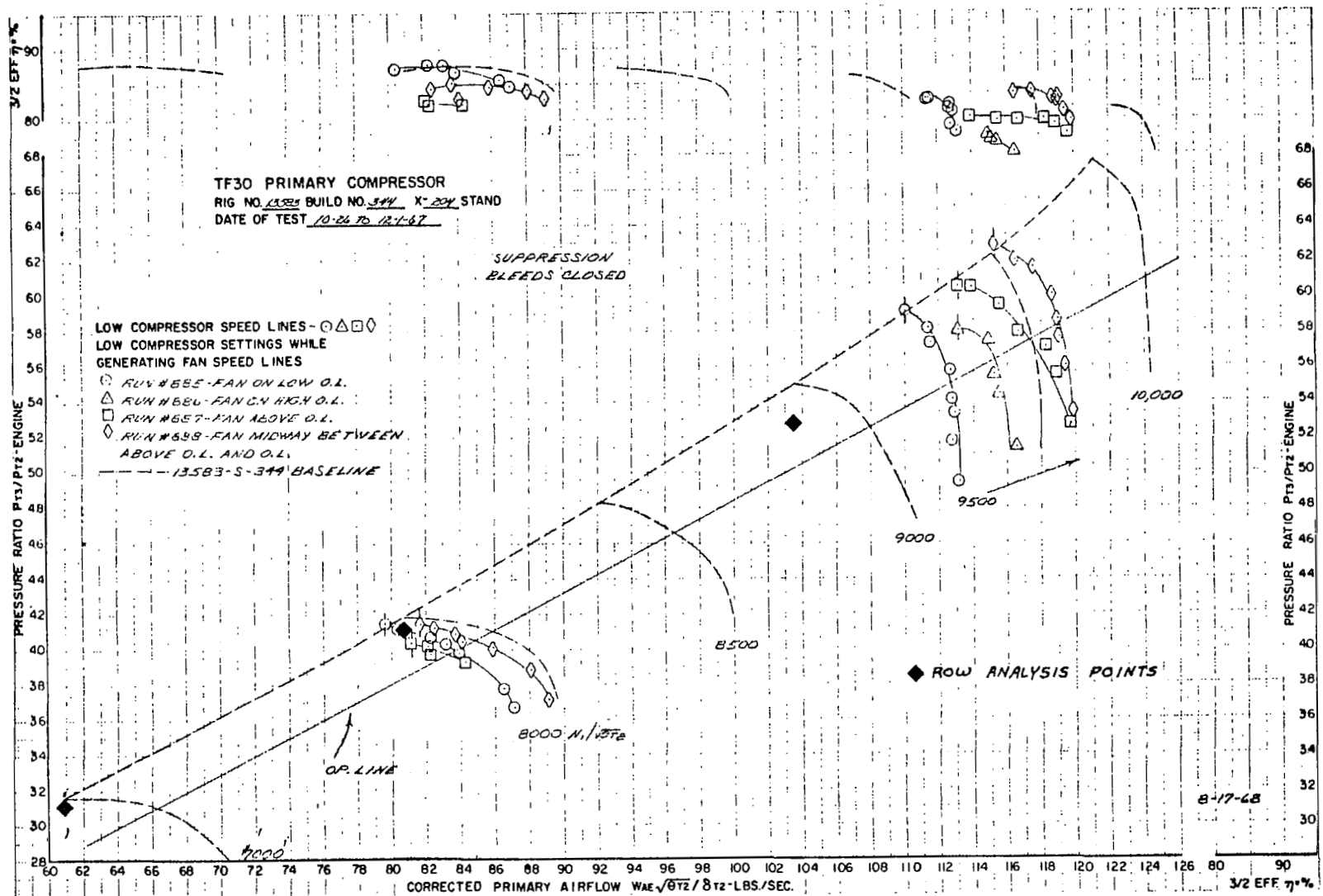
Figure 8. – Row by row analysis, low compressor match points.
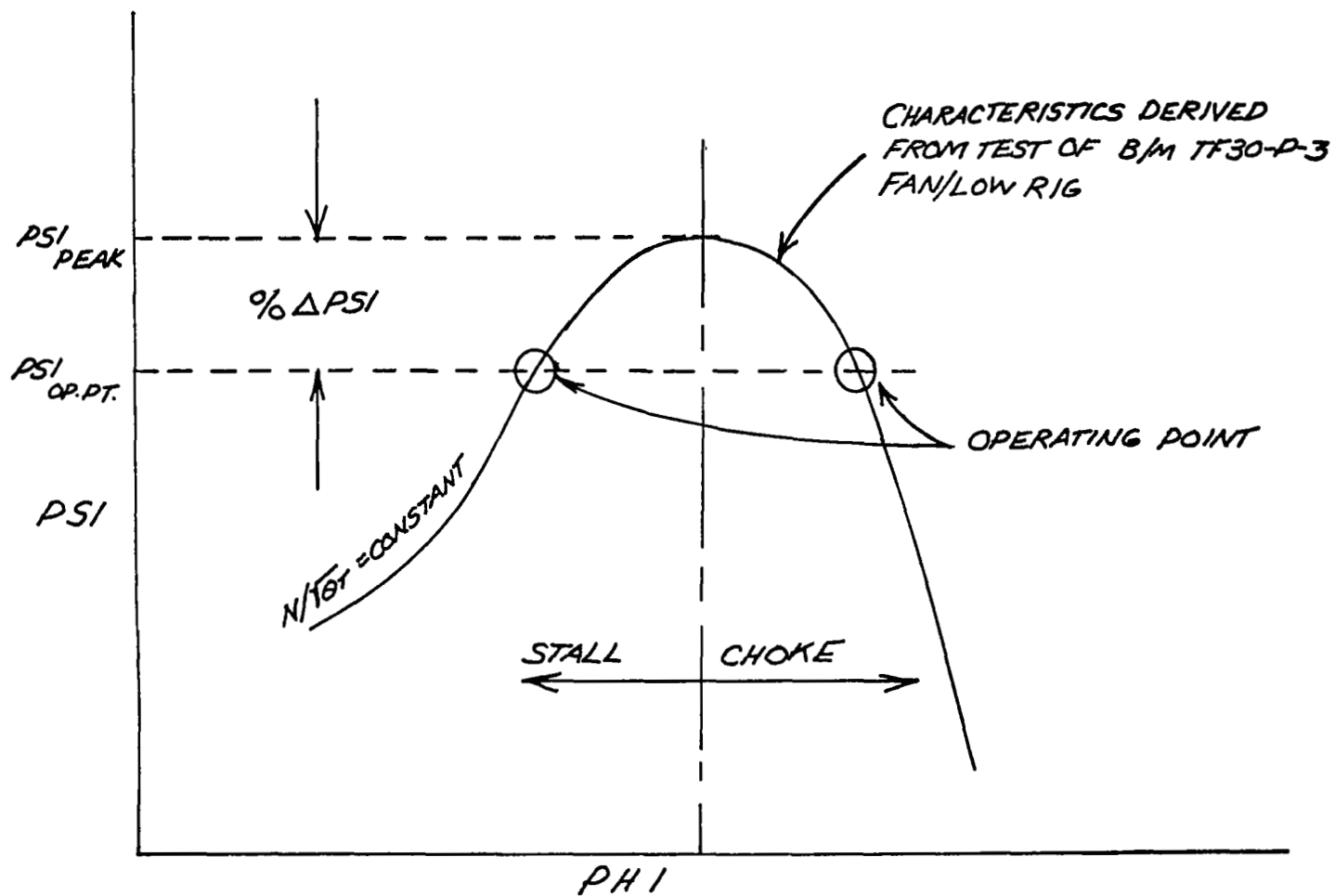
Figure 9. – Row by row analysis.
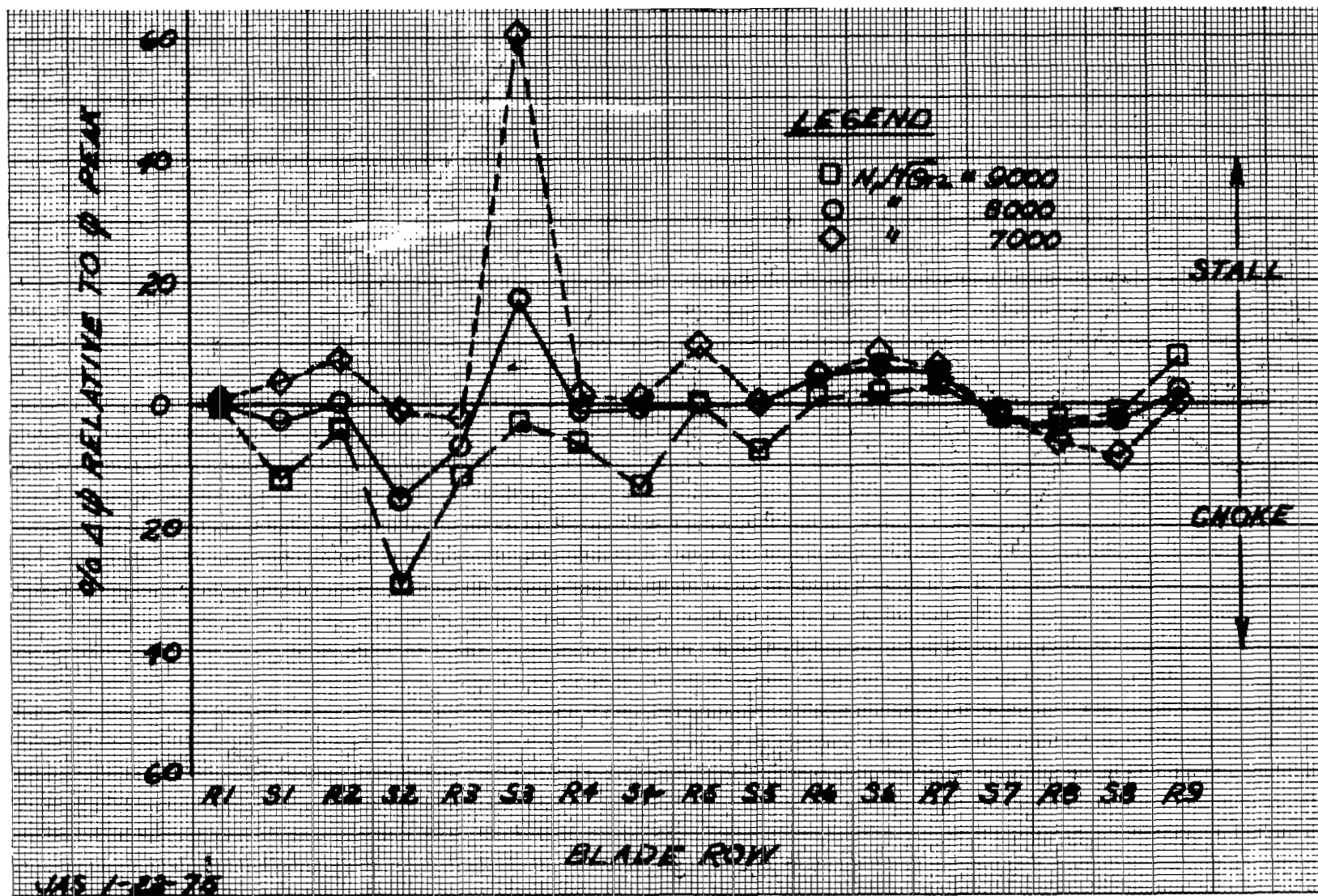
Figure 10. - Pratt and Whitney aircraft TF30-P-3 low pressure compressor - blade row match
variation with speed at near surge conditions; standard fan operating line; no bleed.
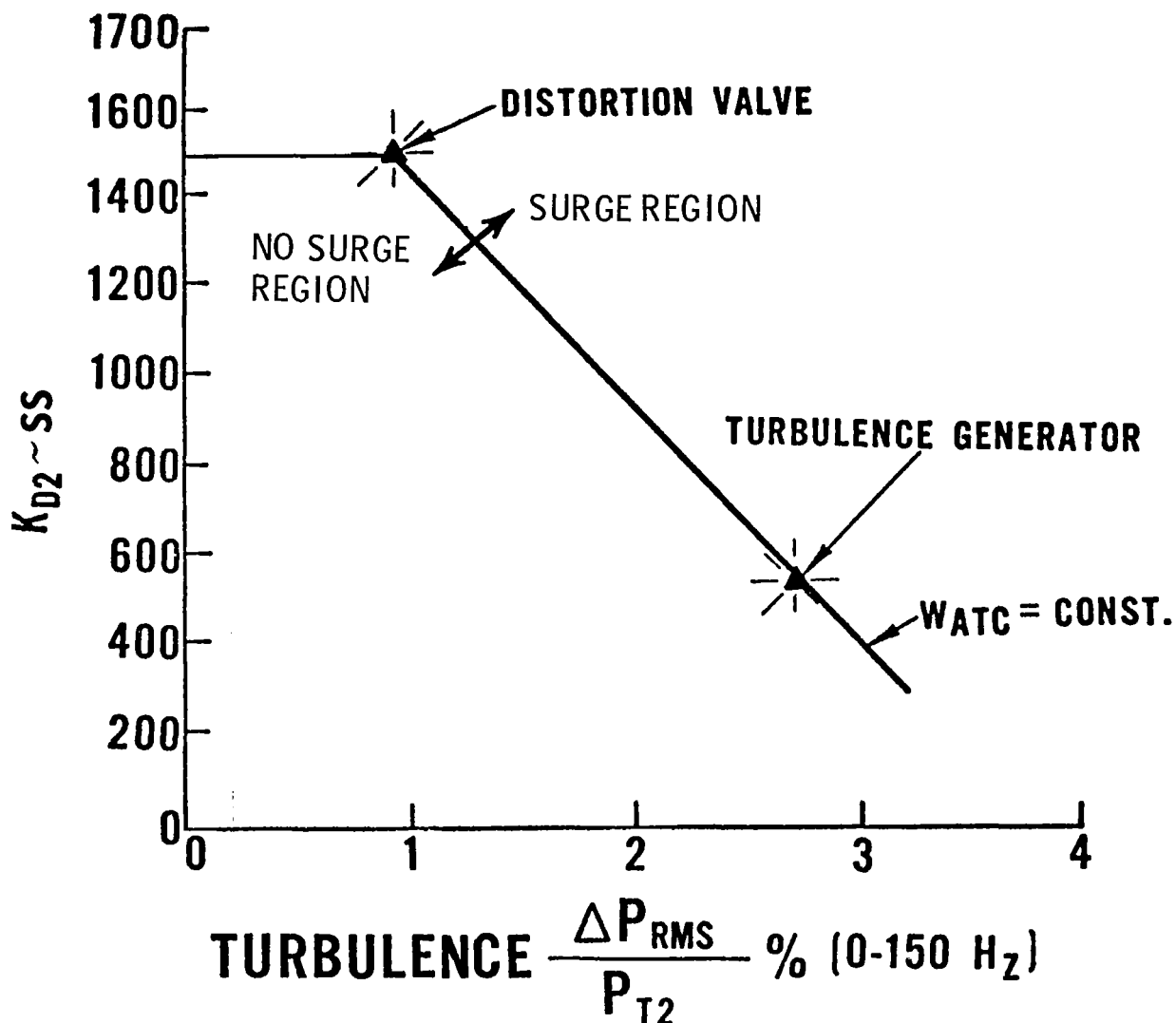
DISTORTION AND TURBULENCE INTERACTION

Figure 11. – Development of K_{D2} versus turbulence.

TRANSITION
SECTIONS

BELLMOUTH

INLET
SCREEN

ENGINE
INLET
CASE

FOUR QUADRANT
CIRCUMFERENTIAL
DISTORTION VALVE

HORIZONTAL STRUT

VANES
OPEN

VANES
PARTIALLY CLOSED

DISTORTION VALVE

INLET
PLENUM

ADJUSTABLE CENTER BODY
CYLINDRICAL SECTION

CONTROL VALVE

BYPASS LINE

INLET AIR
SUPPLY

TO
EXHAUSTERS

NORMAL SHOCK LOCATION

COMPRESSOR RIG
OR ENGINE

Pratt &
Whitney
Aircraft

U
A.

GM-48582
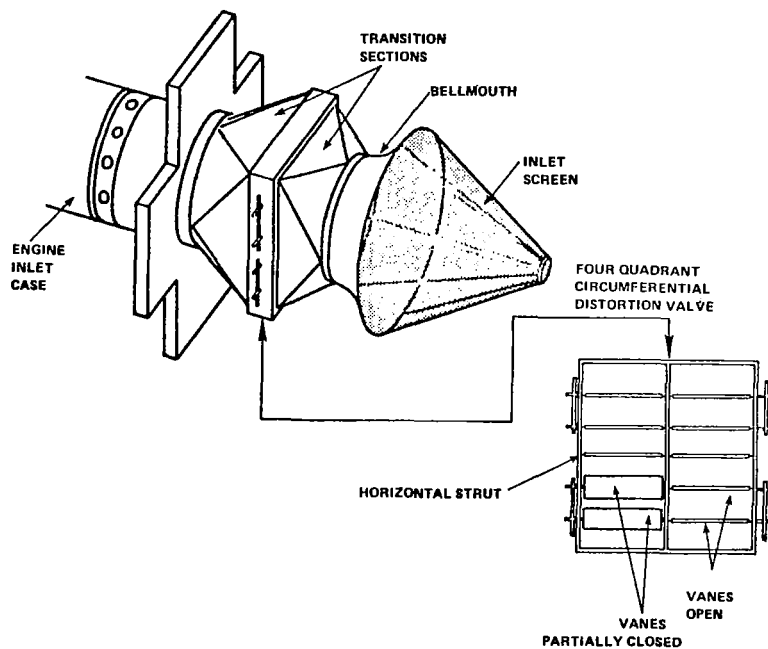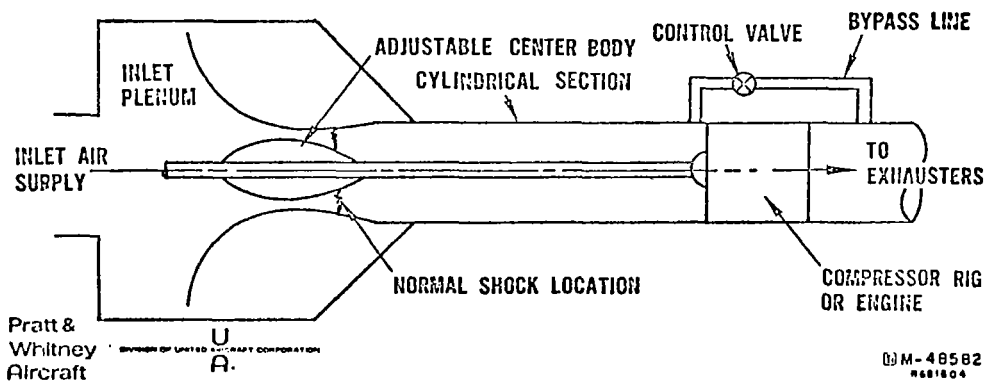
TURBULENCE GENERATOR

Figure 12. – TF30 distortion tolerance development tools.

46

PRATT + WHITNEY AIRCRAFT

TF30 TURBOFAN ENGINE

446-22X-235 DISTORTION VALVE CAL. PHASE I X446-22 VERGE

DATE (MONTH.DAY)   7/11/69
TIME   0
WATC ≈ 145   N1/√θₙ = 6512.0
ALPHA(DEGREES)   -.0
BETA(DEGREES)   -.0
MAP. DISTORTION FACTOR(KD)   692.8
VERGE OF SURGE
                   B/C

SAMPLE OF "KIT"
DISTORTION PATTERN
DISTORTION VALVE

BULLET
NOSE
% ΔP/P_average
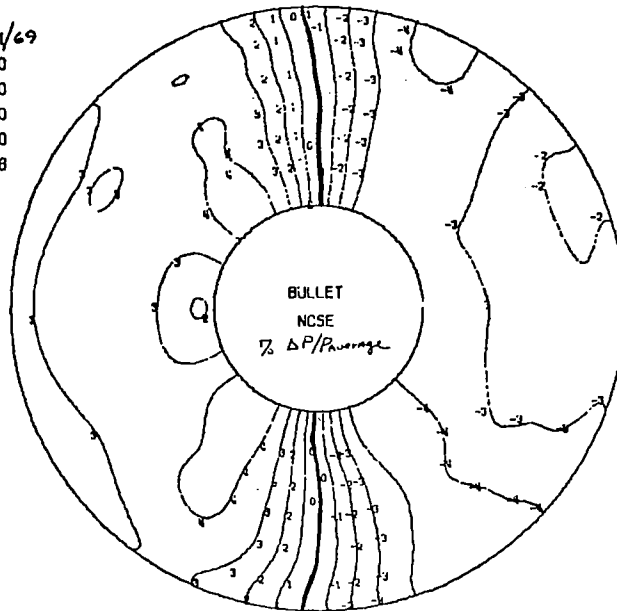
VIEW LOOKING AFT

PRATT + WHITNEY AIRCRAFT

TF30 TURBOFAN ENGINE

P446   Y-446-25 TURBULENCE GEN X210 STAND PHASE 2 KD2

DATE (MONTH.DAY)   5/20/70
TIME (HOURS.MINUTES)   1647
N1/ROT2   0.
K_{D_2} 340

SAMPLE OF "KIT"
DISTORTION PATTERN
TURBULENCE GENERATOR

BULLET
NOSE
% ΔP/P_ave.
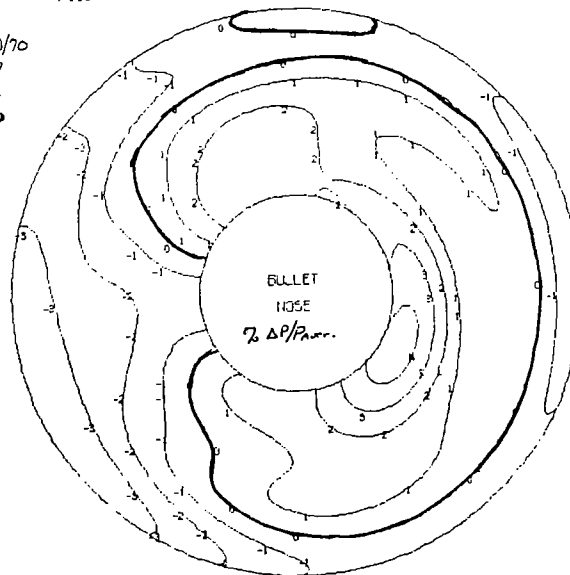
VIEW LOOKING AFT

7^{u} Δ/0

Figure 13. - Distortion patterns.
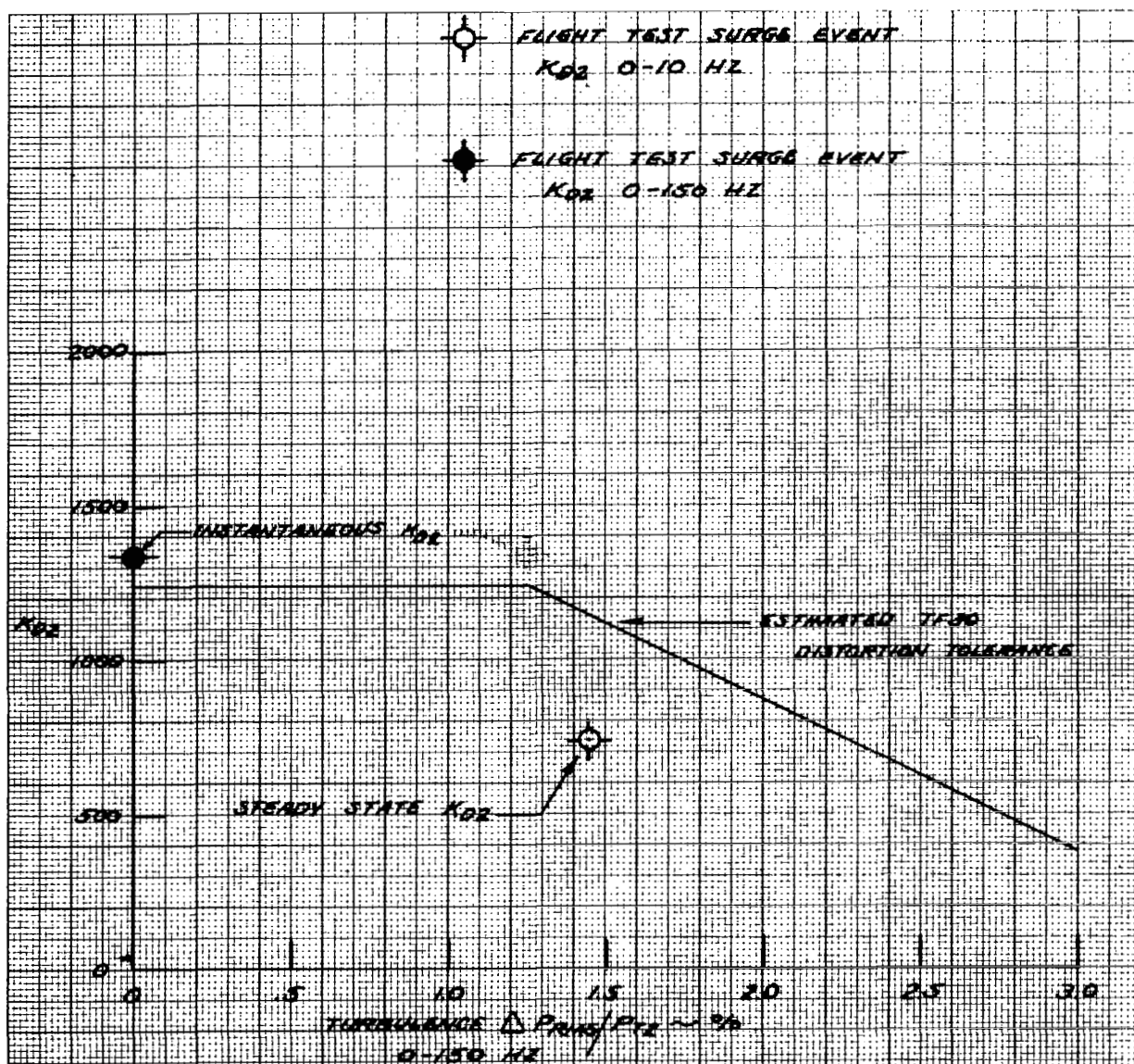
Figure 14. – TF30 aircraft compatibility; WATC = 190 lb/sec; bleeds closed.

○ COMBINATION STEADY STATE & DYNAMIC PROBE
○ STEADY STATE PROBE
  - 72 STEADY STATE PROBES
  - 36 HIGH RESPONSE PROBES

RAKE
1

CENTER BODY SUPPORT
STRUTS

4

10

7

LOOKING AFT
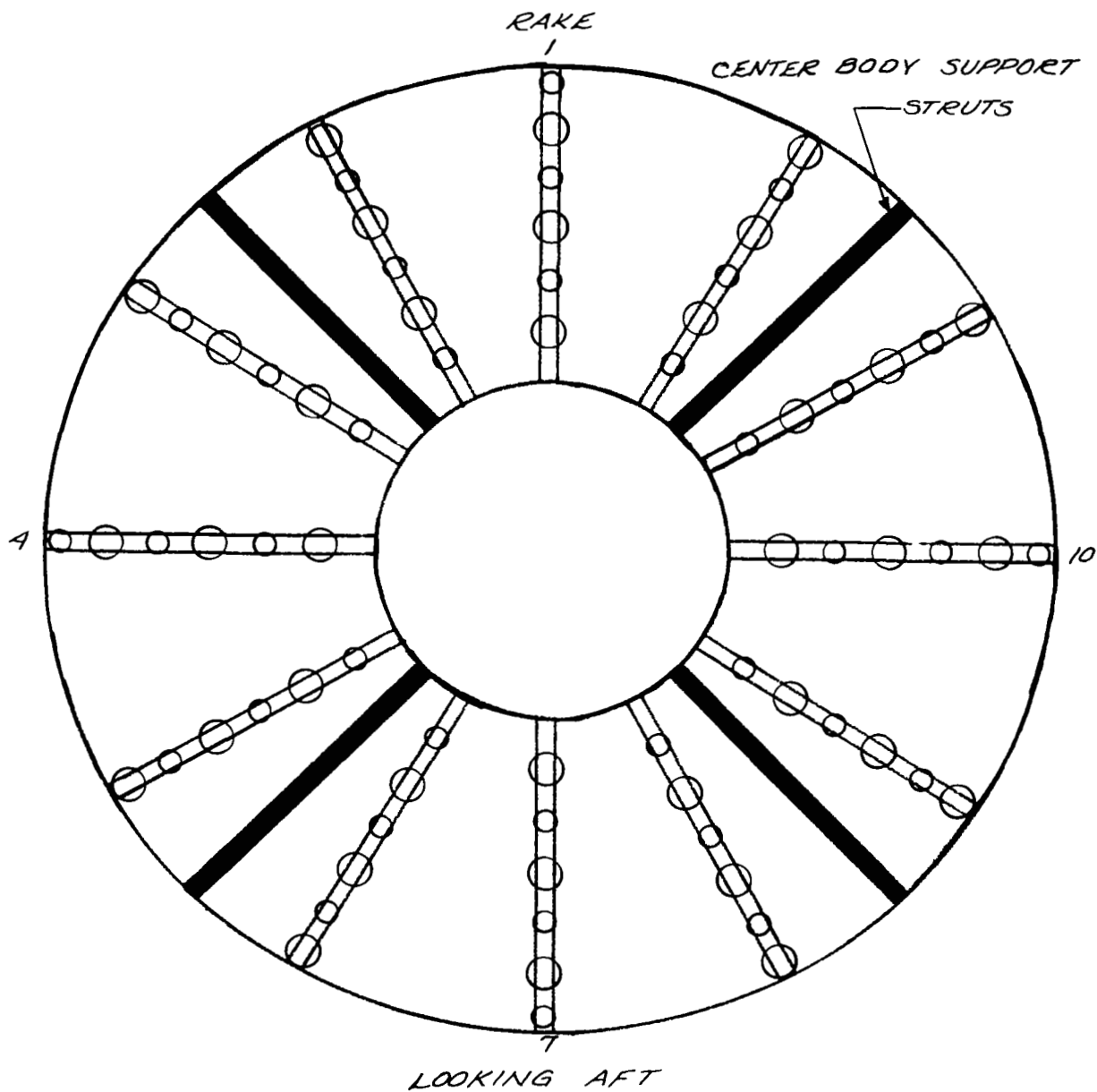
Figure 15. - Engine compressor face instrumentation for inlet tests in NASA/
Lewis 10 × 10 SWT.

"A"

PRATT & WHITNEY AIRCRAFT
ENGINE TF30 TURBOFAN
TF30P3 10X10 NASA/LEWIS   INLET TEST/TF30P-3 KD2

POINT NUMBER   3940
WATC   148.60
ALPHA(DEGREES)   0.0
BETA(DEGREES)   0.0
MAP DISTORTION FACTOR(KD)   401.15

$\Delta P / P_{AVG} \sim \%$

OVERBOARD
BYPASS DOORS

SUPPORT
STRUTS

VIEW LOOKING AFT
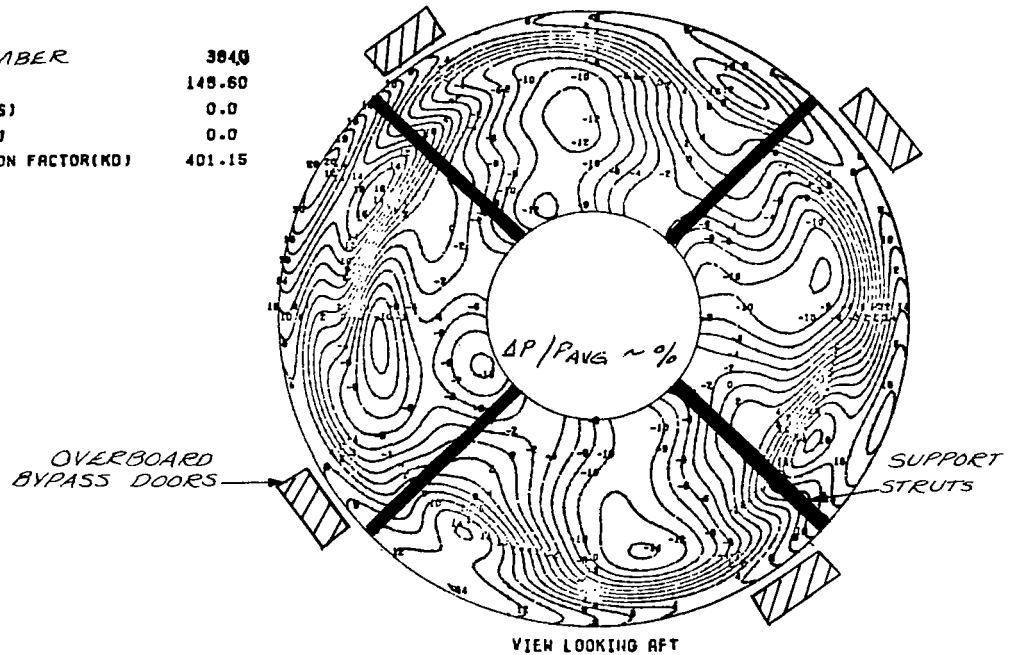
"B"

PRATT & WHITNEY AIRCRAFT
ENGINE TF30 TURBOFAN
TF30P3 10X10 NASA/LEWIS   INLET TEST/TF30P-3 KD2

POINT NUMBER   4570
WATC   150.10
ALPHA(DEGREES)   5.60
BETA(DEGREES)   0.0
MAP DISTORTION FACTOR(KD)   1198.96

$\Delta P / P_{AVG} \sim \%$

VIEW LOOKING AFT
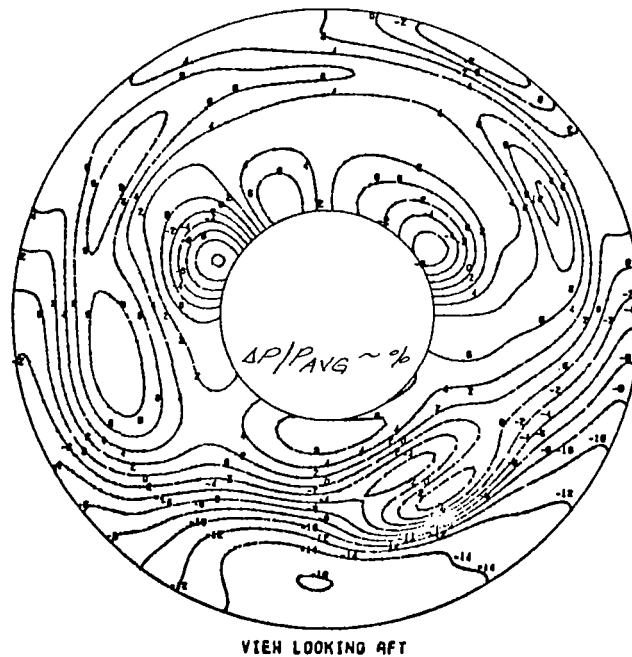
Figure 16. – Steady state inlet pressure profiles; mixed compressor inlet; 2.5 MN.

50

Figure 17. - NASA Lewis inlet test of TF30-P-3 - normalized power spectral density.
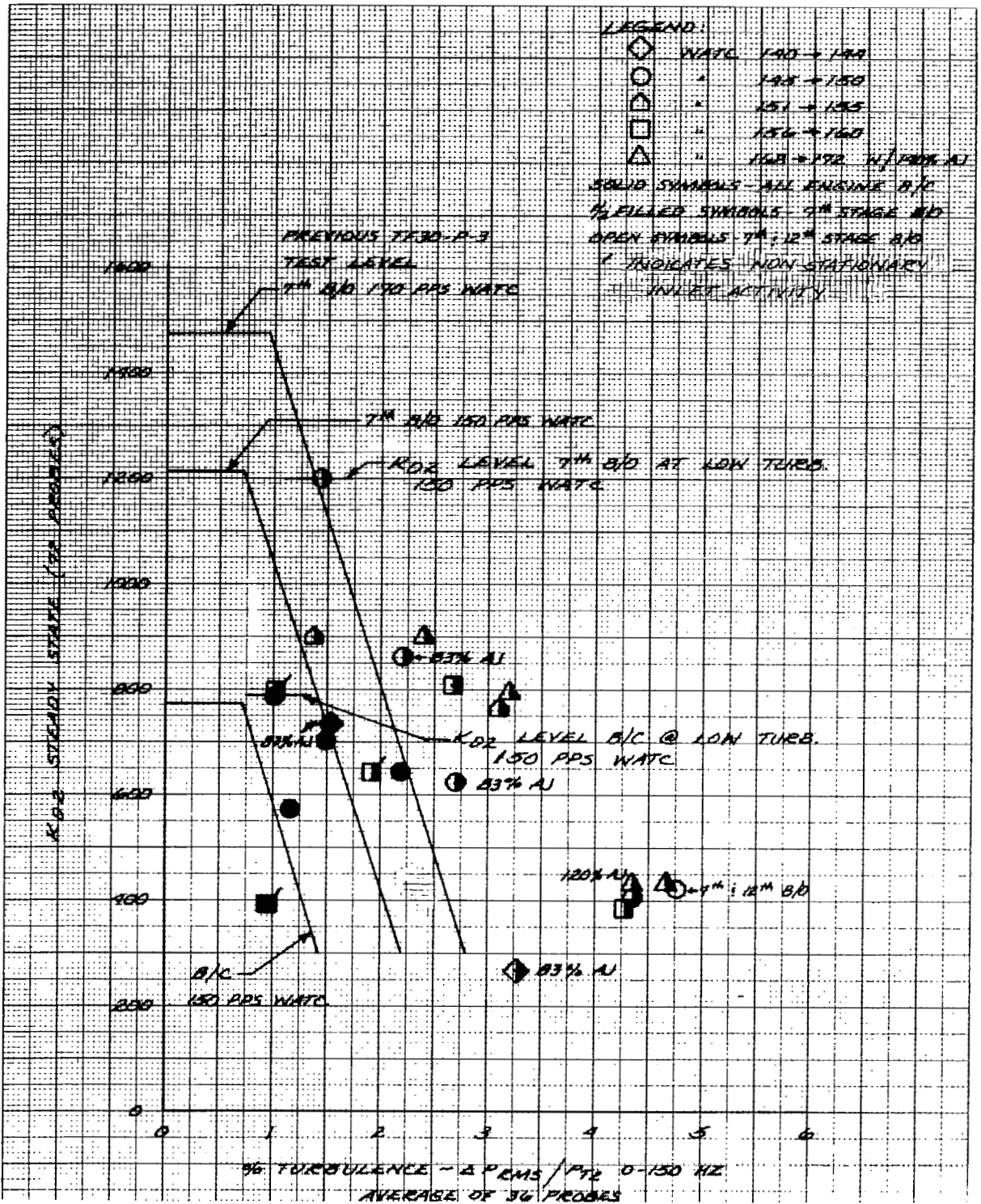
Figure 18A. – TF30-P-3 engine distortion tolerance; NASA/
Lewis inlet test.
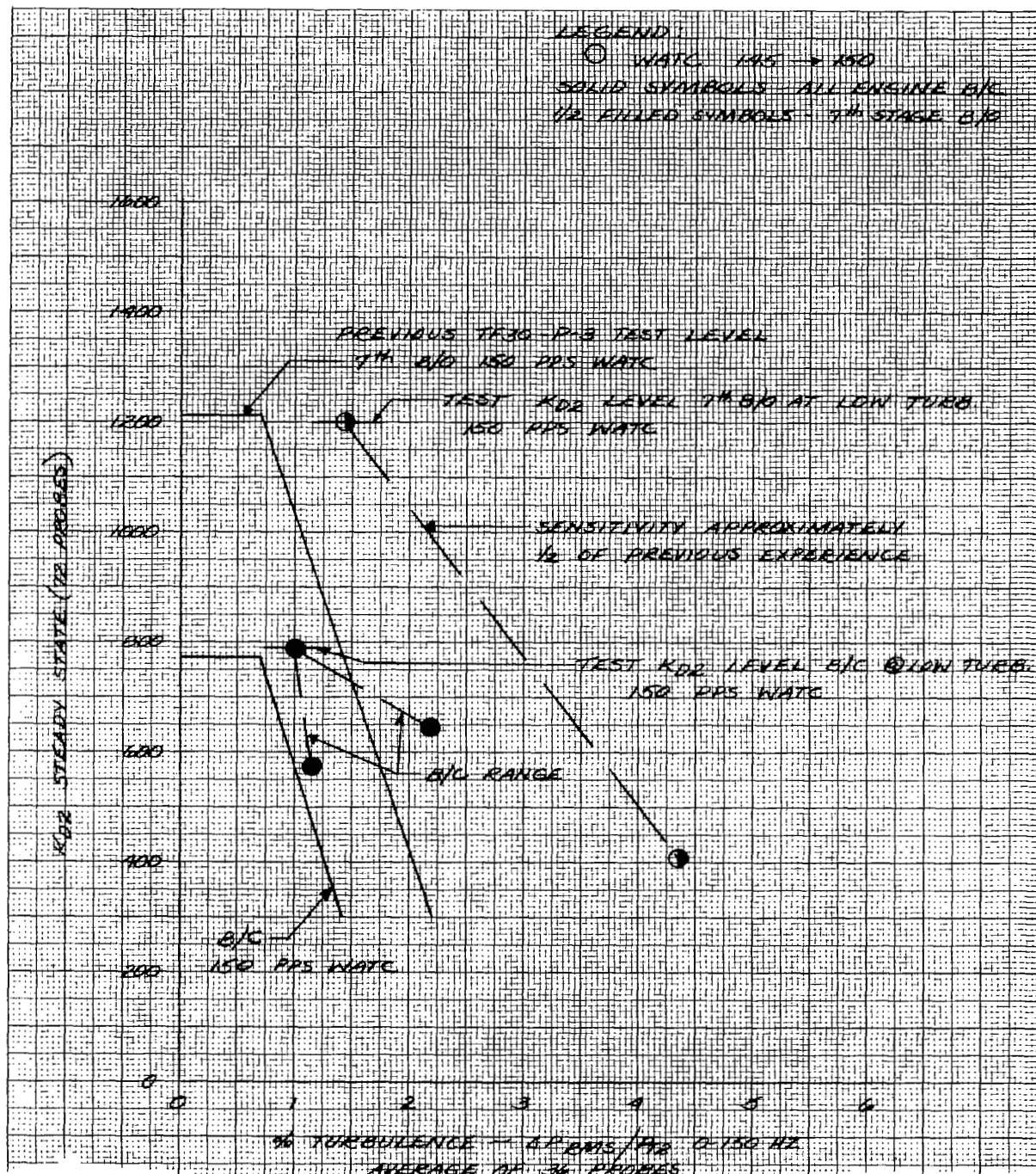
Figure 18B. – TF30-P-3 engine distortion tolerance; NASA/
Lewis inlet test.

Figure 19. – TF30-P-3 engine distortion tolerance; NASA/
Lewis inlet test.
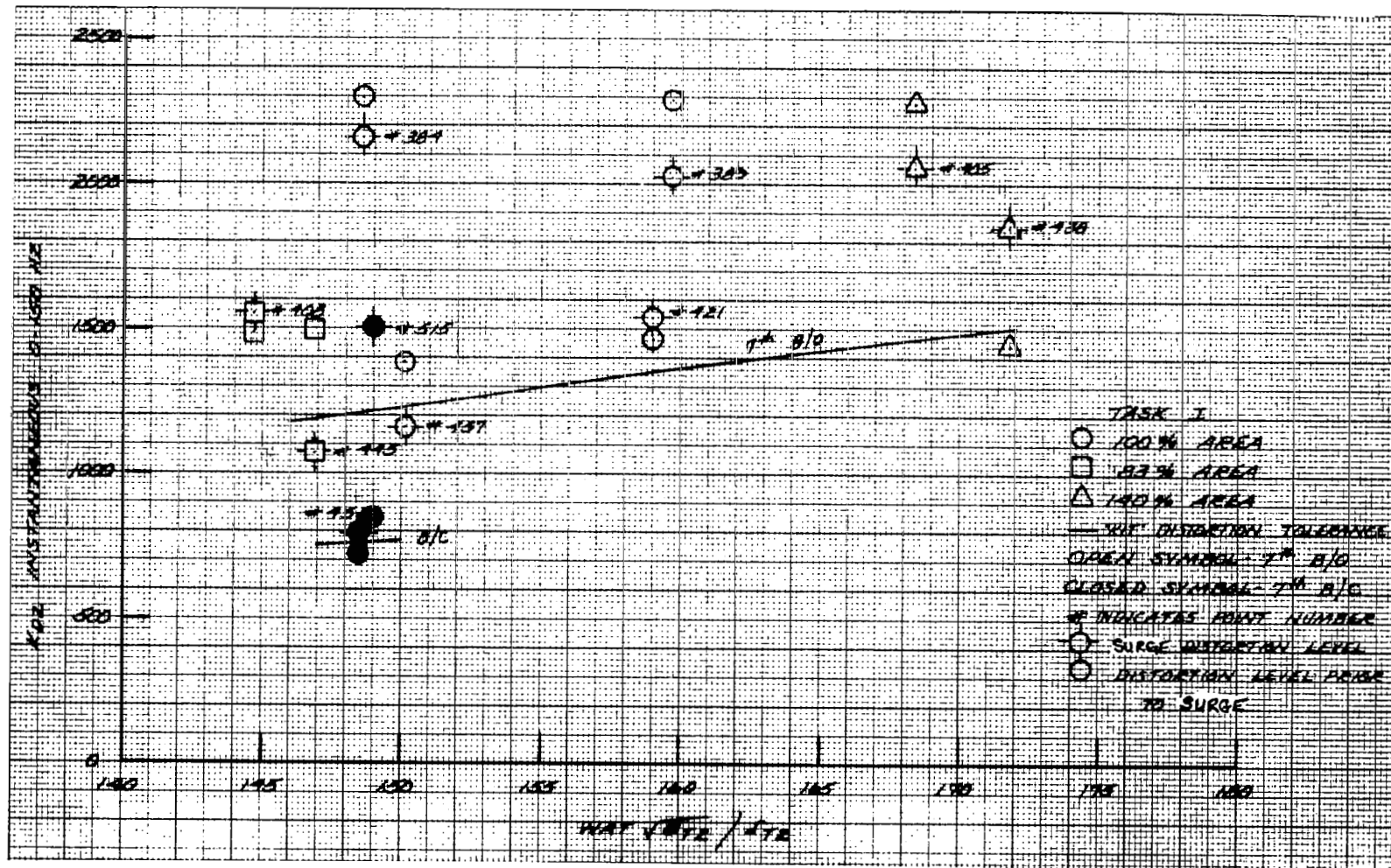
Figure 20. - TF30-P-3 engine distortion tolerance; NASA/Lewis inlet test; K_{D2} instantaneous
analysis; 0-150 Hz.
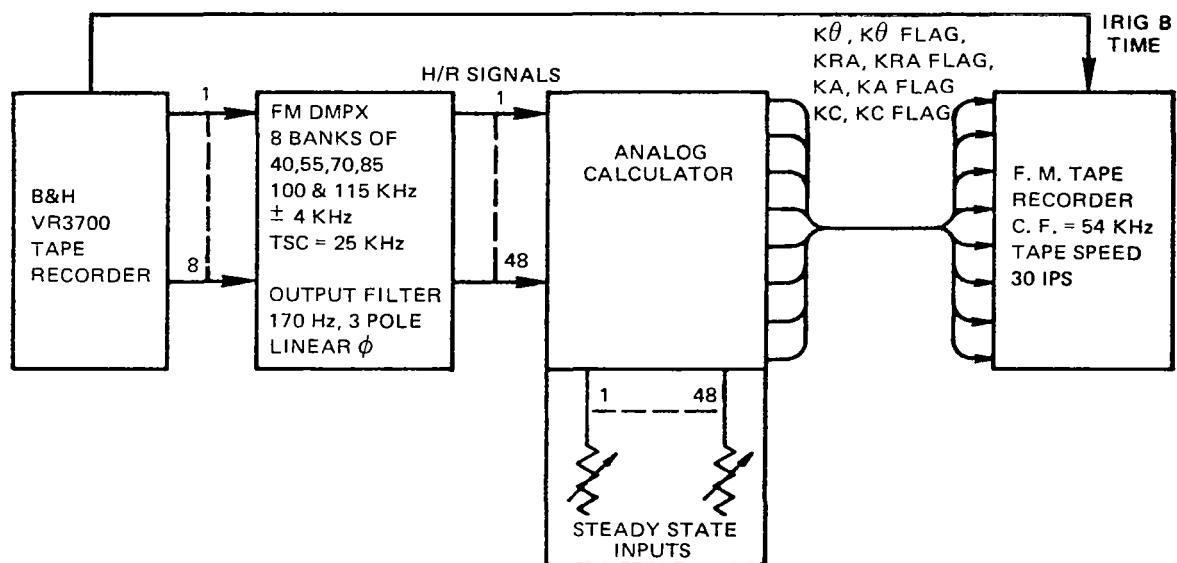
Figure 21. – Screening system; calculator handles eight rakes, six probes per rake, and provides analog distortion indices.
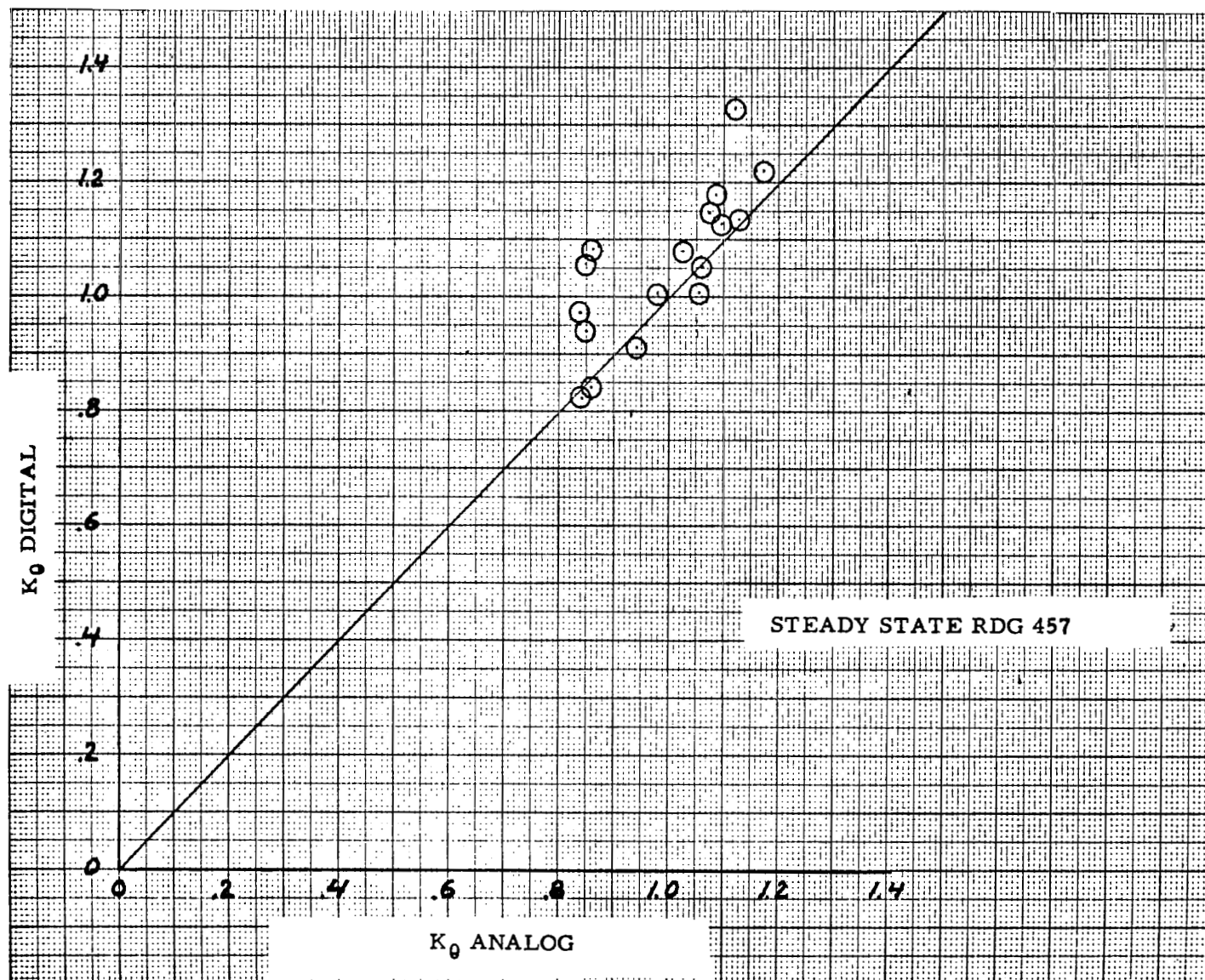
Figure 22. - Comparison of analog to digital distortion calculation.

S.S. RDG #515

PEAK DISTORTION FLAG

KA₂

KO₂

KRA₂

HAMMERSHOCK

KC₂

MAX. DISTORTION
INDICATOR OUTPUT
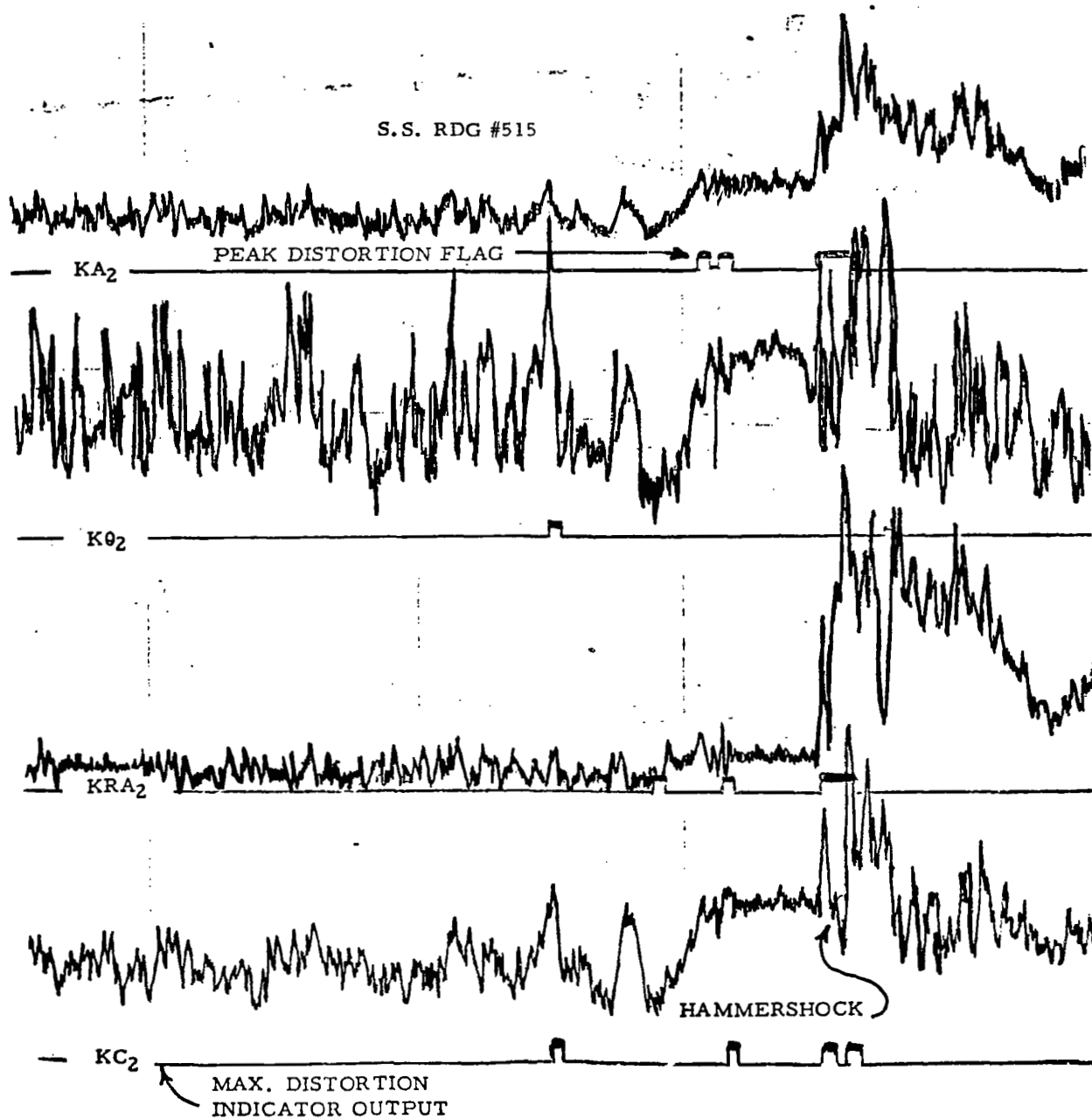
Figure 23. – Sample analog trace.

58
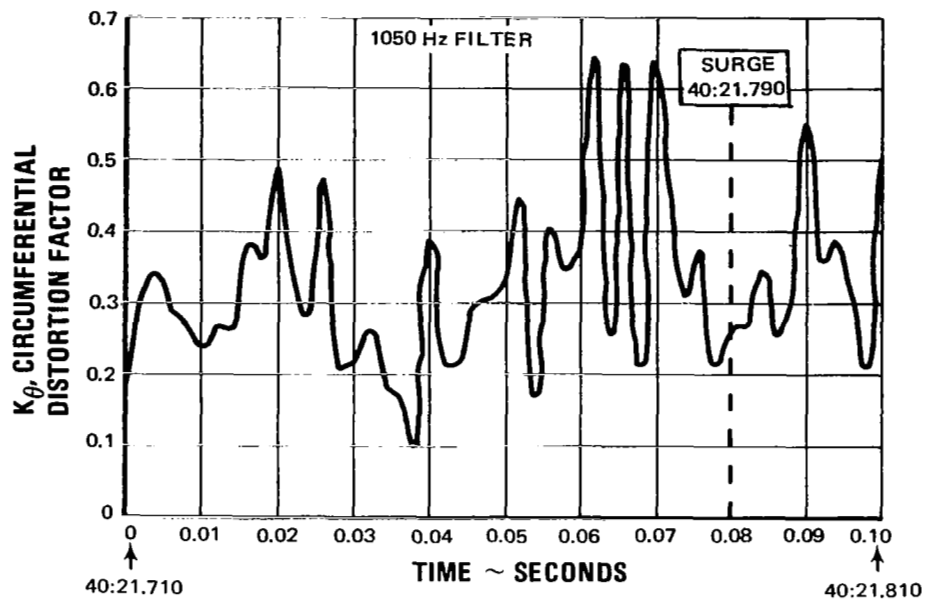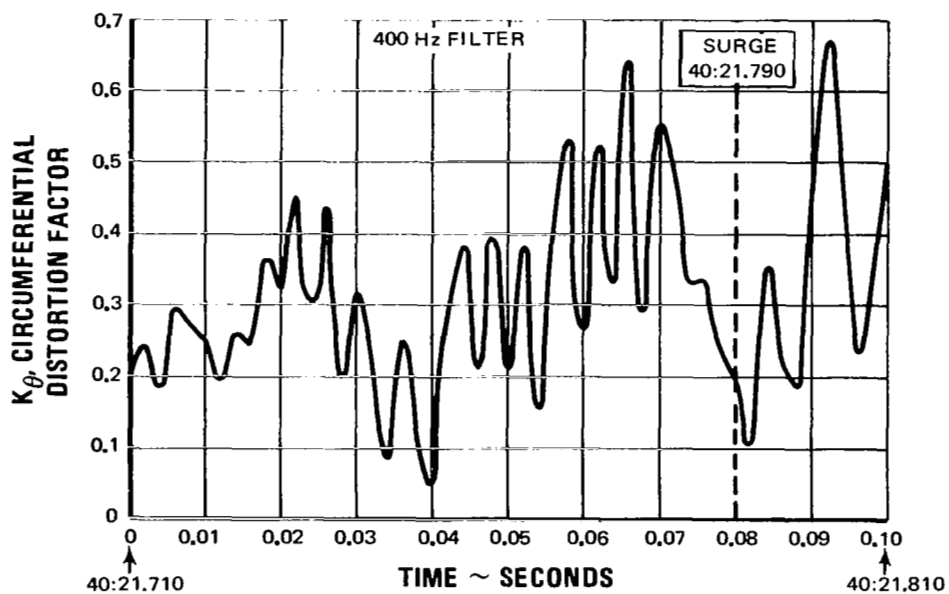
Figure 24. – Instantaneous distortion index, record
1209, at surge; trends observed comparing peak
distortion data.
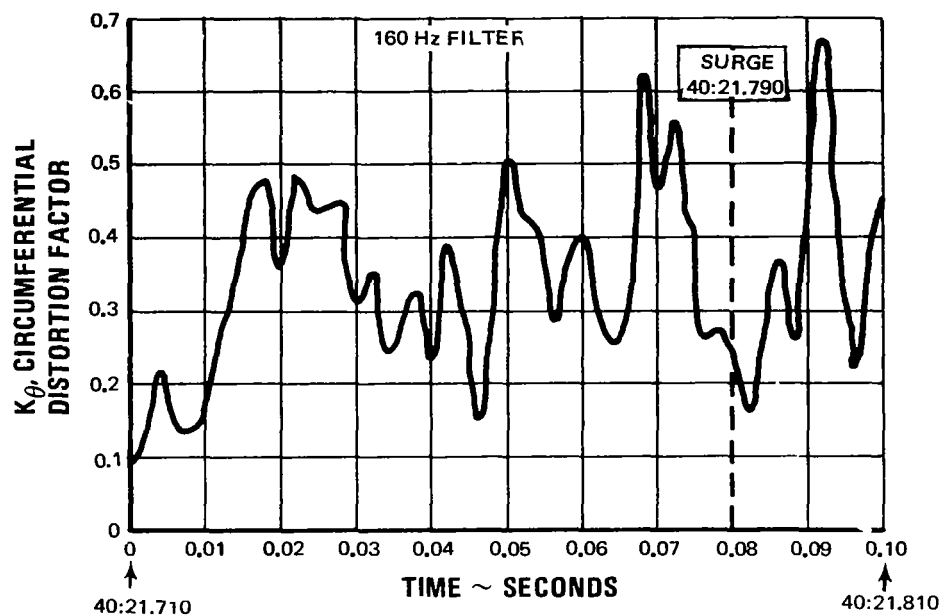
(c)
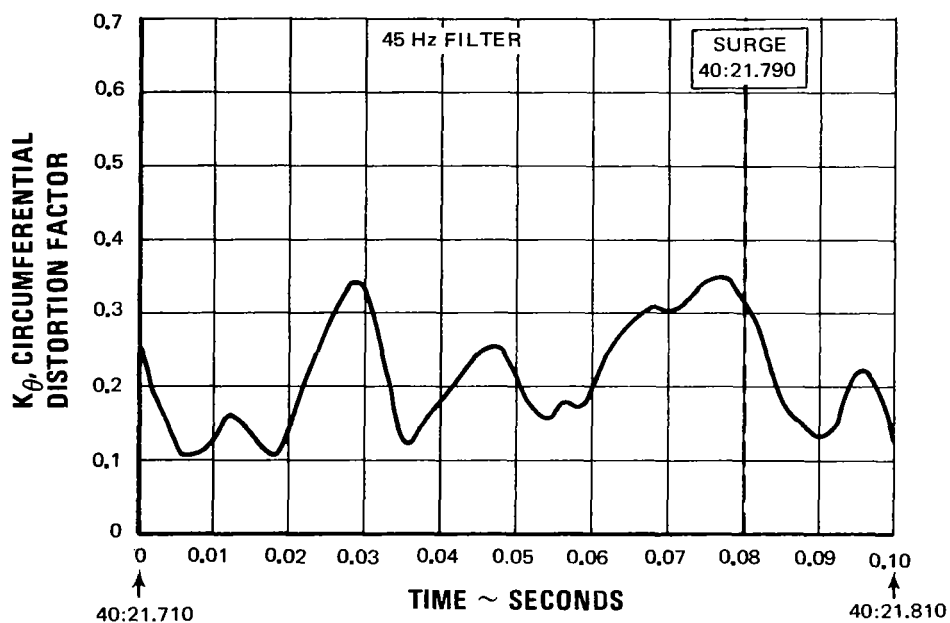
(d)

Figure 24. – Concluded.
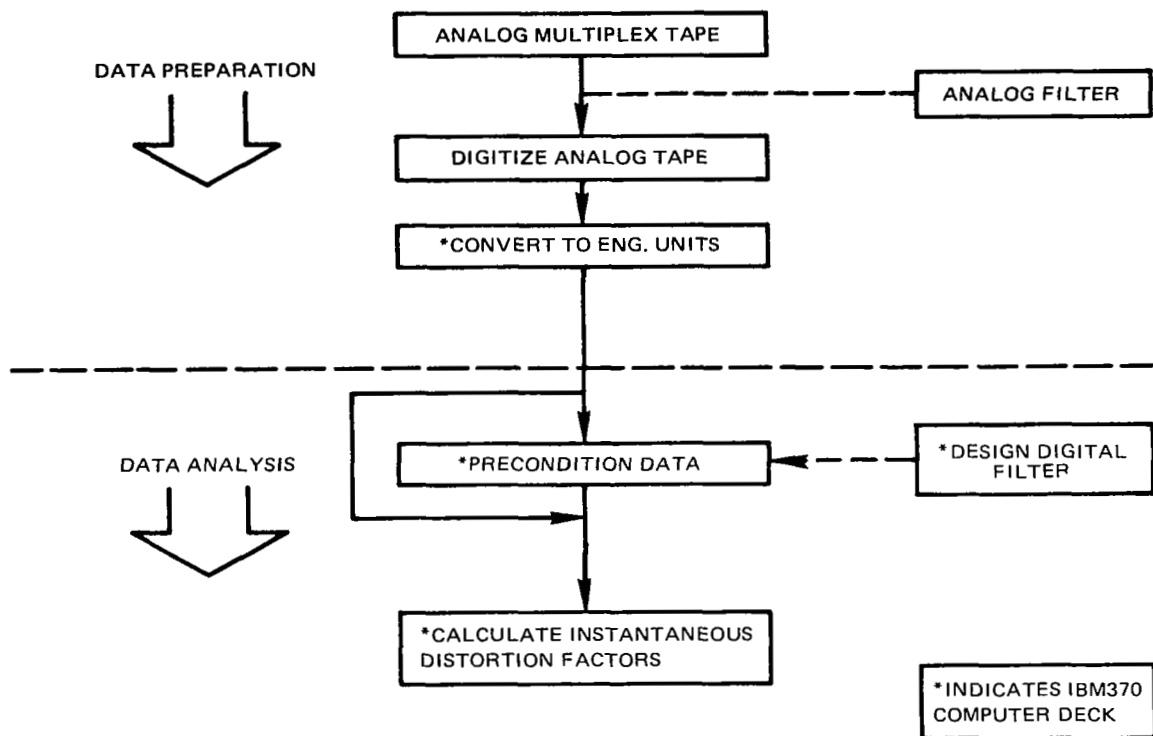
Figure 25. – Pratt and Whitney aircraft data reduction system; instantaneous distortion indices are end result of 2-part flow system.

61
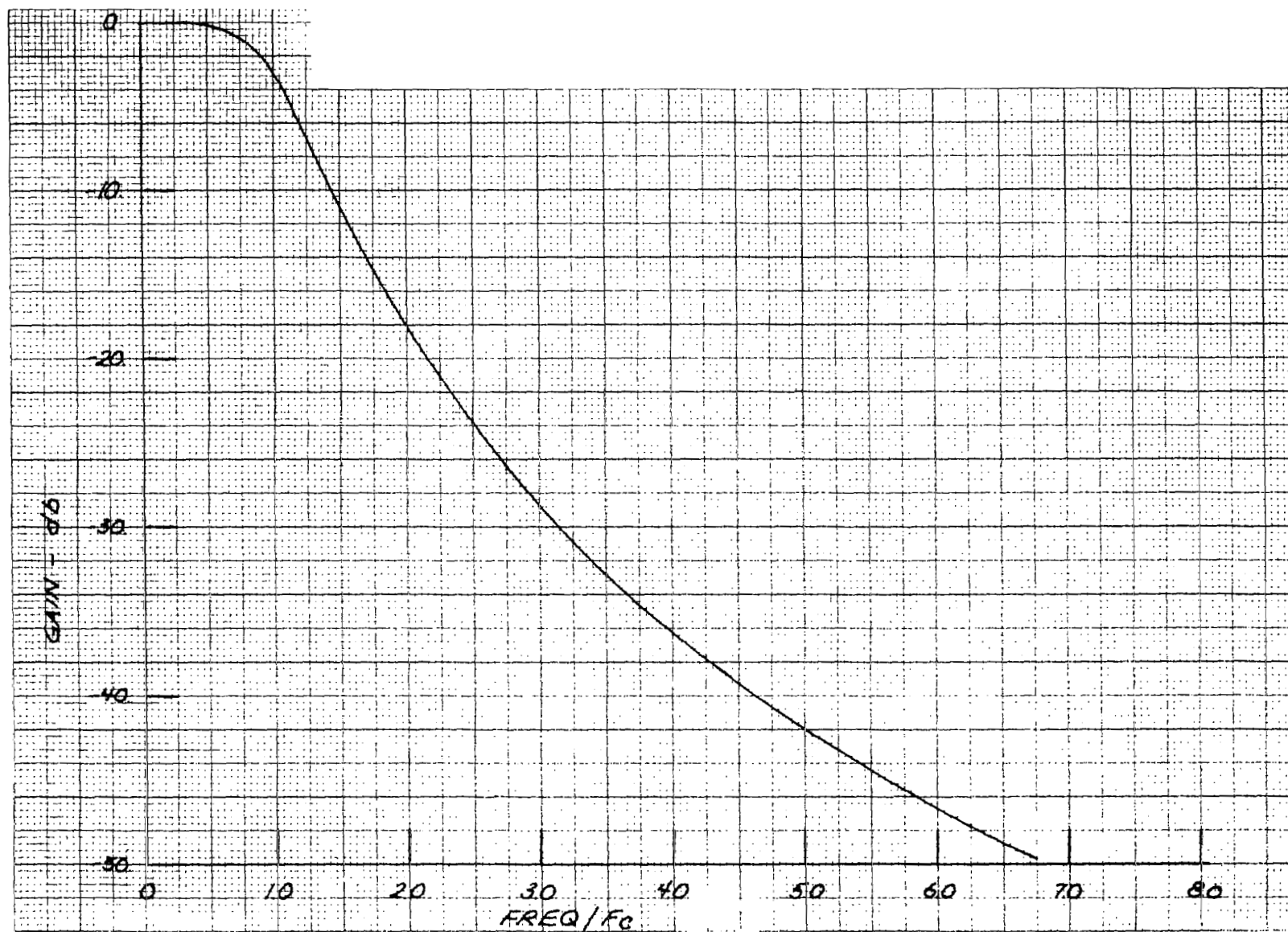
Figure 26. - Phaseless filter design; non-dimensional form.
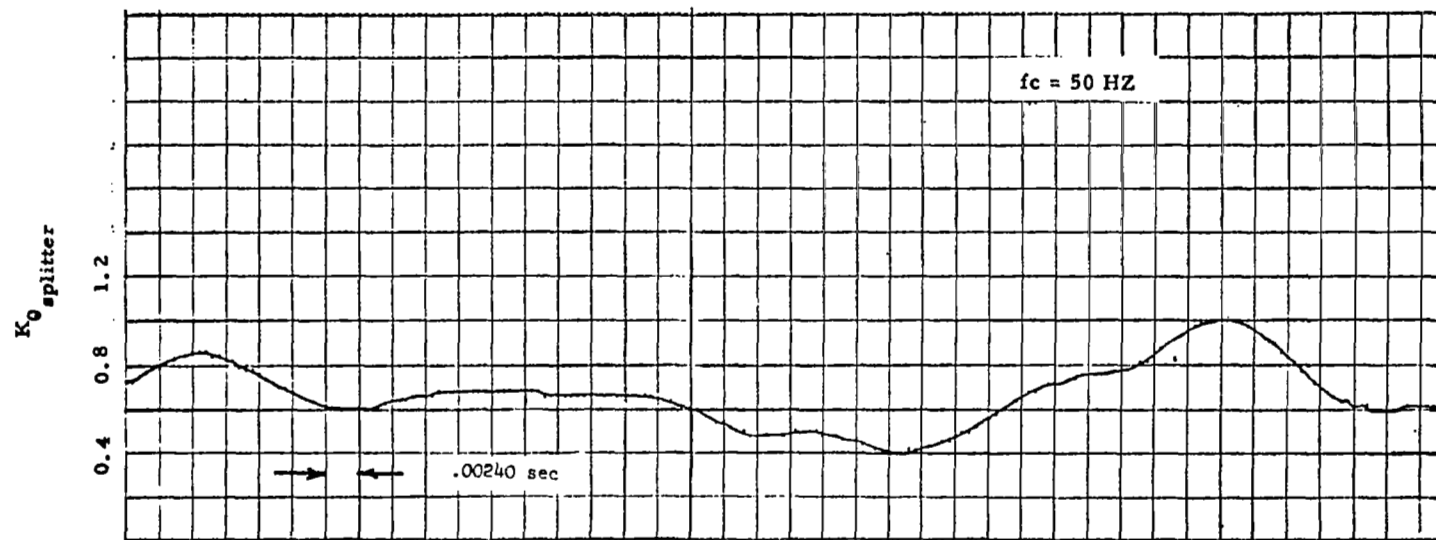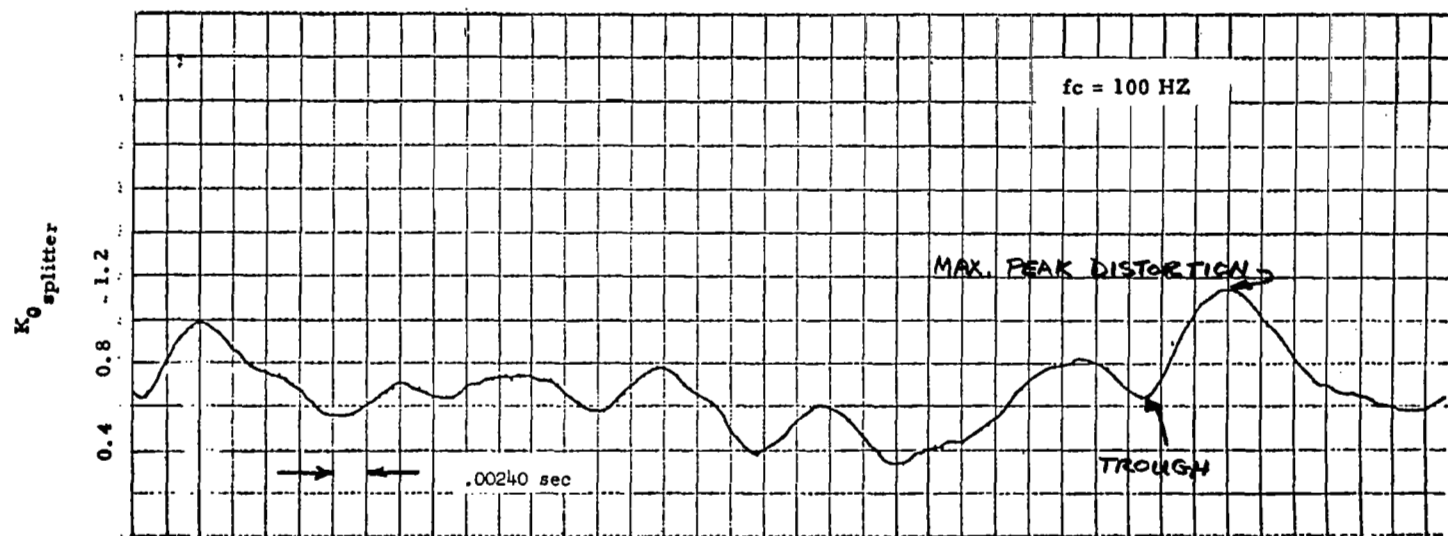
Figure 27. - Effect of filter cut-off frequency on distortion factor.
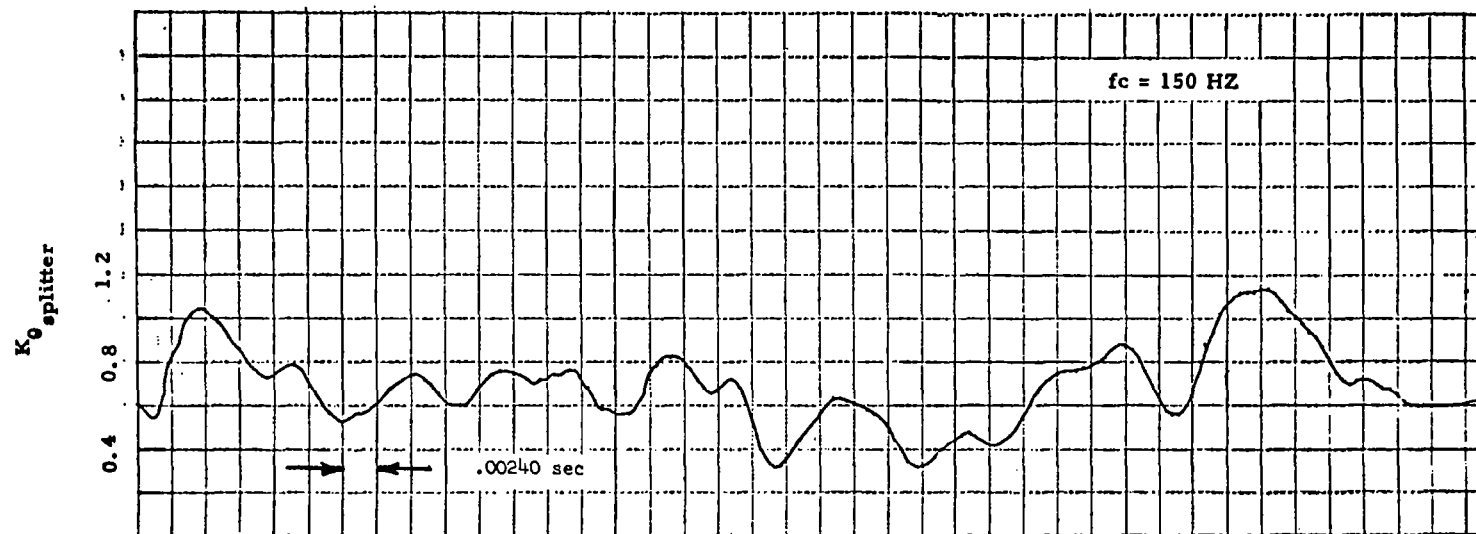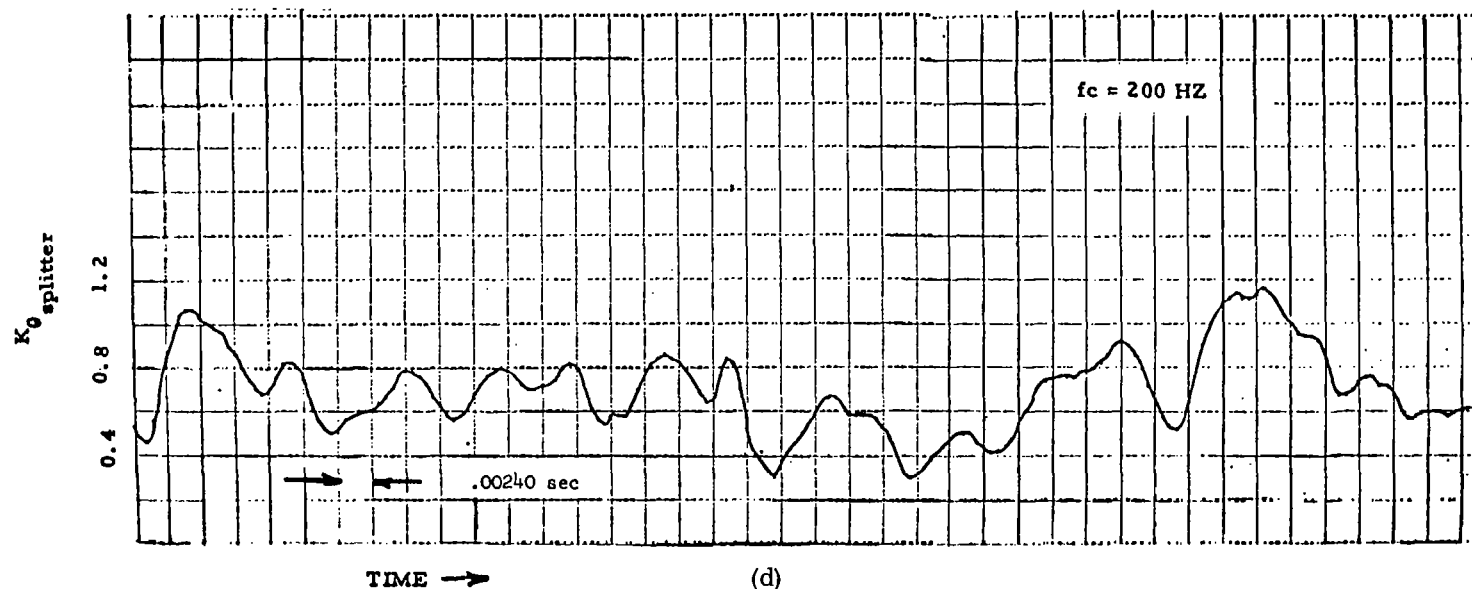
Figure 27. - Concluded.
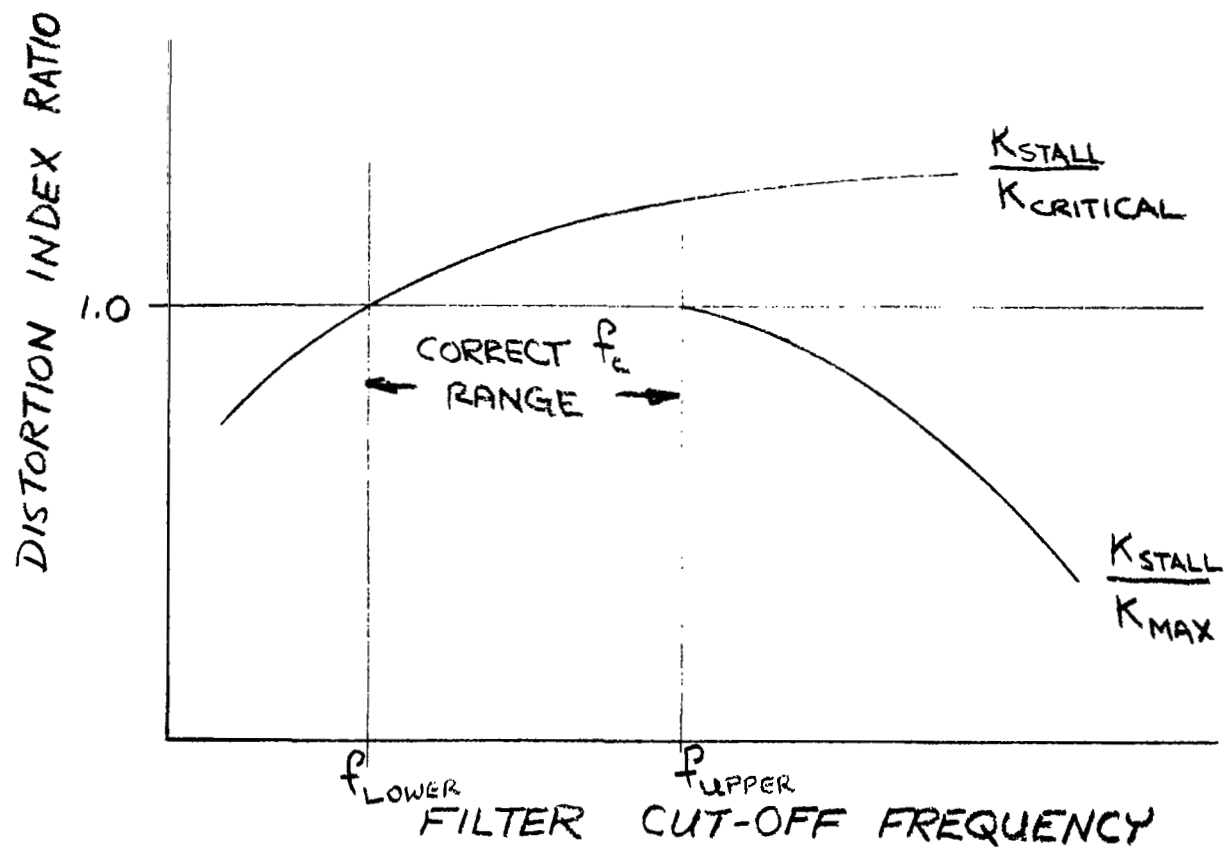
Figure 28. – Approach to analysis of reduced data.
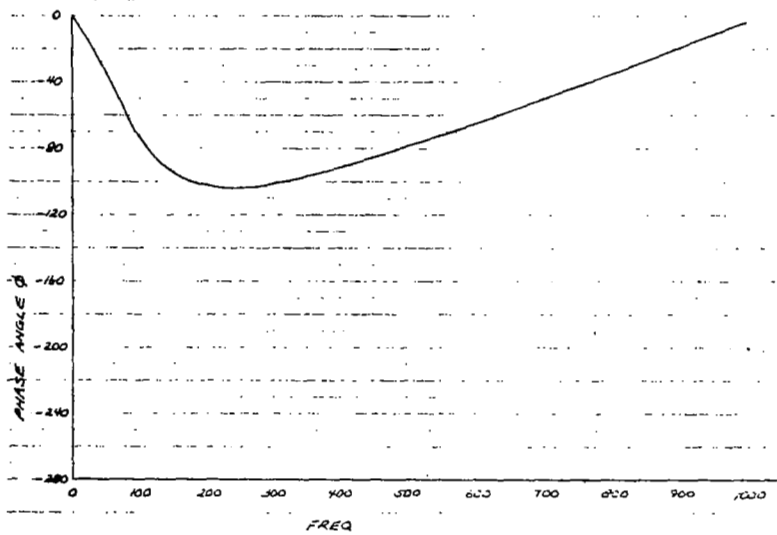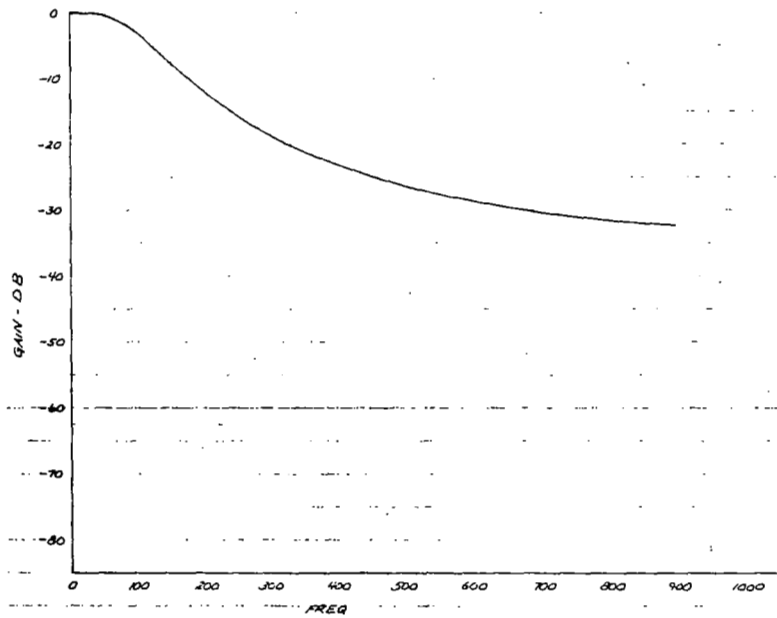
Figure 29. – Sine Butterworth filter; 2 pole.
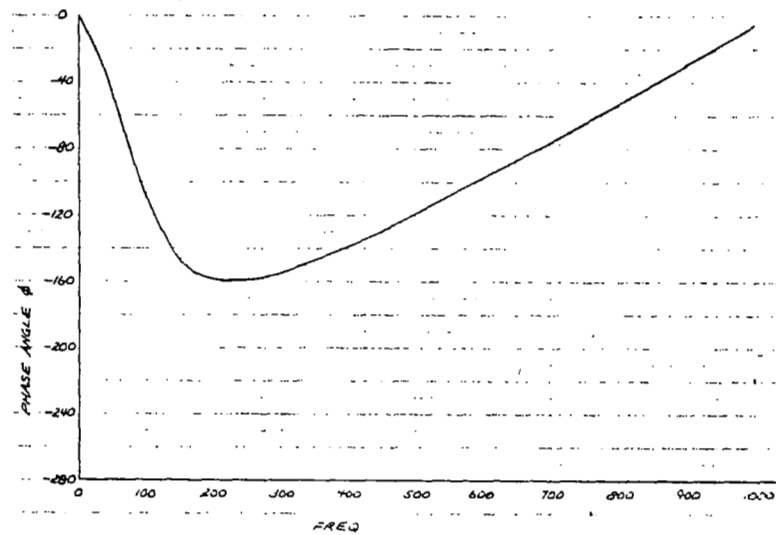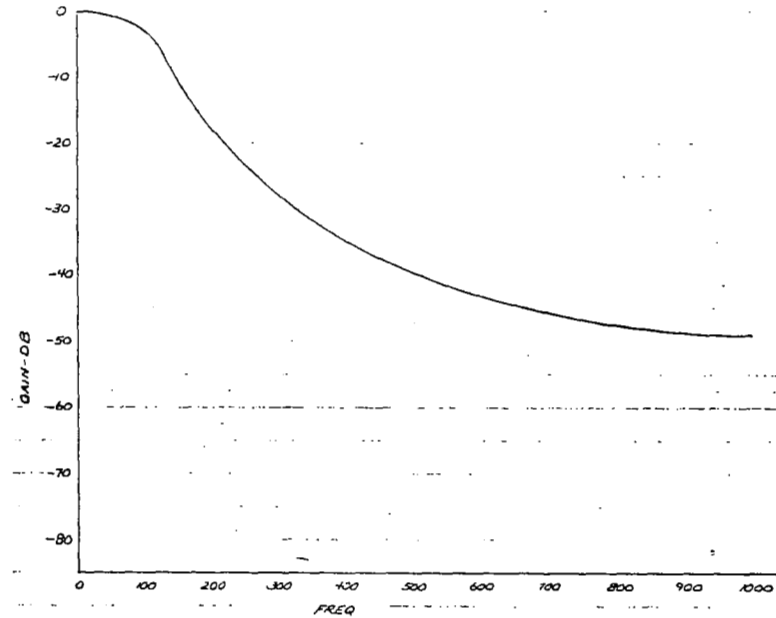
Figure 30. – Sine Butterworth filter; 3 pole.
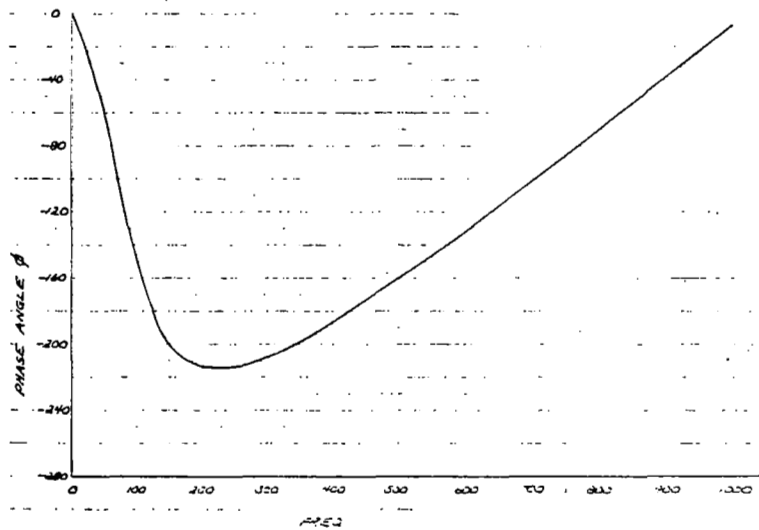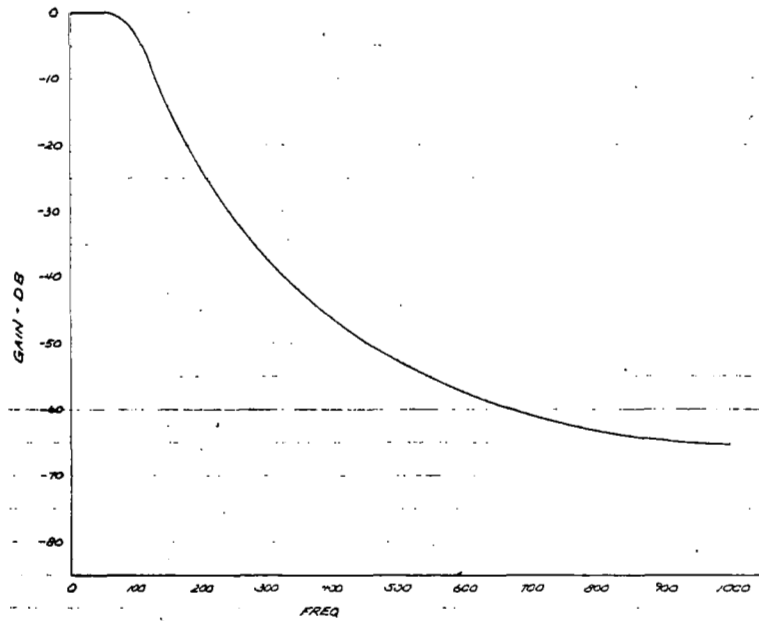
Figure 31. - Sine Butterworth filter; 4 pole.
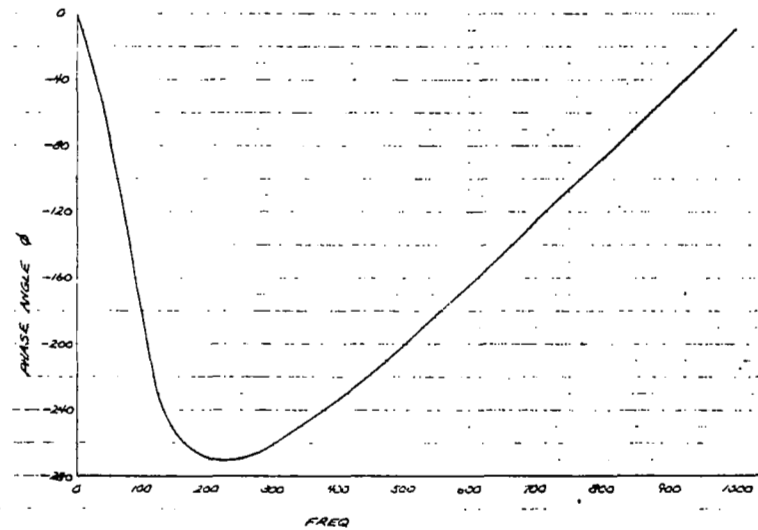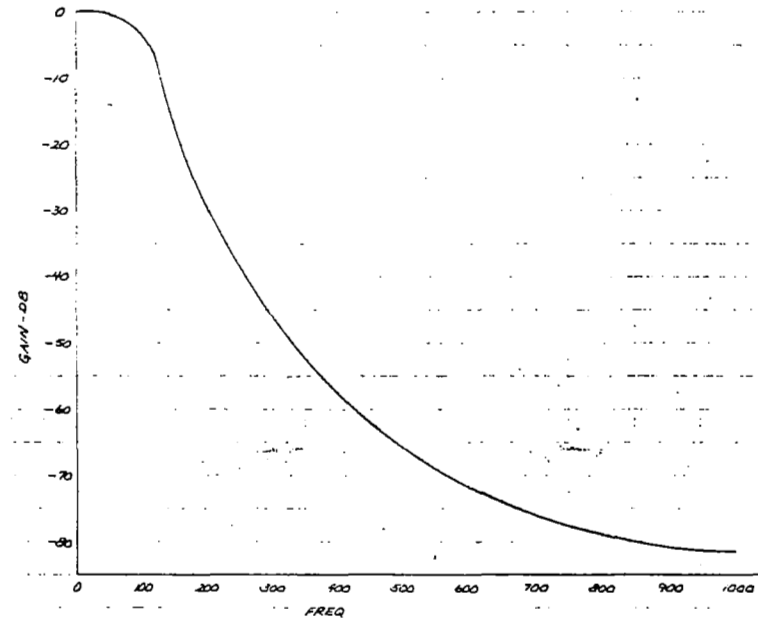
Figure 32. - Sine Butterworth filter; 5 pole.
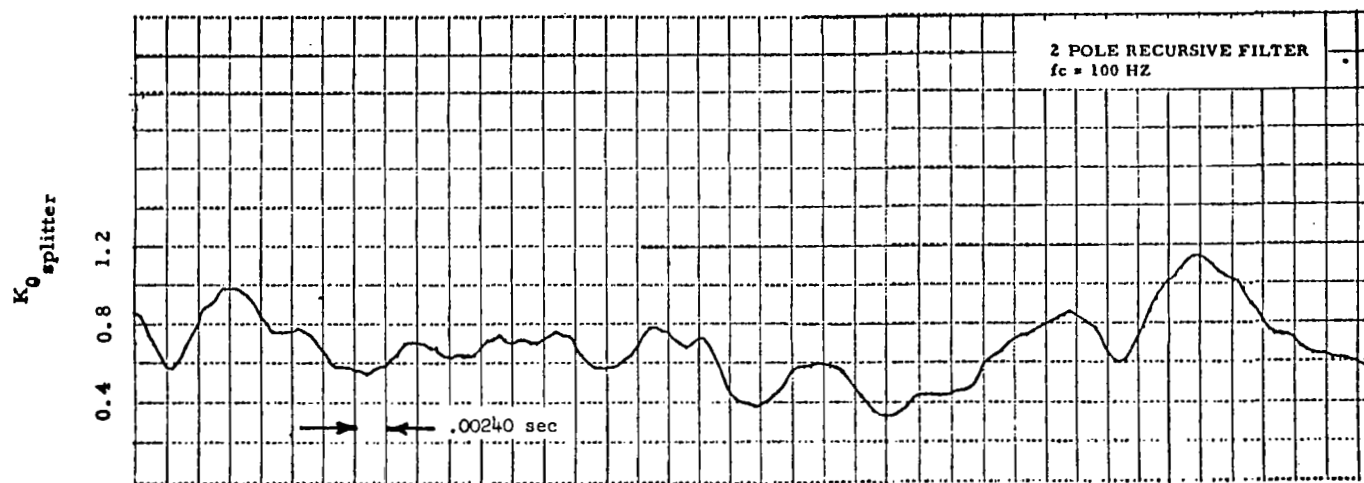
(a)
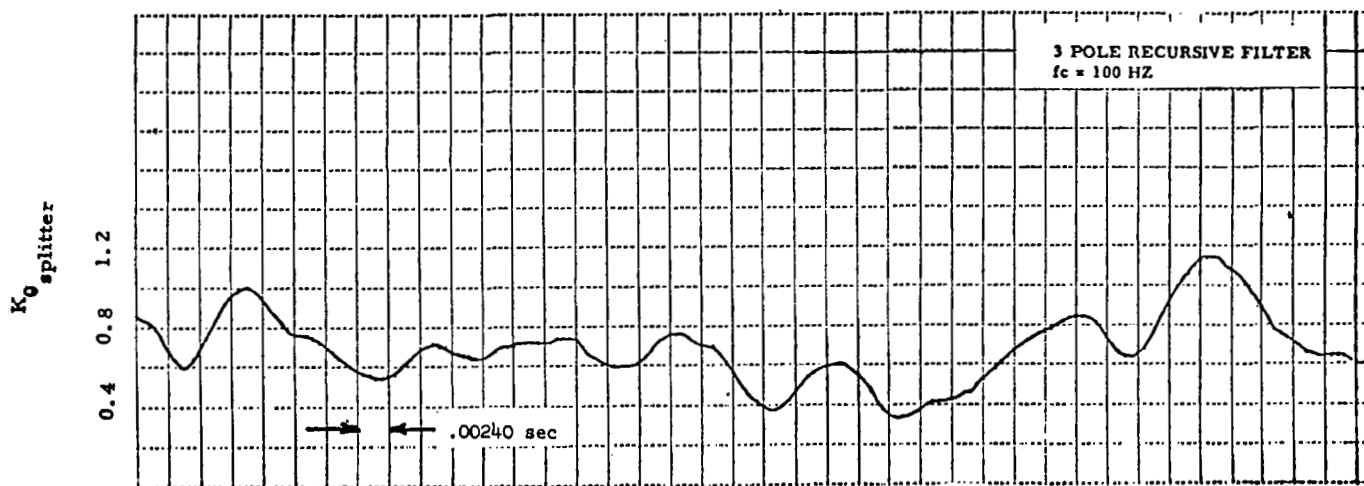
(b)

Figure 33. - Effect of roll-off rate and phase shift on distortion factors.

(c)

(d)

TIME ⟶
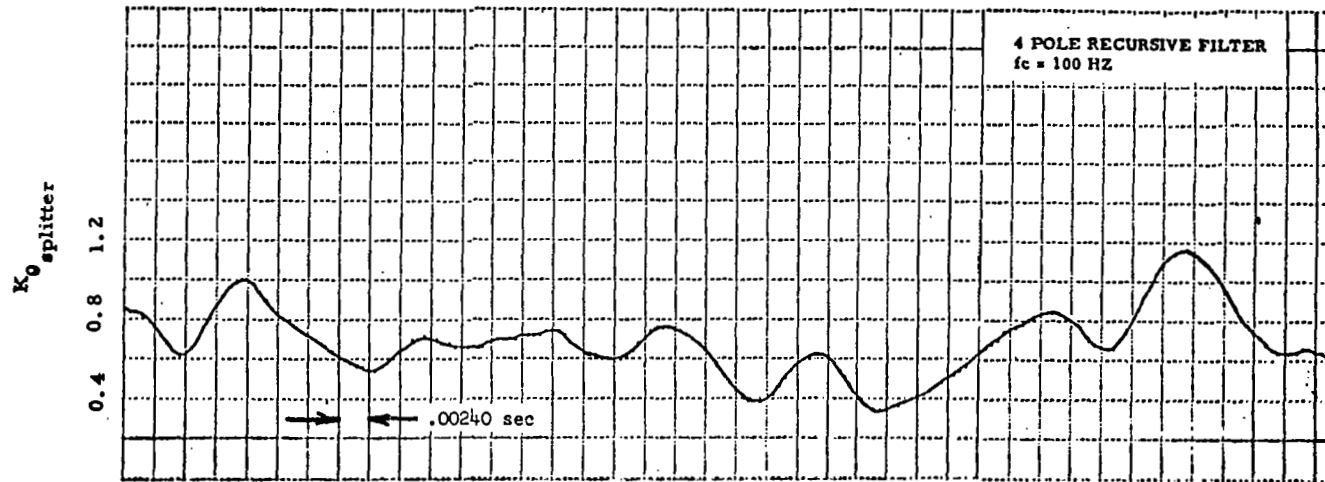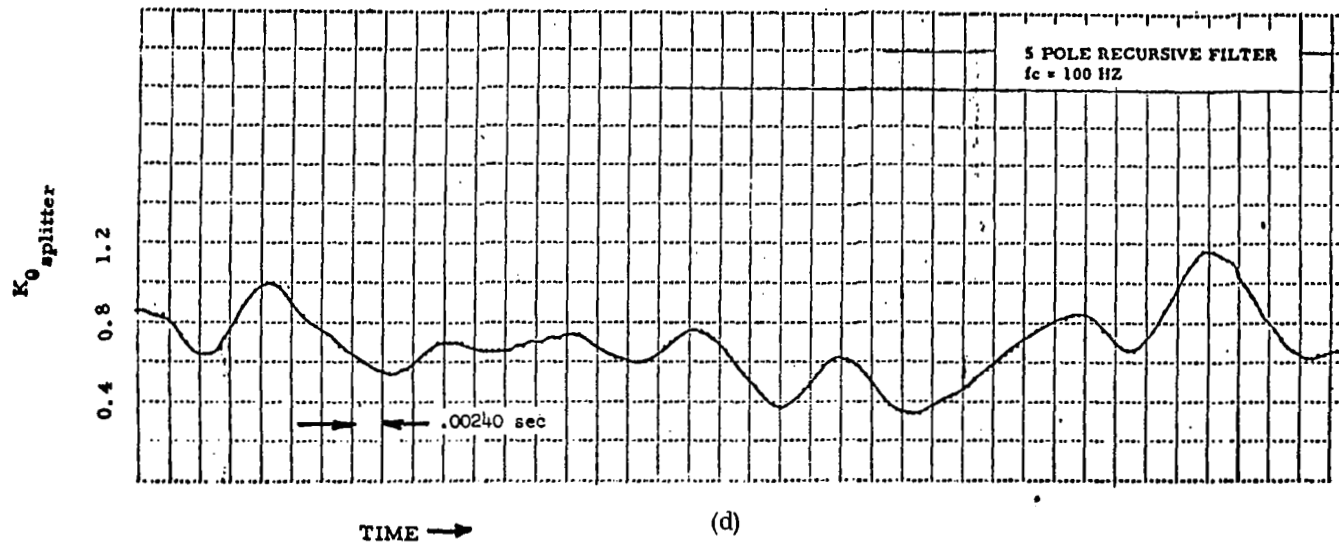
Figure 33. - Concluded.
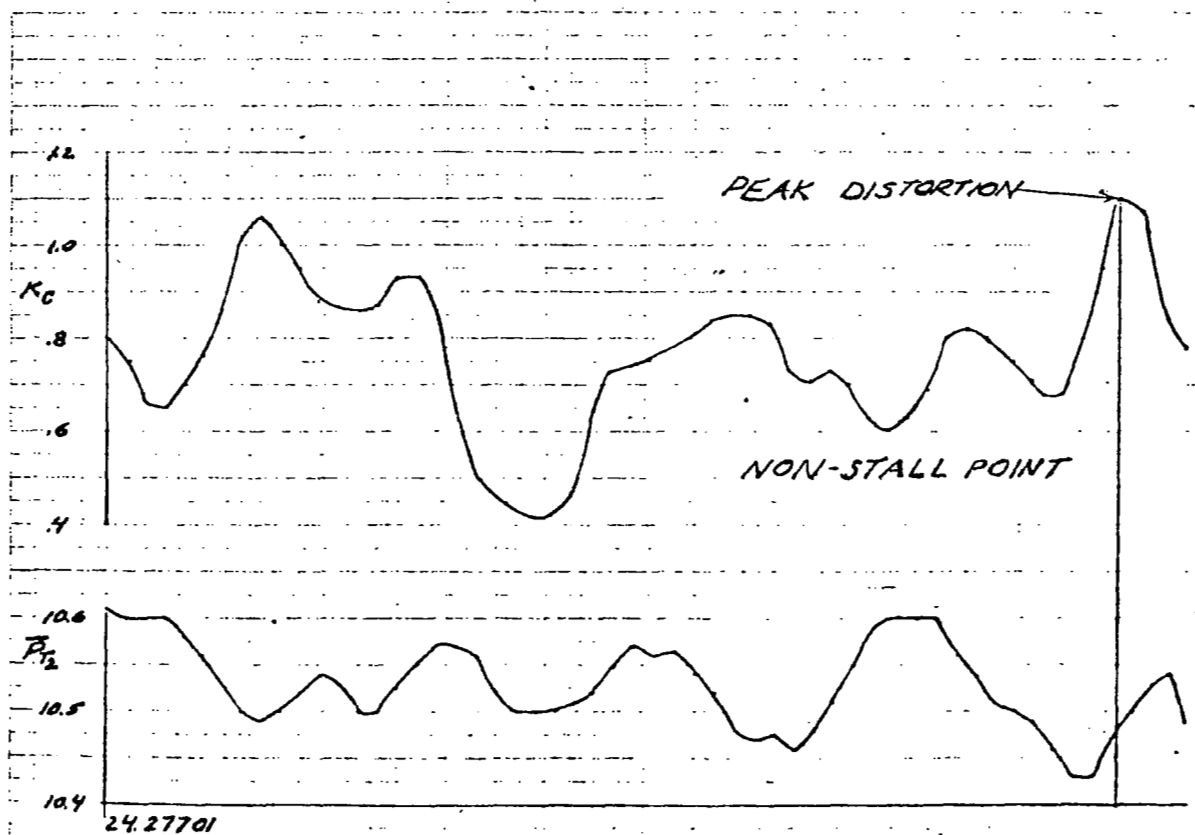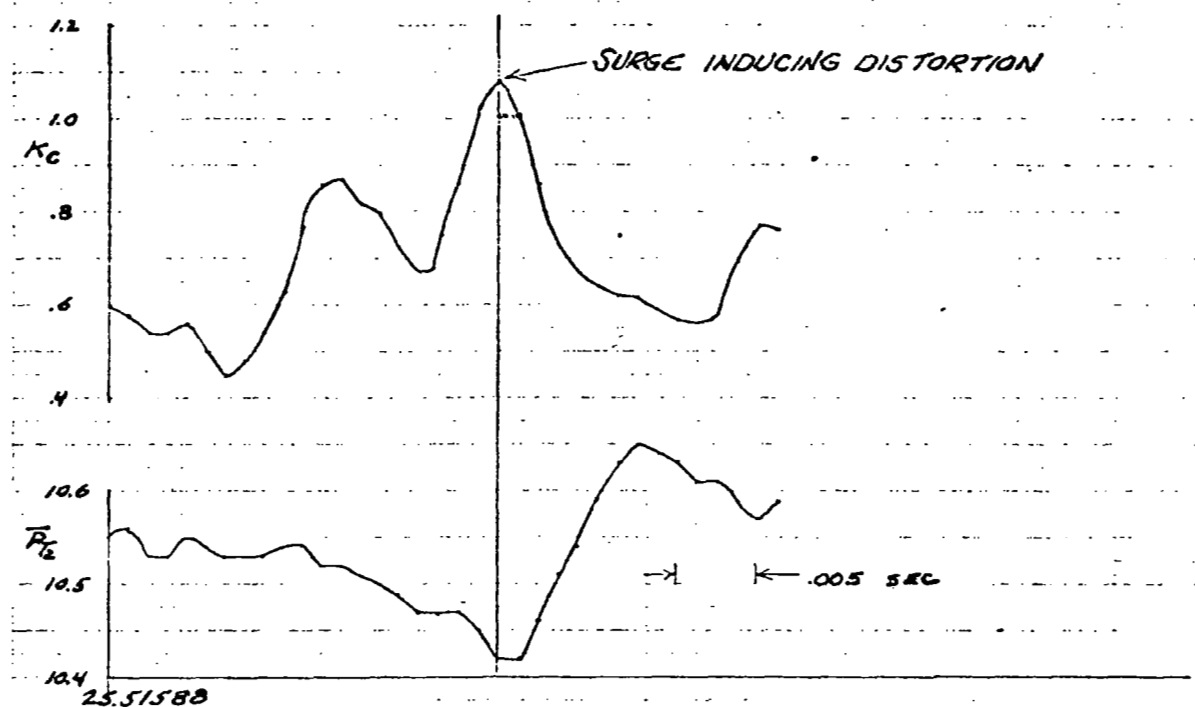
Figure 34. – Comparison of surge inducing distortion with peak distortion;
RDG #438, f_c = 100 Hz.

70
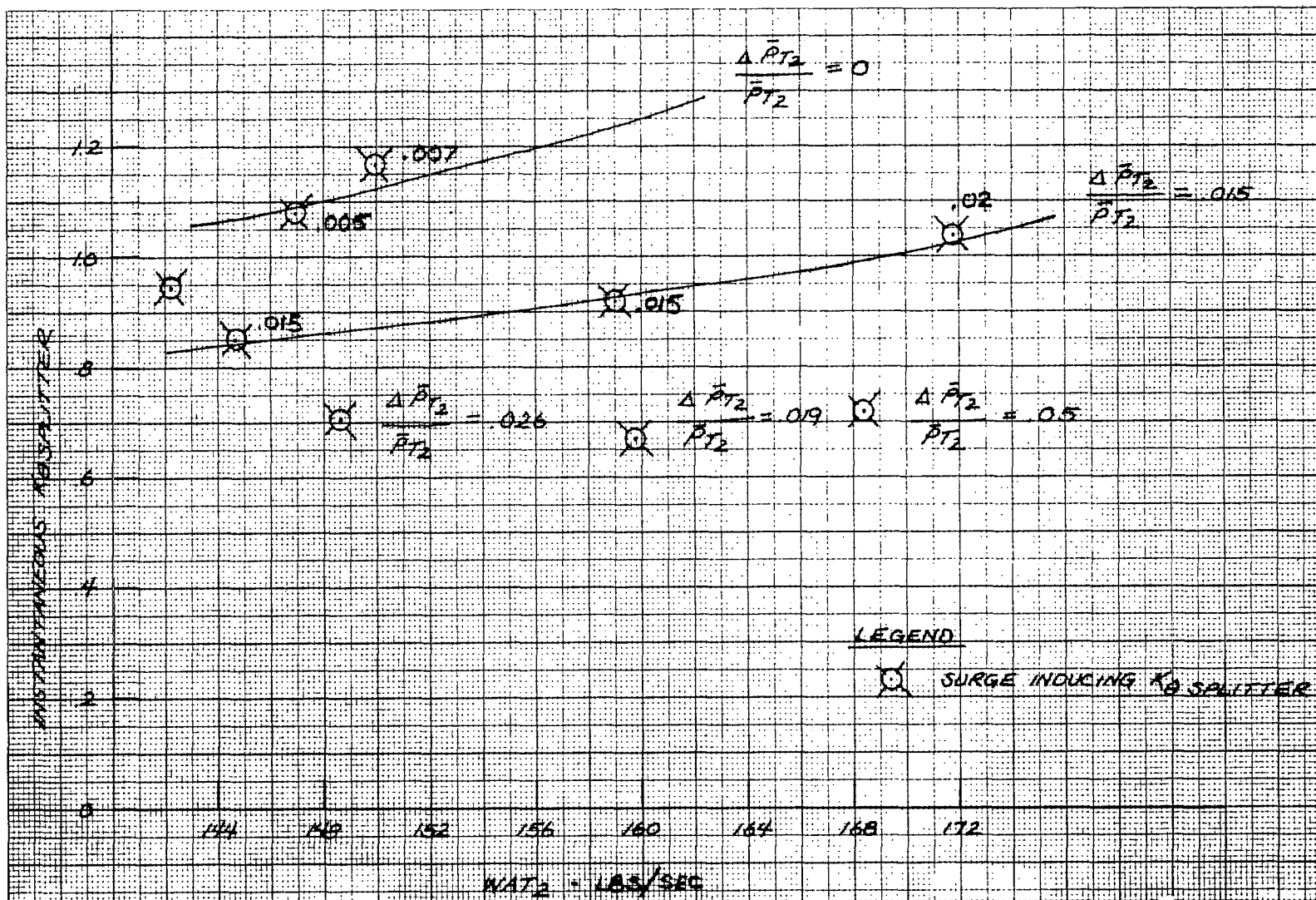
Figure 35. - Surge inducing levels of distortion.
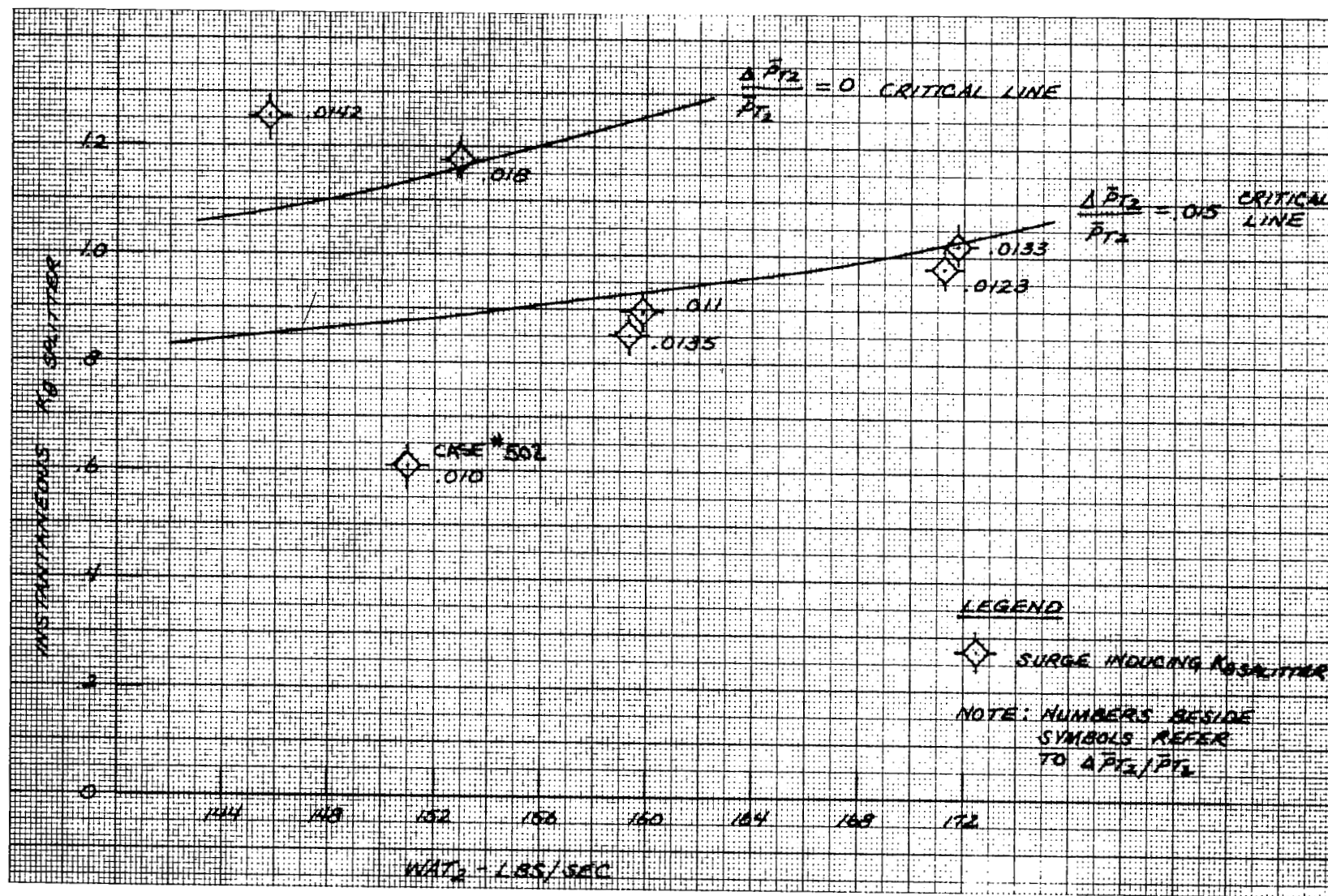
Figure 36. - Verification of critical distortion levels.
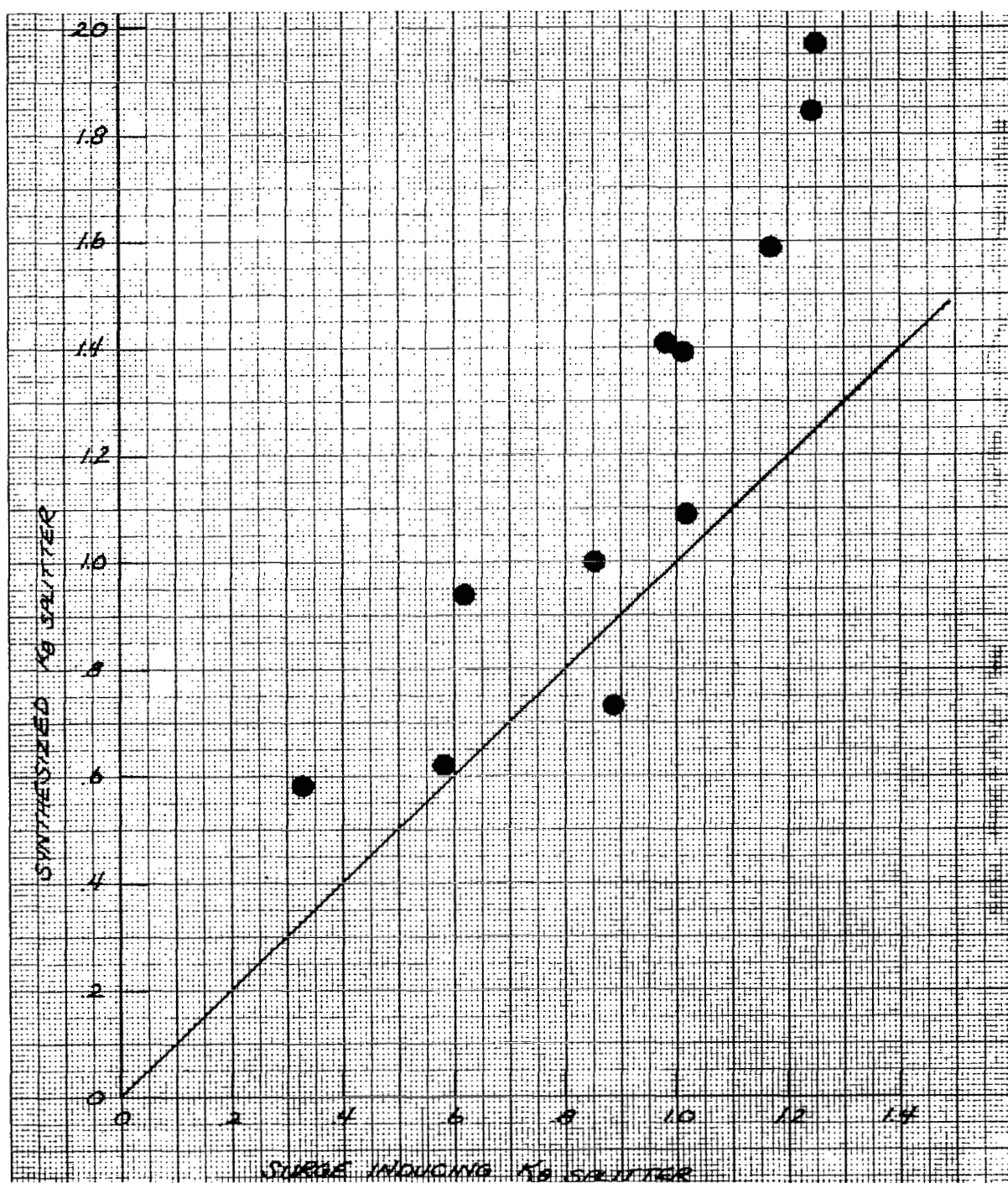
Figure 37. – Comparison of synthesized distortion to observed distortion; 1st asymptote method.
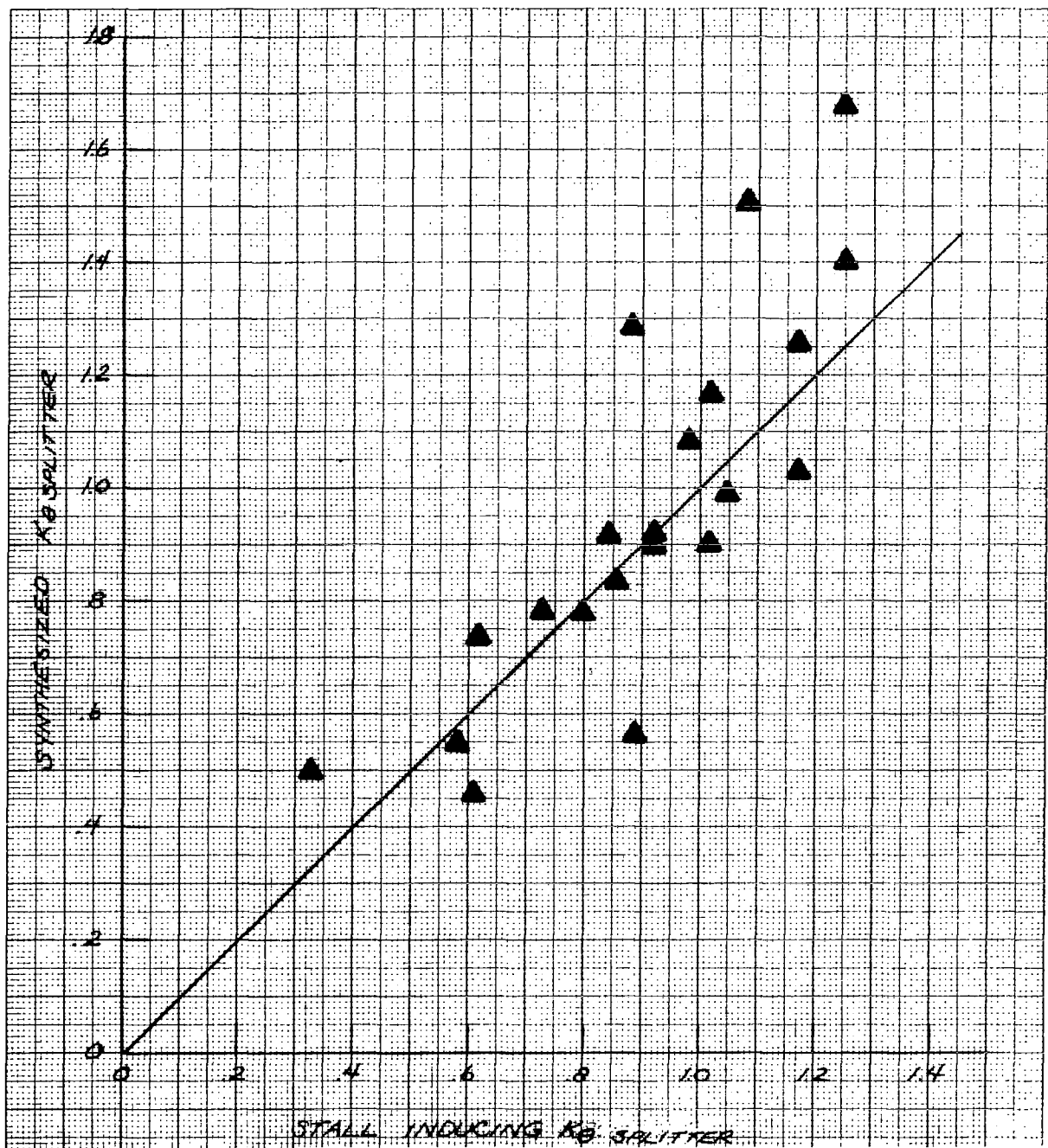
Figure 38. - Comparison of synthesized distortion to observed distortion; refined synthesis method.

APPENDIX A

Definition of Distortion Factors

The equations used to define the distortion factors are presented below.

K_θ

$$K_\theta = \frac{\sum_{ring=1}^{J} \left[\left(\frac{A_n}{N^2} \right)_{max} \right]_{ring} \frac{W_{ring}}{D_{ring}}}{q / \overline{P}_T \sum_{ring=1}^{J} \frac{W_{ring}}{D_{ring}}} \qquad (A-1)$$

where

J = number of total rings which is equal to number of probes per rake

D = diameter of the ring or radial probe

W = ring area weighting factor

$\overline{P}_T$ = face average total pressure

$q / \overline{P}_T$ = dynamic head/average total pressure

To define the term $\left(\frac{A_n}{N^2} \right)_{max}$, a more detailed explanation is required. In general, the circumferential distribution of total pressure at a given radius can be represented by a Fourier series. A particularly useful form of such an expression is:

$$\frac{P_T}{\overline{P}_T} = \frac{a_o}{2} + \sum_{n=1}^{\infty} (a_n \cos n\theta + b_n \sin n\theta)$$

where

$$a_n = \frac{1}{\pi} \int_{-\pi}^{\pi} \frac{P_T}{\overline{P}_T} (\theta) \cos n\theta \, d\theta$$

75

$$b_n = \frac{1}{\pi} \int_{-\pi}^{\pi} \frac{P_T}{\overline{P}_T}(\theta) \ \sin n\theta \ d\theta$$

If we define $A_n = \sqrt{a_n^2 + b_n^2}$ then the series can be written as:

$$\frac{P_T}{\overline{P}_T} = \frac{A_o}{2} + \sum_{n=1}^{\infty} A_n \sin(n\theta + \phi_n)$$

Thus defining $\left(\dfrac{A_n}{N^2}\right)_{max}$ as being the largest value of this expression for the sine series representation of the data. The procedure for calculation of the Fourier coefficients that was used on this contract is presented in Appendix C.

$\underline{K_{RA2}}$

$$K_{RA2} = \frac{\displaystyle\sum_{ring=1}^{J} \left[1 - \frac{P_{TRA}}{\overline{P}_T}\right]_{ring} \frac{1}{D_{ring}}}{q/\overline{P}_T \displaystyle\sum_{ring=1}^{J} \frac{1}{D_{ring}}} \qquad (A-2)$$

where: P_{TRA} = ring average total pressure and $\left[1 - \dfrac{P_{TRA}}{\overline{P}_T}\right]$ is set

   equal to zero when the ring average pressure is larger
   than the face average.

$\underline{K_{A2}}$

$$K_{A2} = K_\theta + K_{RA2} \qquad (A-3)$$

K_θ splitter

K_θ splitter is the value for K_θ obtained by using the diameter of the splitter as the outer diameter of the inlet. The area weighting factors are altered to reflect this change and then the K_θ is calculated using the conventional equation.

K_{C2}

$$K_{C2} = K_\theta \text{ splitter} \times \frac{180}{\bar{\theta}_{avg}} \qquad (A-4)$$

where

$\bar{\theta}$ = the greatest angular extent per ring where $P_T/P_{TRA} < 1.0$. If there are two regions of low P_T/P_{TRA} separated by $25°$ or less, they are to be treated as one low pressure region.

$\bar{\theta}_{avg}$ = the average of $\bar{\theta}$ for rings occurring within the splitter flow radius. The lower limit of $\bar{\theta}$ is to be $90°$.

K_{D2}

$$K_{D2} = \frac{\displaystyle\sum_{ring = 1}^{J} \left(\frac{\Delta P_T}{P_{TRA}} \times \bar{\theta}\right)_{ring} \frac{1}{D_{ring}}}{\displaystyle\sum_{ring = 1}^{J} \frac{1}{D_{ring}}} \qquad (A-5)$$

where

ΔP_T = difference between P_{TRA} and minimum probe total pressure reading.

$\bar{\theta}$ = the greatest angular extent per ring where P_T/P_{TRA} 1.0. Magnitude of $\bar{0}$ is defined from largest product of $\frac{P_T}{P_{TRA}} \times \bar{\theta}$

APPENDIX B

Digital Filter Design

Time variant data often requires filtering to aid in its interpretation. In the case of analog data, filtering is achieved by putting the raw data signal through an electrical circuit that modifies the signal in a prescribed manner. Such hardware can be designed to modify the frequency content of the raw data in a great variety of combinations; such as lowpass, highpass, bandpass, and band reject type filters. If the data is in digital form, filtering must be obtained through the use of digital arithmetic rather than electrical hardware. The simplest of such digital filters is a straight arithmetic average of the data. By varying the weighting coefficients and the arithmetic application techniques, an equivalent digital filter can be found for every type of electrical filter.

There are two basic types of digital filters; non-recursive filters and recursive filters. The arithmetic averaging process is a member of the non-recursive filter family. Non-recursive filters are essentially data averaging techniques that use variable value weighting coefficients. Recursive filters make use of their own previous output, as well as the raw data, to generate filtered data. In other words, recursive filters make use of the process of feedback in altering data.

Design of Phaseless Filters

Determination of the effect of filter cut-off frequency on the analysis of distortion data was conducted with the use of phaseless digital filters. Such characteristics are obtained through the use of symmetric non-recursive digital filters. The equation used to implement such filters is:

$$Y_n = h_o \overline{X}_n + \sum_{k=1}^{M} h_k \left(X_{n-k} + \overline{X}_{n+k} \right) \tag{B-1}$$

where

Y_n = filter output for time t

X_n = input data for time t

X_{n+k} = input data for time $t + k\Delta t$

h_k = filter weighting coefficient

Δt = time interval between successive digital data points

$M = \dfrac{N-1}{2}$

N = number of terms averaged

78

Gain-frequency characteristics of the filter are defined by the set of weighting coefficients, h_k. As demonstrated by Anders, et al (Reference 8), the values of h_k required to simulate a specific filter design are equal to the coefficients of the Fourier series fit of the gain-frequency properties of the filter. Thus, the weighting coefficients are defined by:

$$h_k = \frac{2}{f_s} \int_o^{f_a} H(f) \cos \left(\frac{k \, 2\pi \, f}{f_s} \right) df \qquad (B-2)$$

where

$H(f)$ = function defining the arbitrary gain-frequency relationship

f_s = digitizing frequency (sample/sec.)

$f_a = \dfrac{f_s}{2}$

f = frequency (Hz)

The selection of the number of terms to be averaged is dependent upon the accuracy desired in the simulation of the specified filter characteristics. The gain-frequency characteristics of a digital filter, given by

$$H(f) = h_o + 2 \sum_{k=1}^{M} h_k \cos \left(\frac{k \, 2\pi \, f}{f_s} \right) \qquad (B-3)$$

is compared to the desired filter properties for different values of M. The value of M that results in a gain-frequency curve that is within the desired tolerance is used to define the number of terms averaged. Filters designed for the cut-off frequency study used 35 coefficients to simulate the gain-frequency characteristics presented in Figure 26. Figure B1 presents the resultant properties for a digital filter with a cut-off frequency of 50 Hz.

Design of the Sine-Butterworth Filters

The study of the effect of filter phase shift and roll-off rate on inlet distortion data was conducted through the application of recursive digital filters. A simple type of recursive filter is given by:

$$Y_n = g\overline{X}_n + \sum_{k=1}^{N} h_k Y_{n-k} \qquad (B-4)$$

79

where

g, h_k = weighting coefficients

Y_{n-k} = filtered data output for time $t-k\Delta t$

N = number of values of h_k required to define filter

The filter type used in the study was the sine-Butterworth lowpass digital filter. This particular filter has a gain-frequency curve defined by the following equation:

$$H(f) = \sqrt{\frac{1}{1 + \left(\frac{\sin \pi \Delta t\, f}{\sin \pi \Delta t\, f_c}\right)^{2N}}} \qquad \text{(B-5)}$$

where

f_c = cut-off frequency. N is referred to as the number of poles of the specified filter.

A procedure for the calculation of the weighting factors g and h_k is presented in Reference 9. A brief outline of that procedure follows:

(1) Select values of Δt, f_c, and N to define the desired digital filter.

(2) Calculate for $1 \leq k \leq \frac{N}{2}$

$$b_k = - \sin \pi \Delta t\, f_c \left[\cos \left\{ \pi \left[\frac{1}{2} + \frac{1}{N} \left(k - \frac{1}{2} \right) \right] \right\} \right] \qquad \text{(B-6)}$$

(3) Calculate $C = 1 - \sin^2 \pi \Delta t\, f_c$ \qquad (B-7)

(4) Calculate for $1 \leq k \leq \frac{N}{2}$

$$D_k = \frac{1}{2} \left[-C + \sqrt{C^2 + 4b_k^2} \right] \qquad \text{(B-8)}$$

(5) Calculate for $1 \leq k \leq \frac{N}{2}$

$$E_k = \sqrt{D_k + 1} + \sqrt{D_k} \qquad \text{(B-9)}$$

(6) Calculate for $1 \leq k \leq \frac{N}{2}$

$$h_{k1} = 2 \left(\frac{2b_k^2}{D_k} - 1 \right) \Bigg/ E_k^2 \qquad \text{(B-10)}$$

$$h_{k2} = - E_k^{-4} \qquad \text{(B-11)}$$

(7) Calculate for $1 \leq k \leq N$

$$h_k = \left\{ - \text{coefficients of } Z^{-k} \text{ in } \prod_{k=1}^{N/2} \left(1 - h_{k1} Z^{-1} - h_{k2} Z^{-2} \right) \right\} \quad \text{(B-12)}$$

(8) Calculate

$$g = 1 - \sum_{k=1}^{N} h_k \quad \text{(B-13)}$$

The gain-frequency and phase shift properties of the filters designed for the study are presented in Figures 29 to 32.
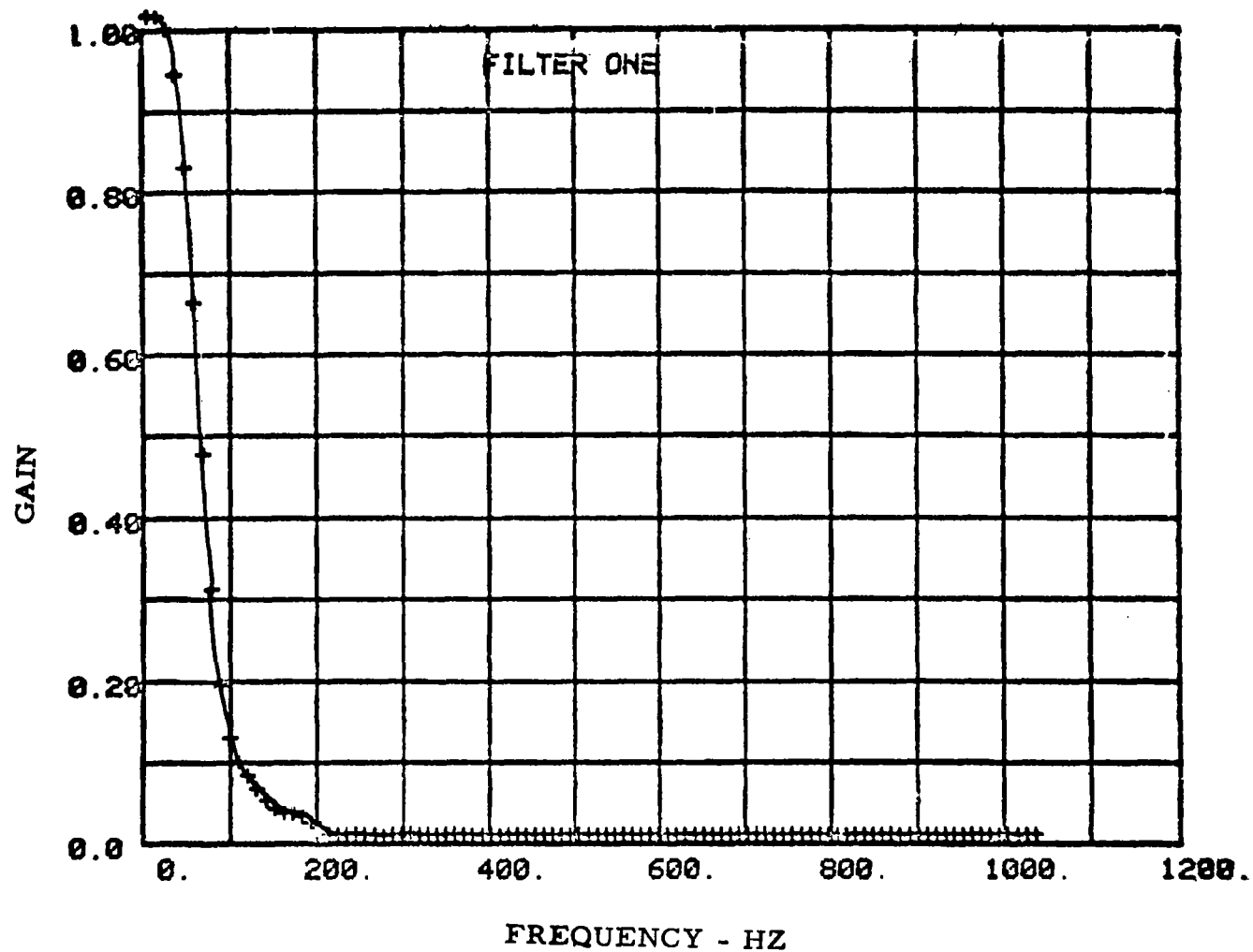
Figure B1. - 50 Hz cutoff frequency filter.

APPENDIX C

Method of Least Squares K_θ Calculation

Current interest in high response inlet distortion testing has led to development of high speed distortion factor calculation techniques. The distortion factor K_θ, described in Appendix A, is easily calculated when rake spacing is equal. However, no general procedure has been available for fast K_θ calculation.

A general procedure of K_θ calculation has been developed for data reduction. The approach taken was to least squares fit a trigometric series to the circumferential total pressure. The resulting coefficients were used as the Fourier coefficients of the data. These values were then used for calculation of K_θ.

This approach does not require special geometric rake conditions to be applicable. The only requirement is that the number of harmonics of the trig. equation be less than or equal to $(N/2 - 1)$; where N is the number of data rakes.

The basic of the least squares approach is the minimization of:

$$S = \sum_{i=1}^{N} (P_i - Q_i)^2 \qquad (C-1)$$

where

P_i = actual pressure values

Q_i = curve fit pressure values

N = number of rakes

The equation used to generate Q_i is a trignometric series and is defined as follows:

$$Q_i = \sum_{j=0}^{M} \alpha_j \, f_{ij} \qquad (C-2)$$

where

M = 2x (number of harmonics)

α_j = the constant coefficients

f_{ij} = 1/2 for j = o

$\quad = \cos j\theta i$ for $1 \leqslant j \leqslant M/2$

$\quad = \sin (j - \dfrac{M}{2}) \, \theta_i$ for $M/2 < j \leqslant M$

To get the minimum value of S, $\partial S/\partial\alpha$ is set equal to zero for all values of $0 \leq j \leq M$. The coefficients, α_j, are then determined from this set of equations. Substituting for Q_i we have:

$$S = \sum_{i=1}^{N} \left[P - \sum_{j=0}^{M} \alpha_j \; f_{ij} \right]^2 \qquad (C-3)$$

The set of simultaneous equations that are used to calculate the curve fit coefficients are defined by:

$$\frac{\partial S}{\partial\alpha_j} = 2 \sum_{i=1}^{N} \left\{ \left[P_i - \sum_{k=0}^{M} \alpha_k \, f_{ik} \right]\left[\; - f_{ij} \right]\right\} = 0 \qquad (C-4)$$

This set of equations reduces to:

$$\sum_{i=1}^{N} P_i \, f_{ij} - \sum_{k=0}^{M} \alpha_k \sum_{i=1}^{N} f_{ik} \; f_{ij} = 0 \qquad (C-5)$$

In matrix shorthand the equations become

$$\left[E_{jk} \right]\left\{ \alpha_j \right\} = \left\{ \lambda_j \right\} \qquad (C-6)$$

where

$$E_{jk} = \sum_{i=1}^{N} f_{ij} \; f_{ik} \qquad \begin{matrix} j = 0 \ldots\ldots M \\ k = 0, 1, \ldots M \end{matrix}$$

$$\left[E_{jk} \right] = (M + 1) \times (M + 1) \, \text{matrix}$$

α_j = curve fit coefficients

$$\lambda_j = \sum_{i=1}^{N} P_i \, f_{ij}$$

84

The values of $\{\alpha\}$ are solved by inverting matrix $[E_{jk}]$ and multiplying $\{\lambda\}$

$$\alpha_j = [E_{jk}]^{-1}\{\lambda_k\} \tag{C-7}$$

The resulting coefficients are assumed to be Fourier coefficients. The cosine coefficients are set equal to α_j (j = 1, ... M/2) and the sine coefficients are α_j (j = M/2 + 1, ... M). The calculations required for K_θ can then be made. It might be mentioned here that one advantage to this particular method is that the matrix $[E_{jk}]$ need only be inverted once for a given instrumentation geometry, thus resulting in rapid calculation of K_θ.

Steady State Case No. 384
LPC Rot. Stall/HPC Surge
Initial Stall Location 2.3-2.6
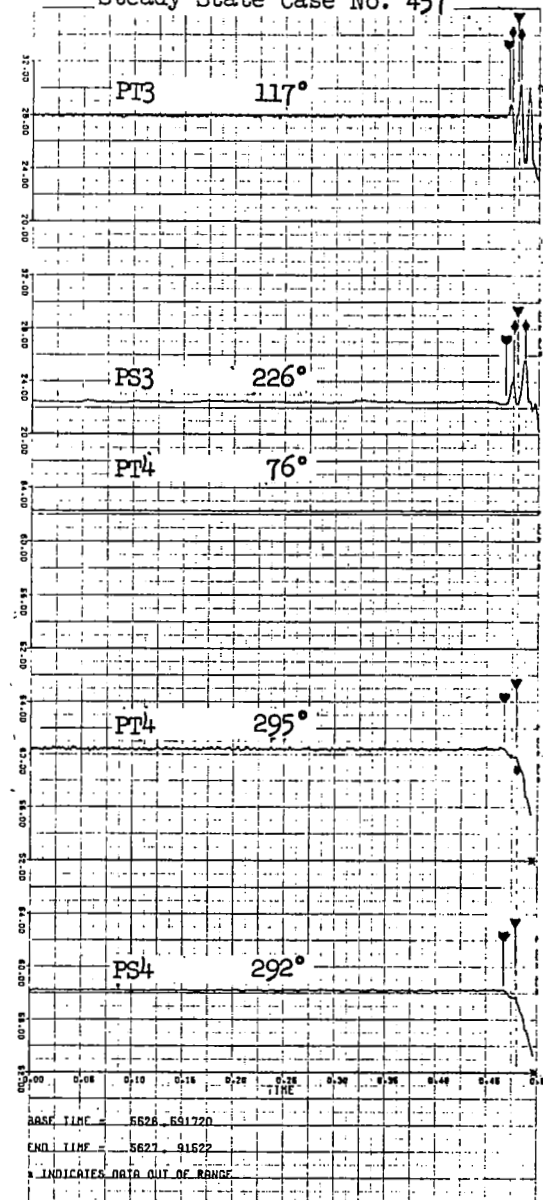
PT2.3   269°

PT2.6   89°

PS2.6   69°

PT2.6   268°

PS2.6   249°
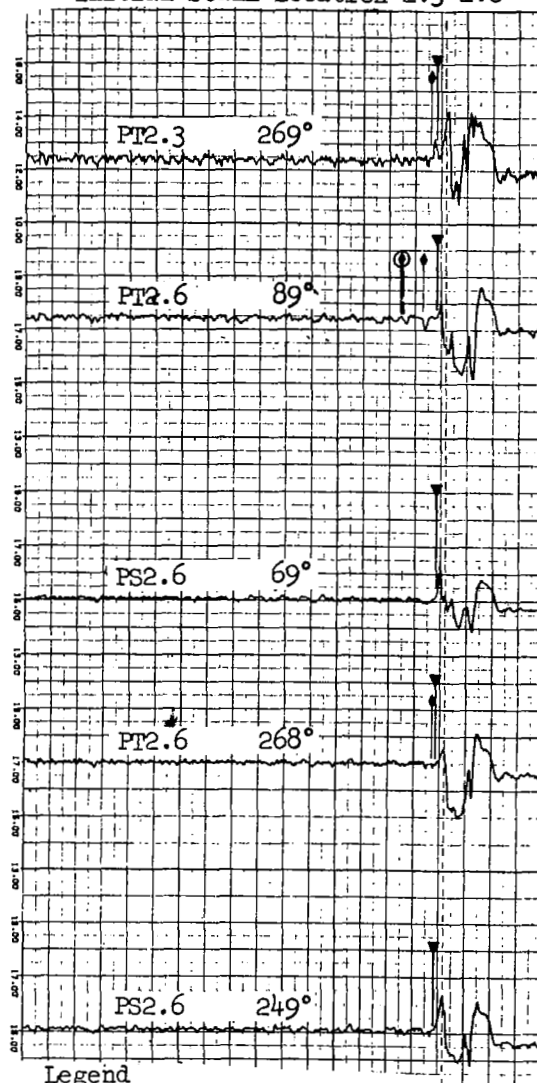
Legend
O Initial Stall Indication
◆ LPC Rotating Stall
▼ HPC Surge
- - - Station 2.0 Overpressure

Steady State Case No. 384

Steady State Case No. 389
LPC Rot. Stall/HPC Surge
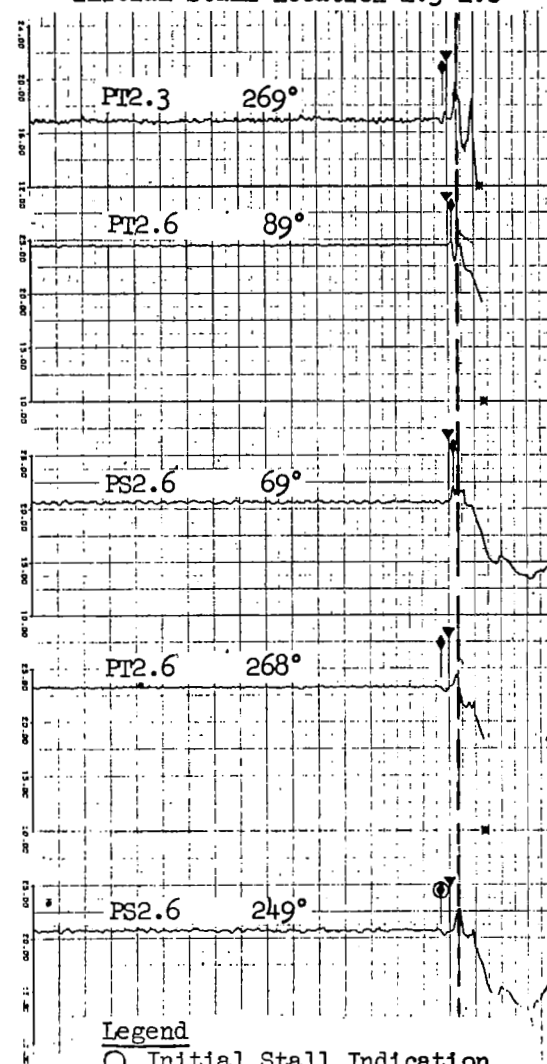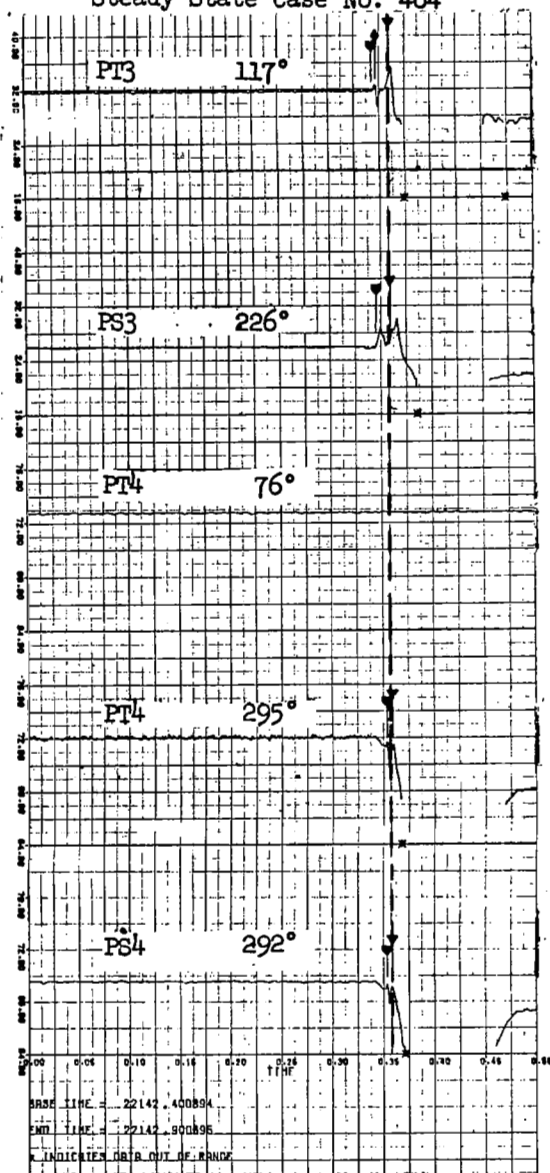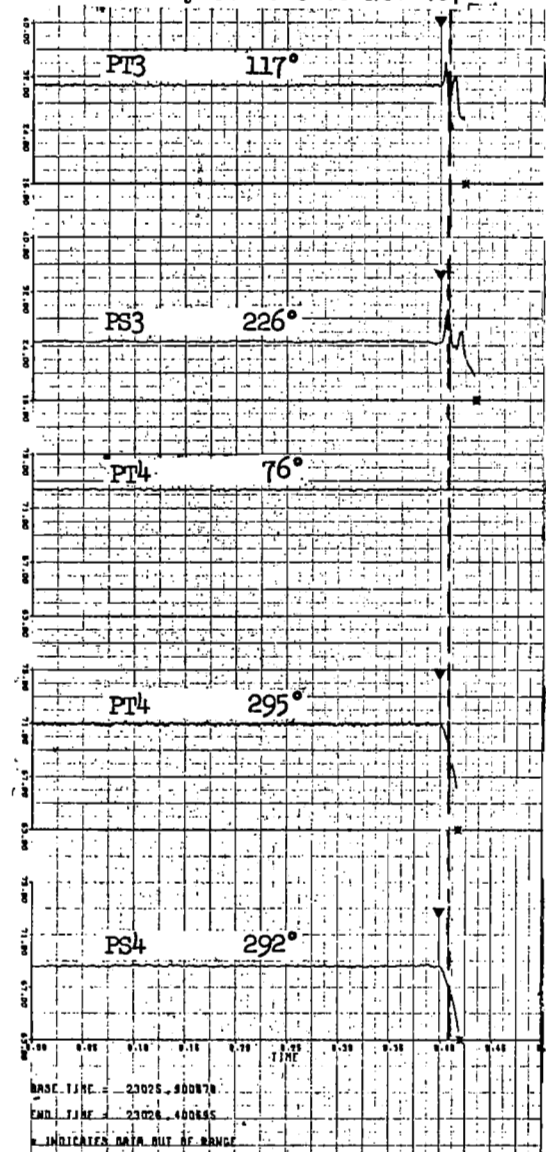Initial Stall Location 2.3-2.6
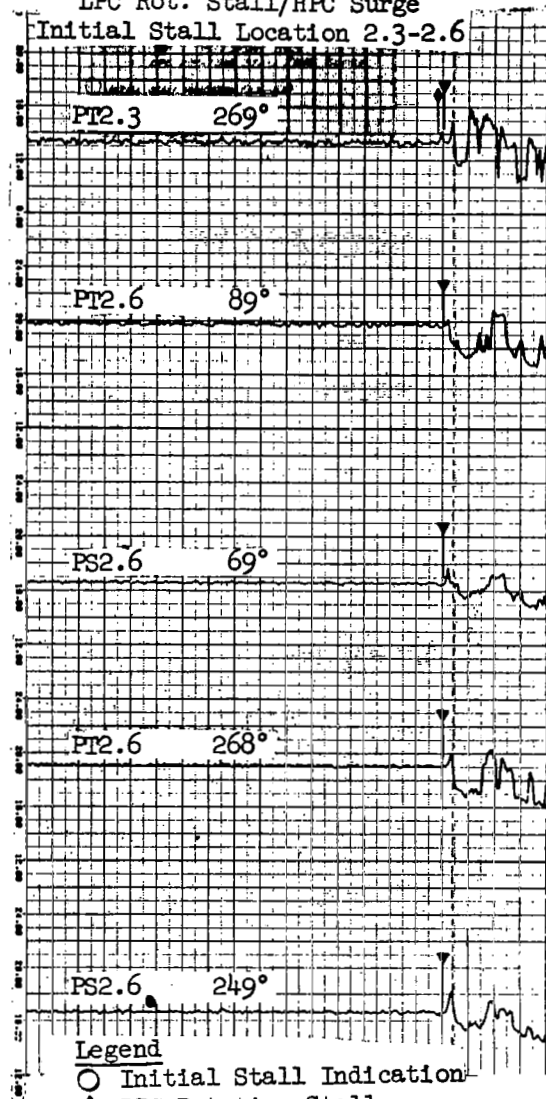
PT2.3   269°

PT2.6   89°

PS2.6   69°

PT2.6   268°

PS2.6   249°

Legend
○ Initial Stall Indication
◆ LPC Rotating Stall
▼ HPC Surge
- - -Station 2.0 Overpressure

Steady State Case No. 405
LPC Rot. Stall/HPC Surge
Initial Stall Location 2.3-2.6

PT2.3   269°

PT2.6   89°

PS2.6   69°

PT2.6   268°

PS2.6   249°

Legend
○ Initial Stall Indication
◆ LPC Rotating Stall
▼ HPC Surge
- - -Station 2.0 Overpressure

88

Steady State Case No. 389

PT3   117°
PS3   226°
PT4   76°
PT4   295°
PS4   292°

Steady State Case No. 405

PT3   117°
PS3   226°
PT4   76°
PT4   295°
PS4   292°

Steady State Case No. 408
LPC Rot. Stall/HPC Surge
Initial Stall Location 2.3-2.6

PT2.3   269°
PT2.6   89°
PS2.6   69°
PT2.6   268°
PS2.6   249°

Legend
○ Initial Stall Indication
◆ LPC Rotating Stall
▼ HPC Surge
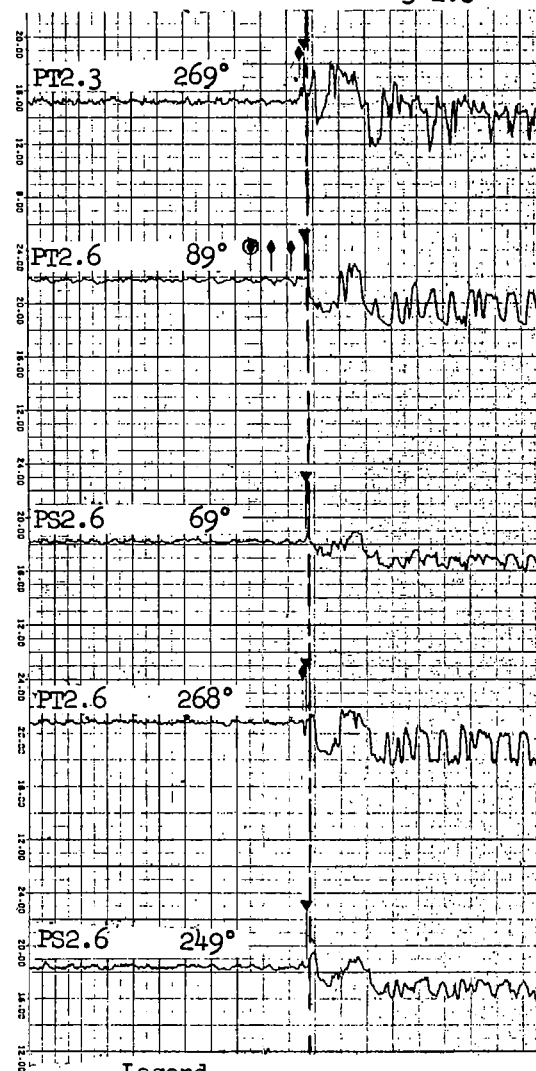- - - Station 2.0 Overpressure

Steady State Case No. 421
LPC Rot. Stall/HPC Rot. Stall/HPC Surge
Initial Stall Location 2.3-2.6

PT2.3   269°
PT2.6   89°
PS2.6   69°
PT2.6   268°
PS2.6   249°

Legend
○ Initial Stall Indication
◆ LPC Rotating Stall
▼ HPC Rotating Stall
▼ HPC Surge
- - - Station 2.0 Overpressure

Steady State Case No. 408

PT3   117°
PS3   226°
PT4   76°
PT4   295°
PS4   292°

Steady State Case No. 421

PT3   117°
PS3   226°
PT4   76°
PT4   295°
PS4   292°

Steady State Case No. 438
LPC Rot. Stall/HPC Surge
Initial Stall Location 2.6-3.0

PT2.3   269°

PT2.6   89°

PS2.6   69°

PT2.6   268°

PS2.6   249°

Legend
○ Initial Stall Indication
◆ LPC Rotating Stall
▼ HPC Surge
− − −Station 2.0 Overpressure

Steady State Case No. 441
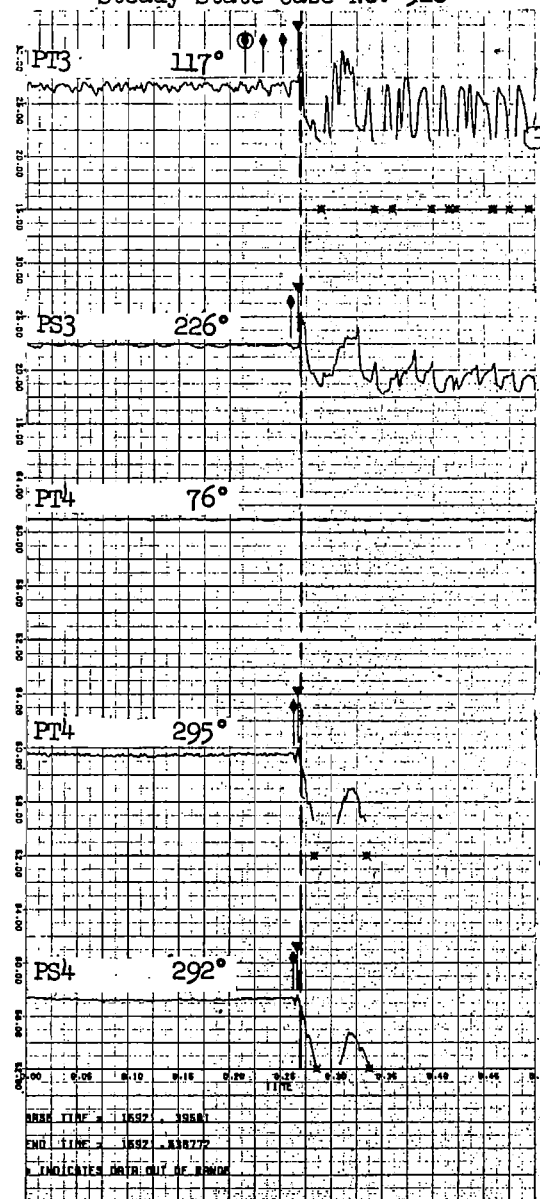LPC Rot. Stall/HPC Surge
Initial Stall Location 2.3-2.6

PT2.3   269°

PT2.6   89°

PS2.6   69°

PT2.6   268°

PS2.6   249°
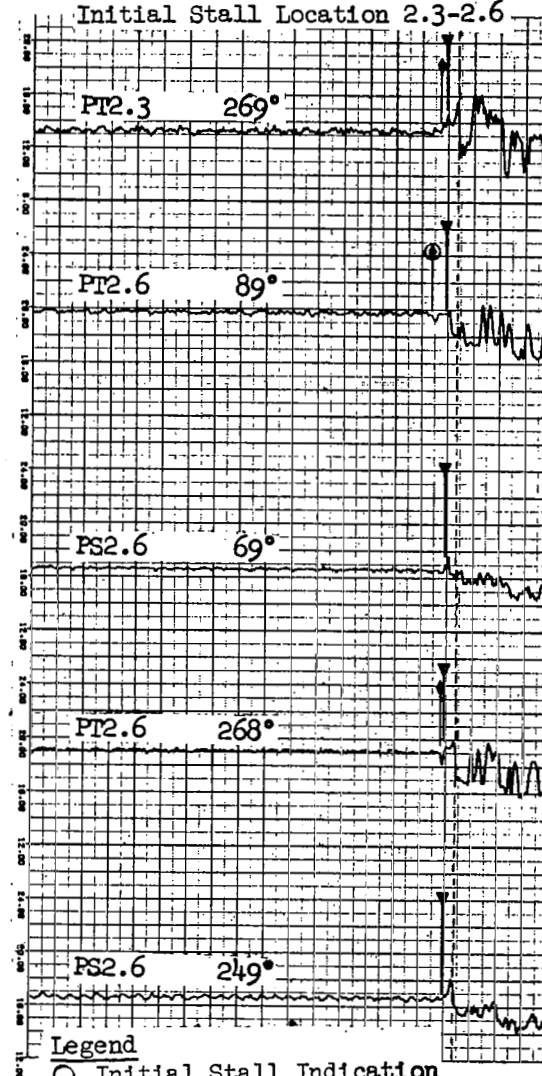
Legend
○ Initial Stall Indication
◆ LPC Rotating Stall
▼ HPC Surge
− − −Station 2.0 Overpressure
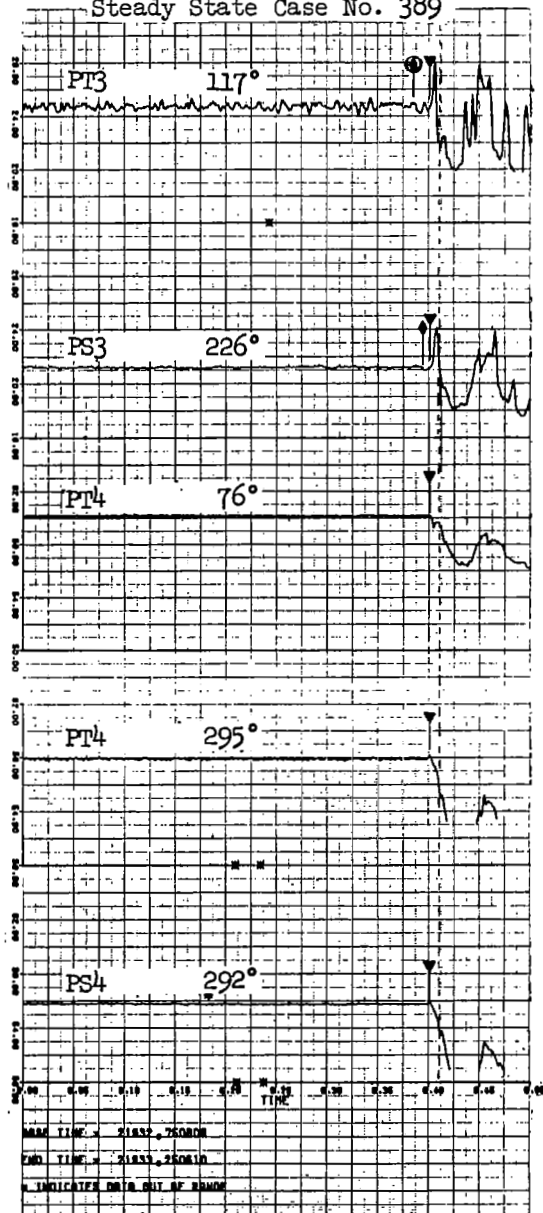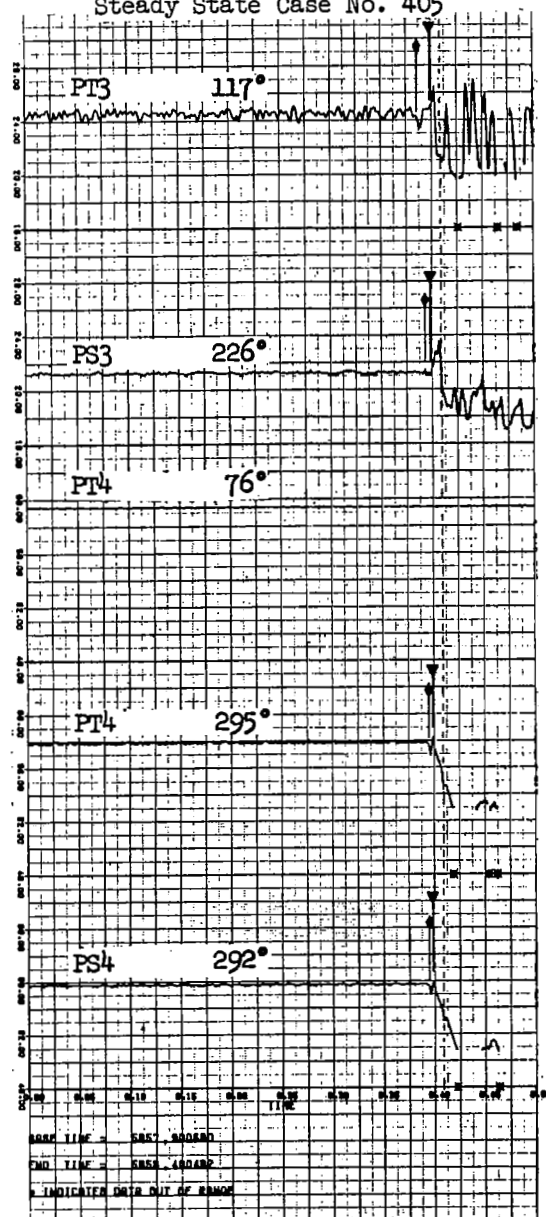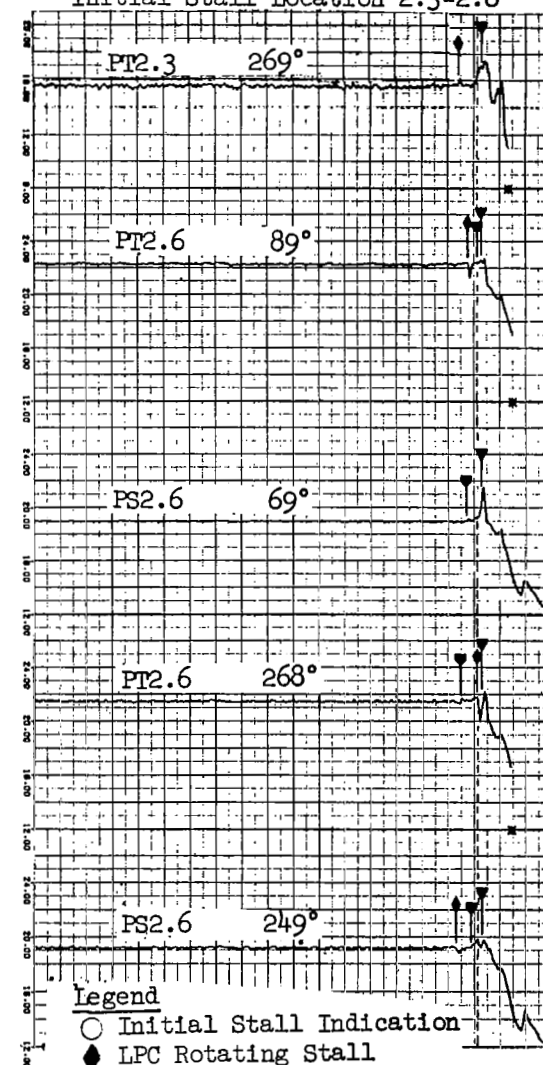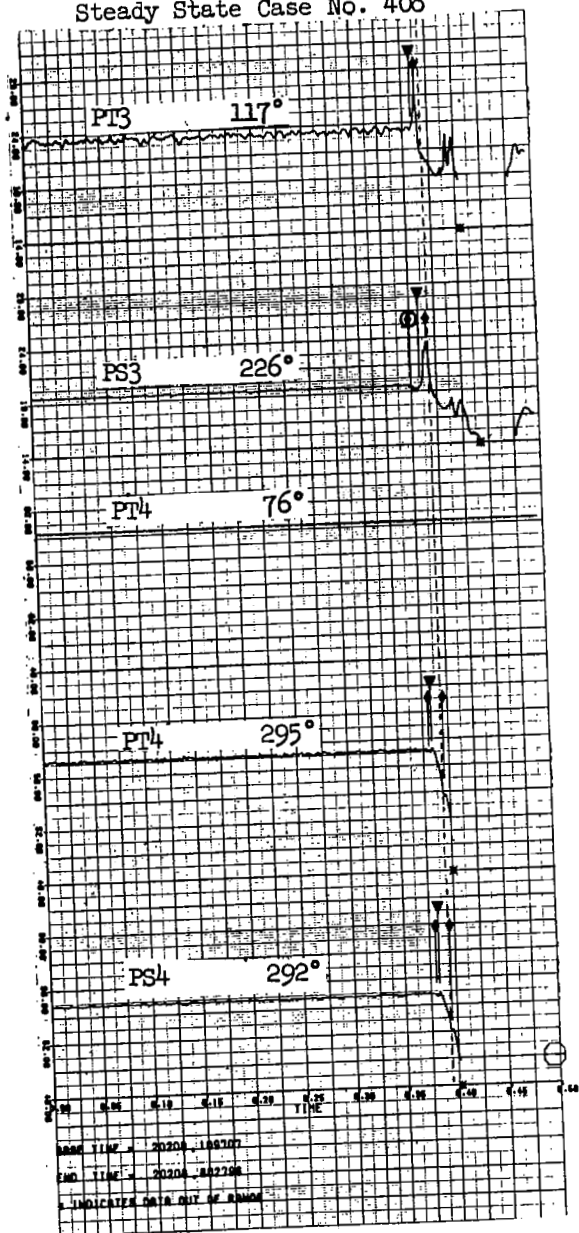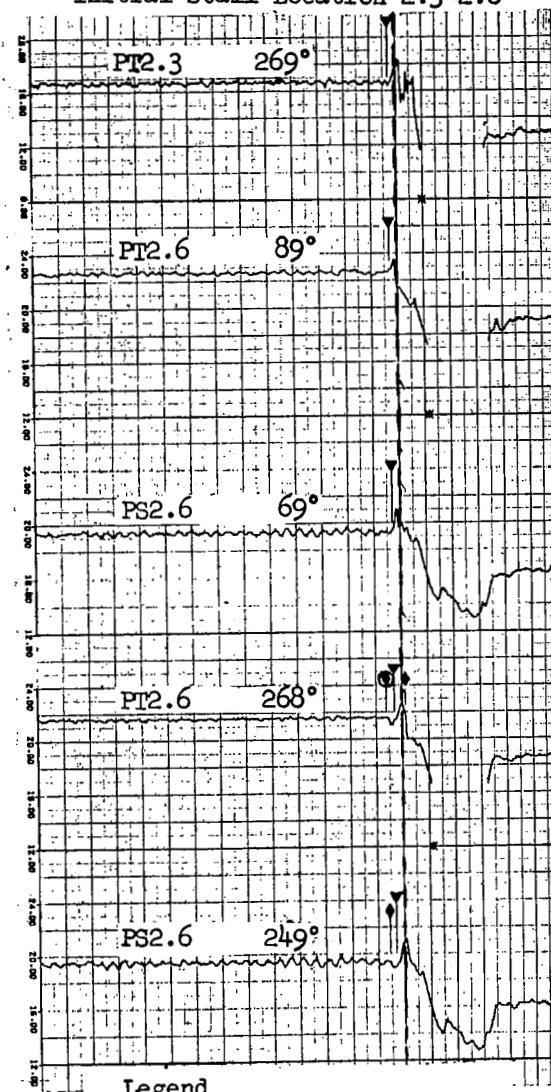
Steady State Case No. 438

Steady State Case No. 441

Steady State Case No. 445
Fan Rot. Stall/LPC Rot. Stall/HPC Surge
Initial Stall Location 2.0-2.3

PT2.3   269°

PT2.6   89°
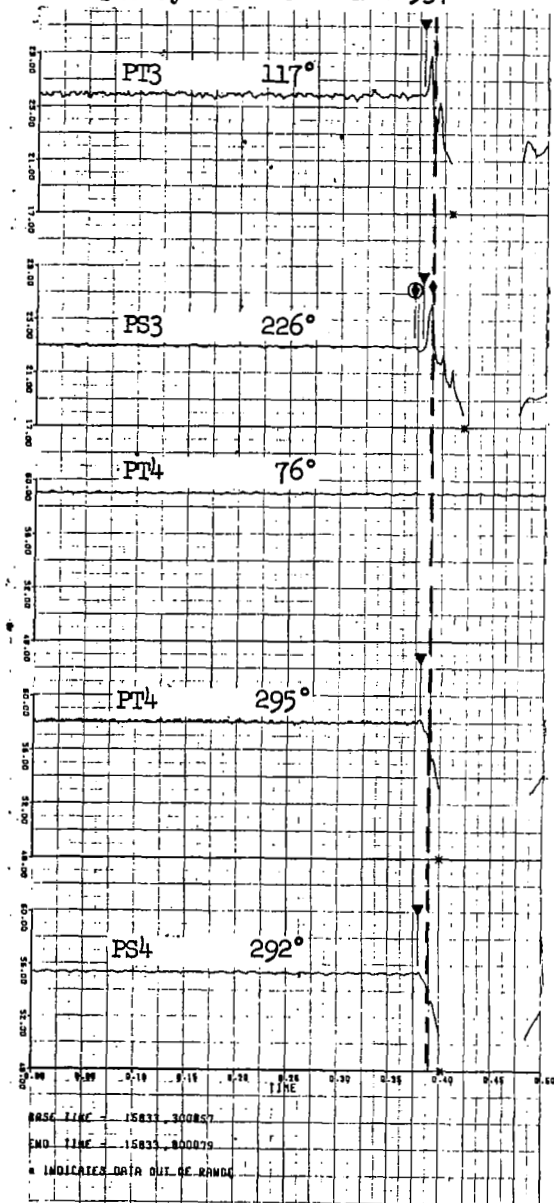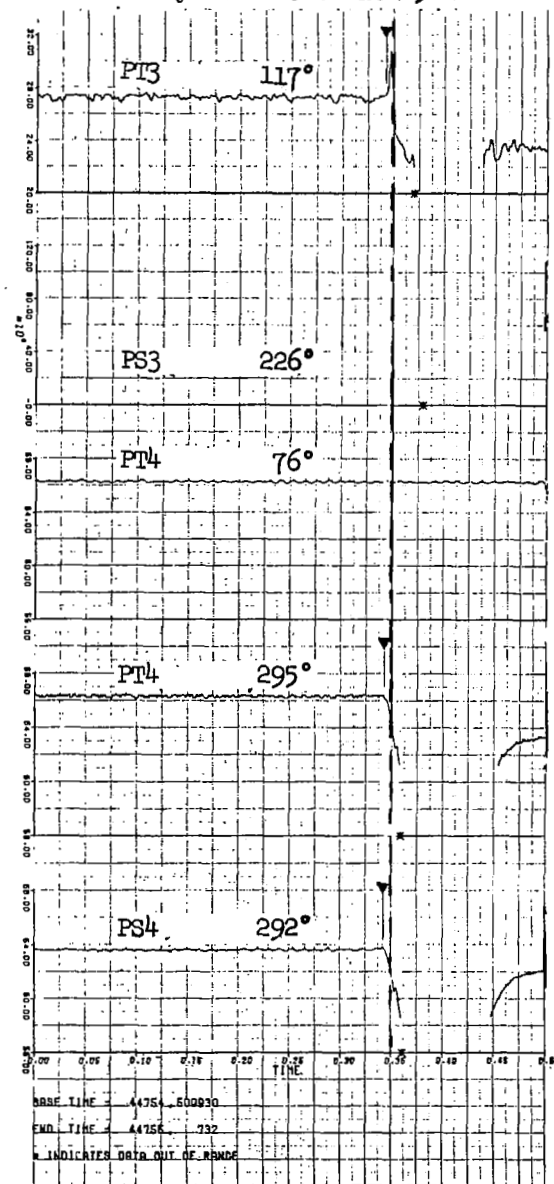
PS2.6   69°

PT2.6   268°

PS2.6   249°

Legend
○ Initial Stall Indication
◆ Fan/LPC Rotating Stall
▼ HPC Surge
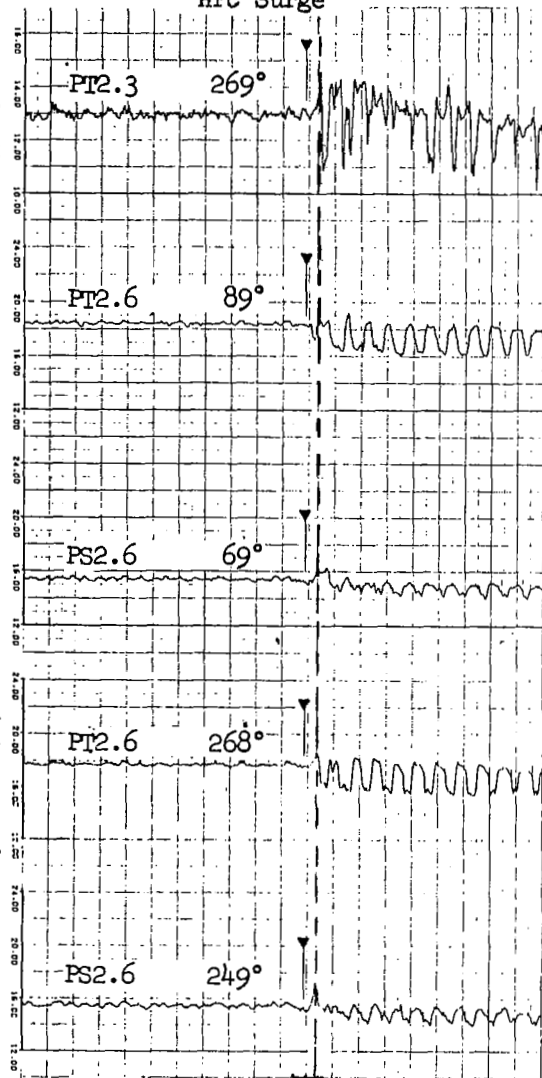- - -Station 2.0 Overpressure

Steady State Case No. 457
LPC Rot. Stall/HPC Rot. Stall/HPC Surge
Initial Stall Location 2.3-2.6

PT2.3   269°

PT2.6   89°

PS2.6   69°

PT2.6   268°

PS2.6   249°

Legend
○ Initial Stall Indication
◆ LPC Rotating Stall
▼ HPC Rotating Stall
▼ HPC Surge
- - -Station 2.0 Overpressure

Steady State Case No. 445

PT3   117°
PS3   226°
PT4   76°
PT4   295°
PS4   292°

Steady State Case No. 457

PT3   117°
PS3   226°
PT4   76°
PT4   295°
PS4   292°

Steady State Case No. 464
LPC Rot. Stall/HPC Rot. Stall/HPC Surge
Initial Stall Location 2.3-2.6

PT2.3   269°
PT2.6   89°
PS2.6   69°
PT2.6   268°
PS2.6   249°

Legend
○ Initial Stall Indication
◆ LPC Rotating Stall
▼ HPC Rotating Stall
▼ HPC Surge
‐ ‐ ‐Station 2.0 Overpressure

Steady State Case No. 467
LPC Rot. Stall/HPC Rot. Stall/HPC Surge
Initial Stall Location 2.3-2.6
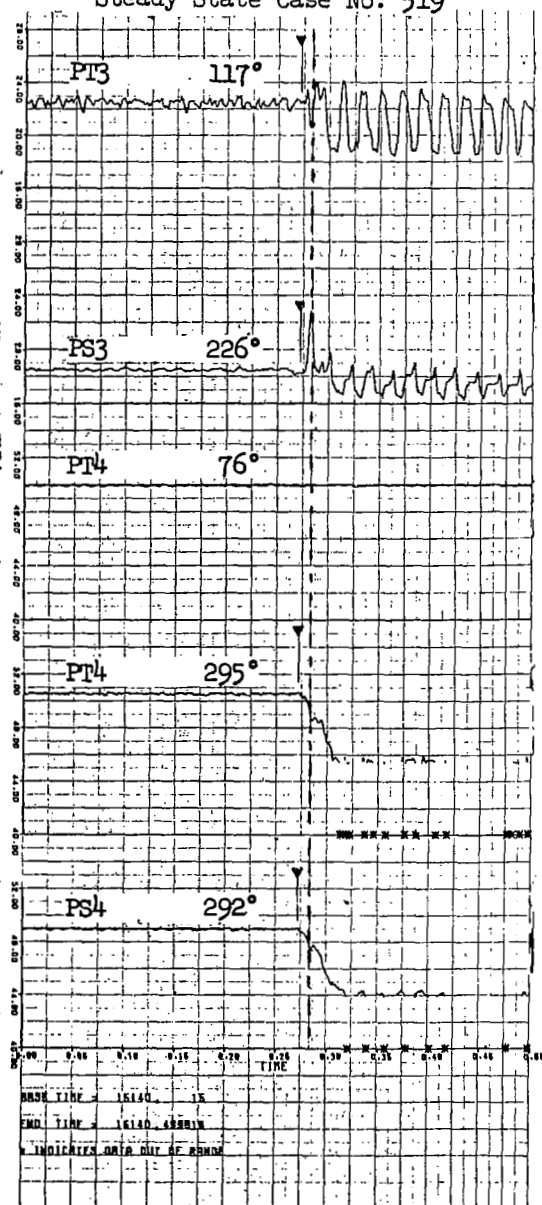
PT2.3   269°
PT2.6   89°
PS2.6   69°
PT2.6   268°
PS2.6   249°

Legend
○ Initial Stall Indication
◆ LPC Rotating Stall
▼ HPC Surge
‐ ‐ ‐Station 2.0 Overpressure

Steady State Case No. 464

PT3   117°

PS3   226°

PT4   76°

PT4   295°

PS4   292°

TIME

BASE TIME = 22142.400894
END TIME = 22142.900895
* INDICATES DATA OUT OF RANGE

Steady State Case No. 467

PT3   117°

PS3   226°

PT4   76°

PT4   295°

PS4   292°

TIME

BASE TIME = 23025.900870
END TIME = 23026.400855
* INDICATES DATA OUT OF RANGE

97

Steady State Case No. 502
Fan Rot. Stall/LPC Rot. Stall/HPC Surge
Initial Stall Location 2.0-2.3

Steady State Case No. 528
LPC Rot. Stall/HPC Surge
Initial Stall Location 2.3-2.6

Legend
◯ Initial Stall Indication
◆ Fan/LPC Rotating Stall
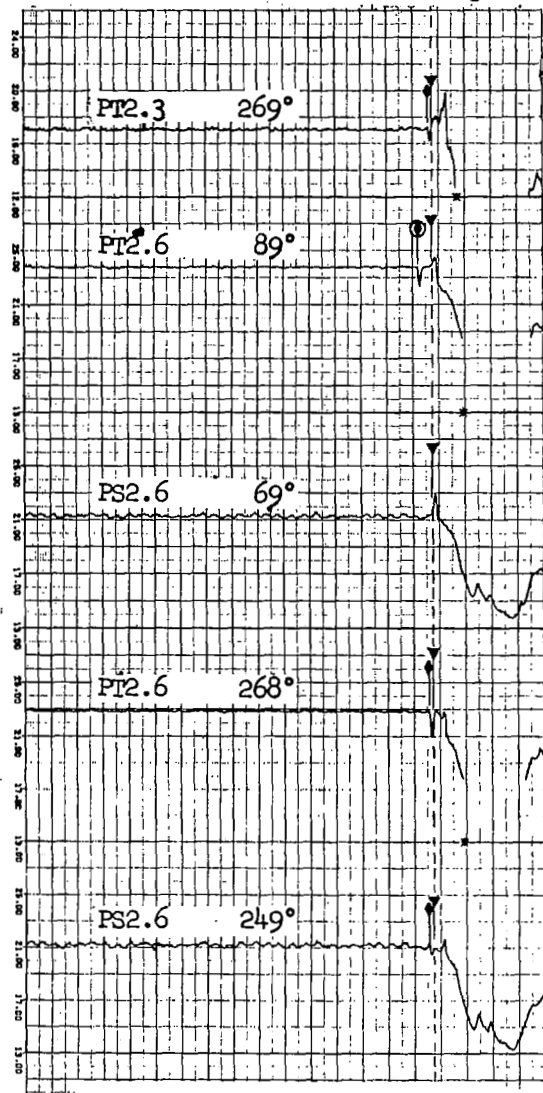▼ HPC Surge
− − −Station 2.0 Overpressure

Legend
◯ Initial Stall Indication
◆ LPC Rotating Stall
▼ HPC Surge
− − −Station 2.0 Overpressure
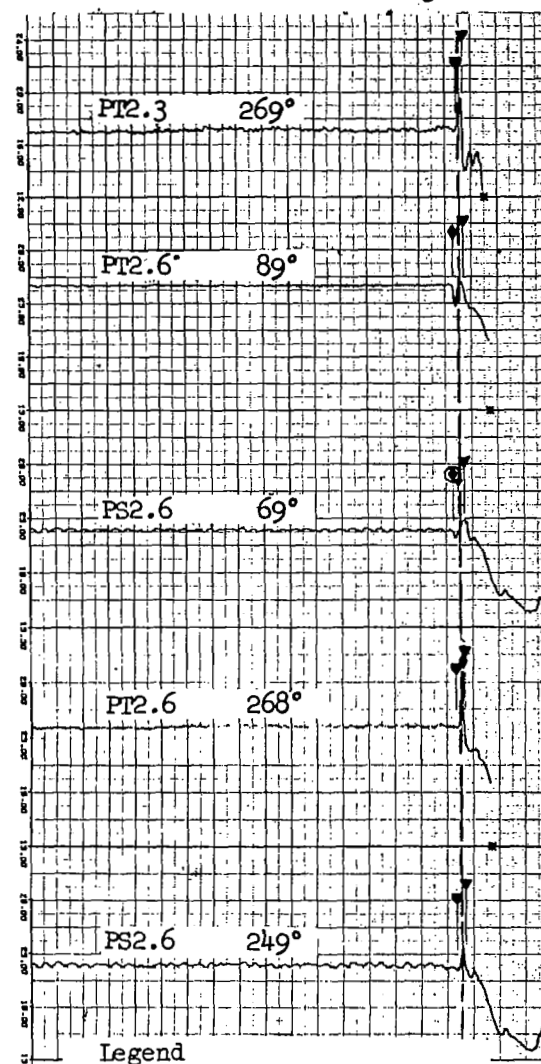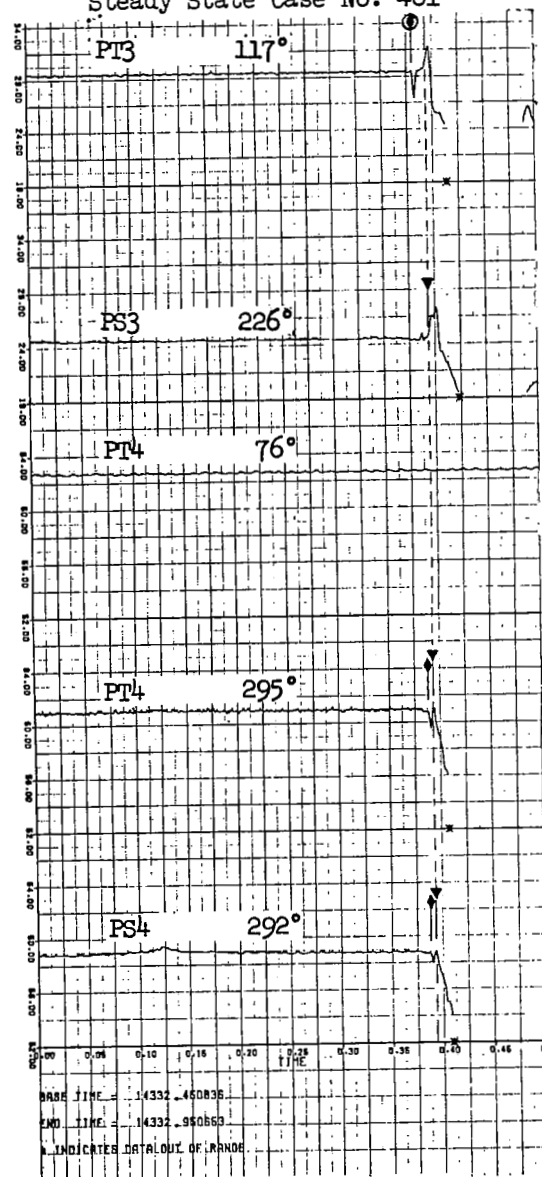
98

Steady State Case No. 502
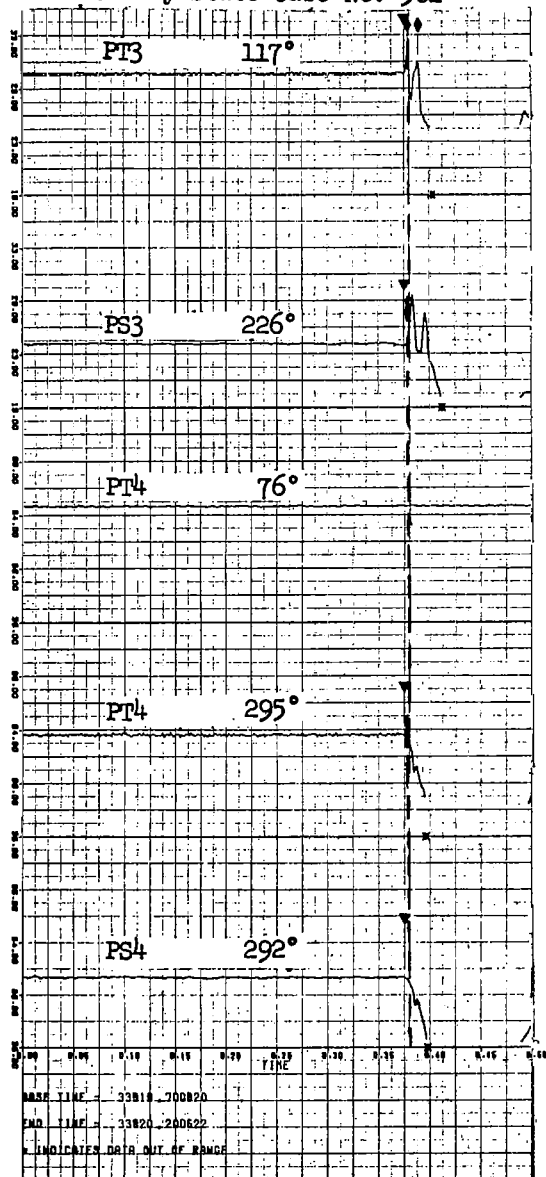
Steady State Case No. 528

Steady State Case No. 537
LPC Rot. Stall/HPC Surge
Initial Stall Location 2.3-2.6

PT2.3   269°

PT2.6   89°

PS2.6   69°

PT2.6   268°

PS2.6   249°

Legend
○ Initial Stall Indication
◆ LPC Rotating Stall
▼ HPC Surge
- - - Station 2.0 Overpressure

Steady State Case No. 561
LPC Rot. Stall/HPC Surge
Initial Stall Location 2.3-2.6

PT2.3   269°
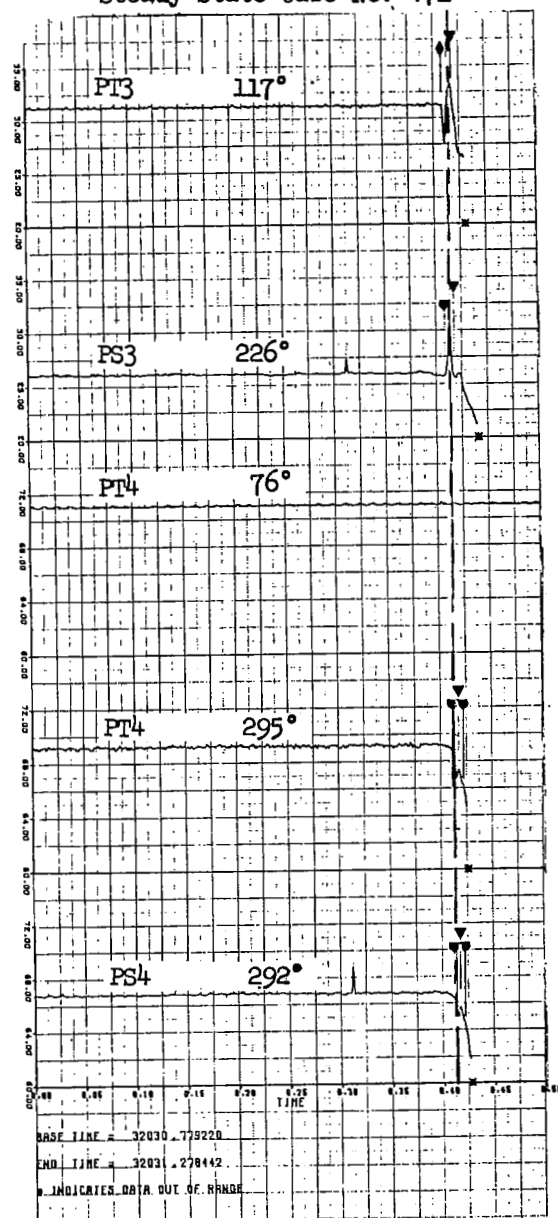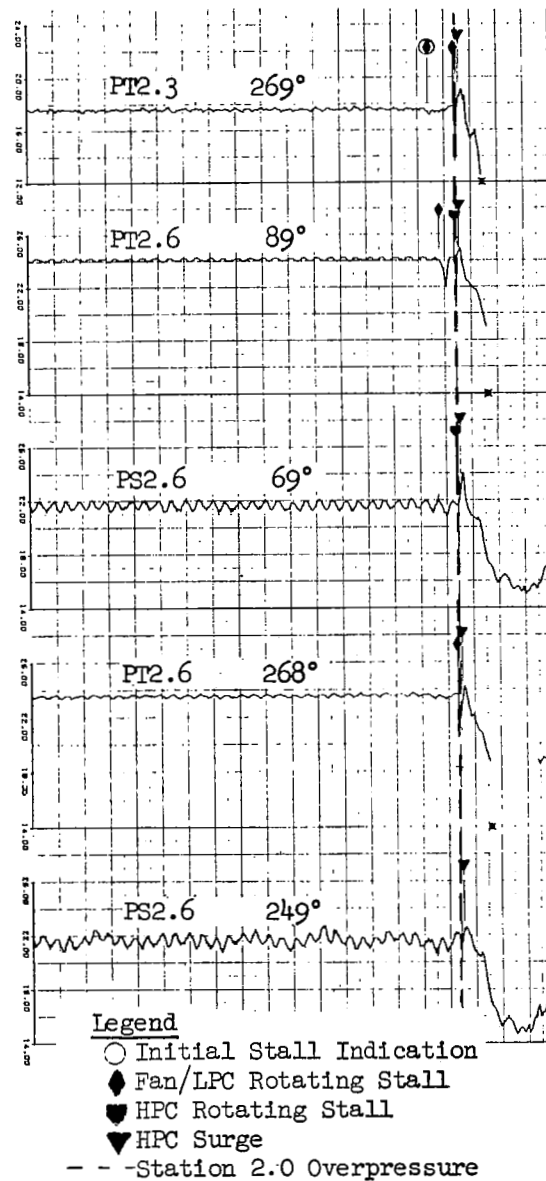
PT2.6   89°

PS2.6   69°

PT2.6   268°

PS2.6   249°

Legend
○ Initial Stall Indication
◆ LPC Rotating Stall
▼ HPC Surge
- - - Station 2.0 Overpressure

Steady State Case No. 537

PT3   117°

PS3   226°
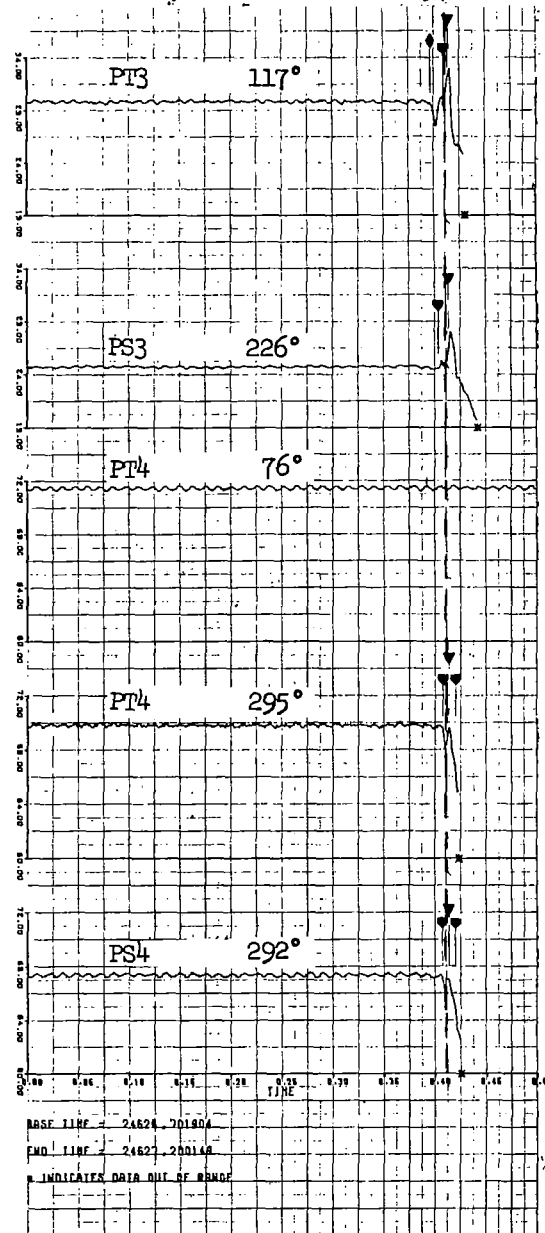
PT4   76°

PT4   295°

PS4   292°

Steady State Case No. 561

PT3   117°

PS3   226°

PT4   76°

PT4   295°

PS4   292°

Steady State Case No. 519
HPC Surge

PT2.3   269°

PT2.6   89°

PS2.6   69°

PT2.6   268°

PS2.6   249°

Legend
▼ HPC Surge
- - -Station 2.0 Overpressure

Steady State Case No. 451
LPC Rot. Stall/HPC Surge
Initial Stall Location 2.3-2.6

PT2.3   269°

PT2.6   89°

PS2.6   69°

PT2.6   268°

PS2.6   249°

Legend
○ Initial Stall Indication
◆ LPC Rotating Stall
▼ HPC Surge
- - -Station 2.0 Overpressure
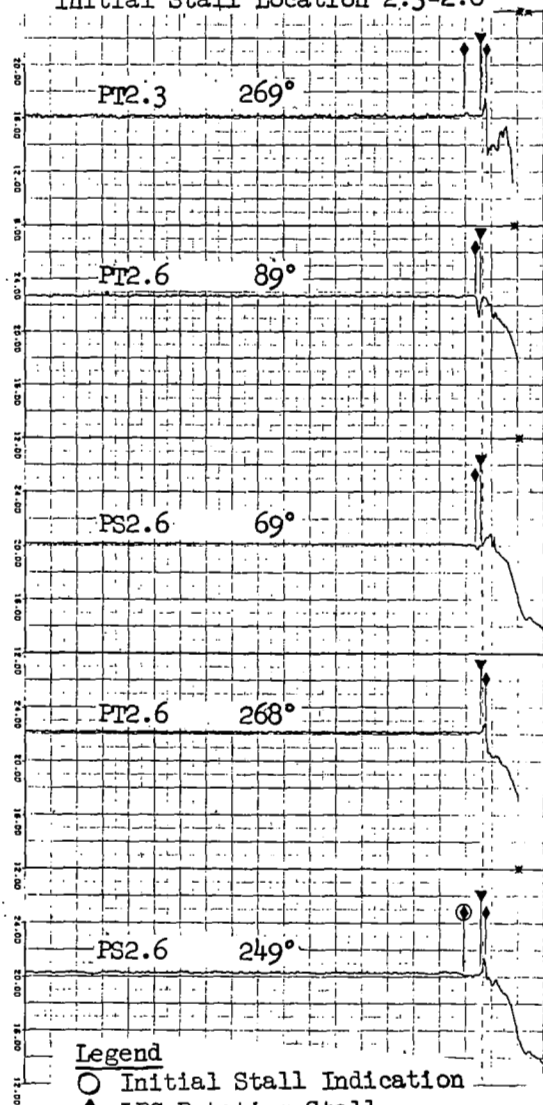
102
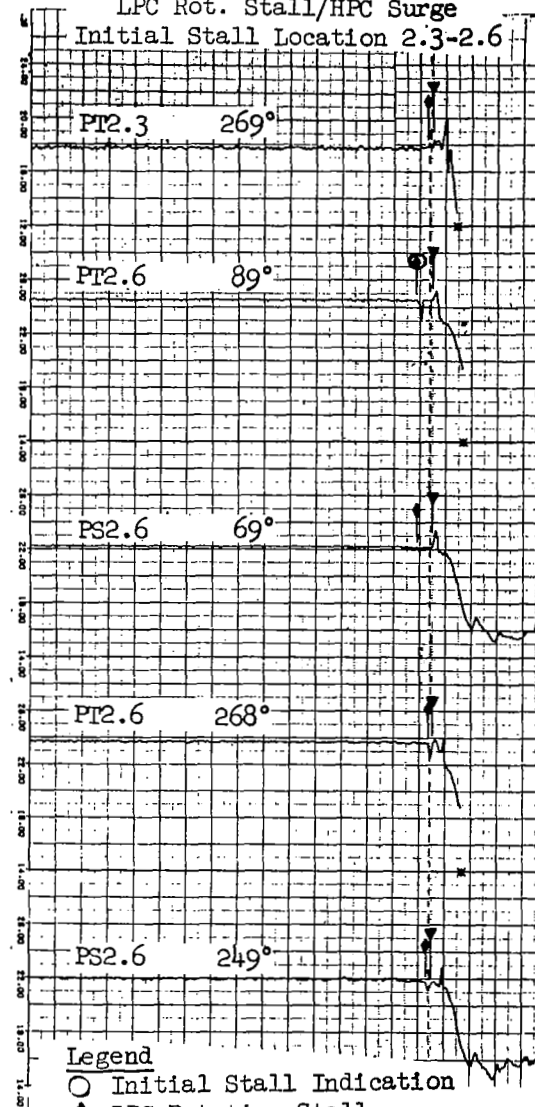
Steady State Case No. 519

Steady State Case No. 451
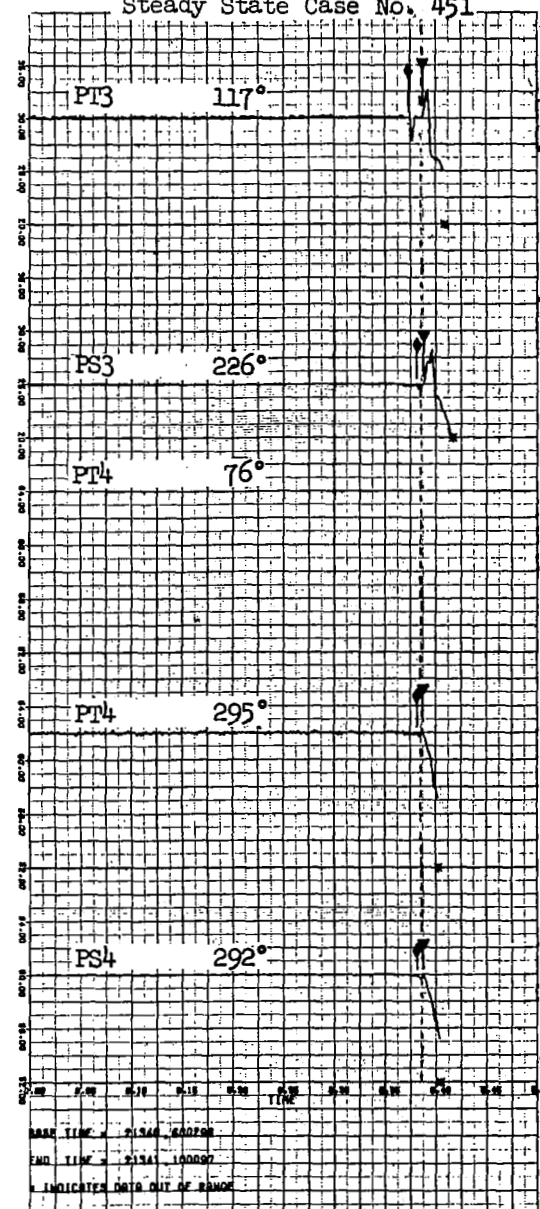
103

Steady State Case No. 461
Fan Rot. Stall/LPC Rot. Stall/HPC Surge
Initial Stall Location 2.0-2.3

Steady State Case No. 471
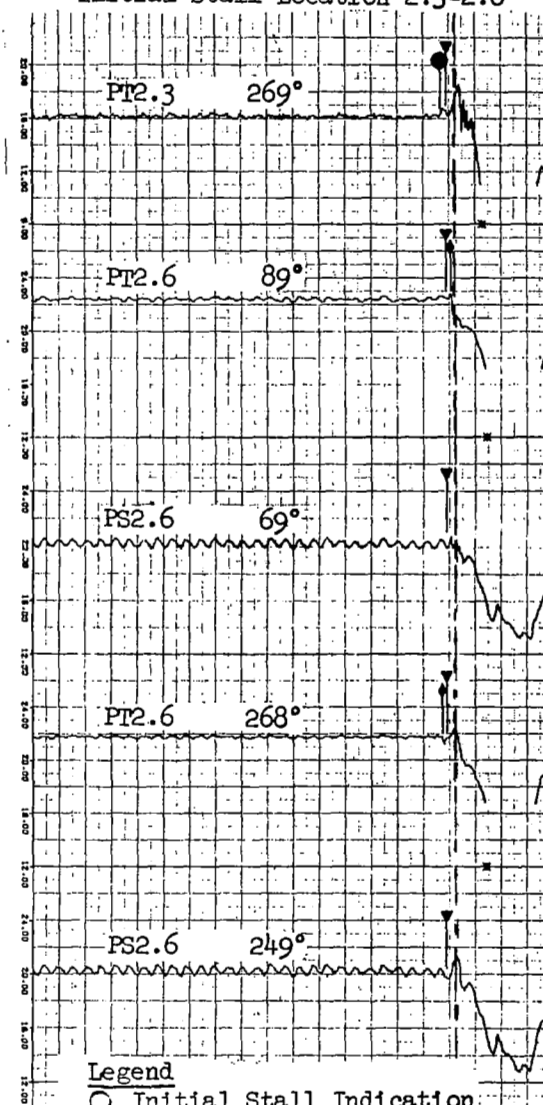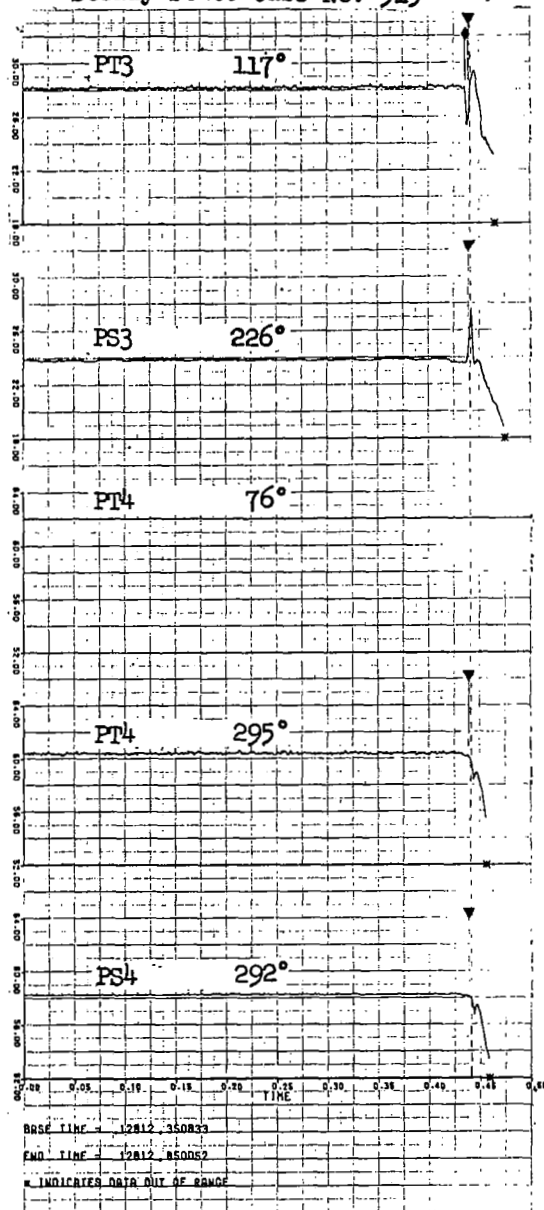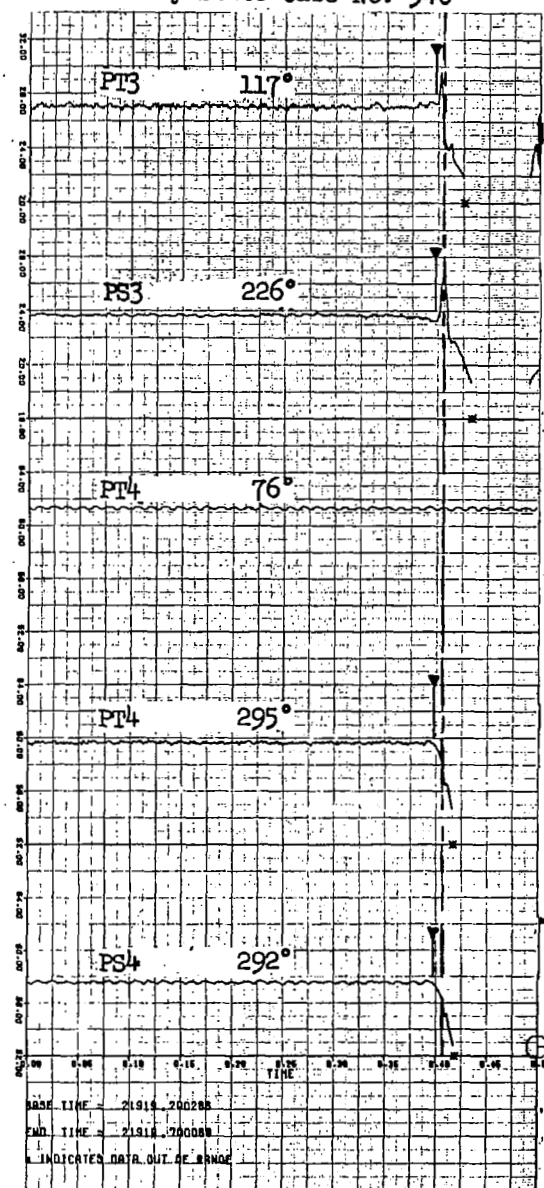LPC Rot. Stall/HPC Rot. Stall/HPC Surge
Initial Stall Location 2.3-2.6

PT2.3   269°

PT2.6   89°

PS2.6   69°

PT2.6   268°

PS2.6   249°

PT2.3   269°

PT2.6   89°

PS2.6   69°

PT2.6   268°

PS2.6   249°

Legend
○ Initial Stall Indication
◆ Fan/LPC Rotating Stall
▼ HPC Surge
- - -Station 2.0 Overpressure

Legend
○ Initial Stall Indication
◆ LPC Rotating Stall
♥ HPC Rotating Stall
▼ HPC Surge
- - -Station 2.0 Overpressure

104

Steady State Case No. 461

PT3   117°
PS3   226°
PT4   76°
PT4   295°
PS4   292°

BASE TIME = 14332.450838
END TIME = 14332.950663
INDICATES DATA OUT OF RANGE

Steady State Case No. 471

PT3   117°
PS3   226°
PT4   76°
PT4   295°
PS4   292°

BASE TIME = 32030.779220
END TIME = 32031.278442
INDICATES DATA OUT OF RANGE

Steady State Case No. 497
Fan Rot. Stall/LPC Rot. Stall/HPC Rot. Stall/HPC Surge
Initial Stall Location 2.0-2.3

PT2.3   269°

PT2.6   89°

PS2.6   69°

PT2.6   268°

PS2.6   249°

Legend
○ Initial Stall Indication
◆ Fan/LPC Rotating Stall
♥ HPC Rotating Stall
▼ HPC Surge
— — Station 2.0 Overpressure

Steady State Case No. 497

Steady State Case No. 515
LPC Rot. Stall/HPC Surge
Initial Stall Location 2.3-2.6

PT2.3   269°

PT2.6   89°

PS2.6   69°

PT2.6   268°

PS2.6   249°

Legend
○ Initial Stall Indication
◆ LPC Rotating Stall
▼ HPC Surge
- - - Station 2.0 Overpressure

Steady State Case No. 540
LPC Rot. Stall/HPC Surge
Initial Stall Location 2.3-2.6

PT2.3   269°

PT2.6   89°

PS2.6   69°

PT2.6   268°

PS2.6   249°

Legend
○ Initial Stall Indication
◆ LPC Rotating Stall
▼ HPC Surge
- - - Station 2.0 Overpressure

108

Steady State Case No. 515

Steady State Case No. 540

109

Rotating Stall Frequency

Steady State Case No. 384
LPC Rot. Stall/HPC Surge
Initial Stall Location 2.3-2.6

Rotating Stall Frequency
Steady State Case No. 389
LPC Rot. Stall/HPC Surge
Initial Stall Location 2.3-2.6

LEGEND
◇ P_{T23} 269°
◻ P_{S3} 226°
⬠ P_{T3} 117°

LPC CELL

SURGE

52.6% N₁

PROBE CIRCUMFERENTIAL LOCATION – DEGREES

RELATIVE TIME – SEC

UAS A22-75

III

Rotating Stall Frequency
Steady State Case No. 405
LPC Rot. Stall/HPC Surge
Initial Stall Location 2.3-2.6

LEGEND

○ P_{T4} ___ 295°
□ P_{S4} ___ 292°
◇ $P_{T2.3}$ ___ 269°
△ $P_{T2.6}$ ___ 268°
⬠ $P_{S.3}$ ___ 226°
⬡ P_{T3} ___ 117°
⬡ $P_{T2.6}$ ___ 89°

PROBE CIRCUMFERENTIAL LOCATION ~ DEGREES

0/360
300
200
100
0/360
300
200
100
0/360

56.0% N_1

LPC CELL
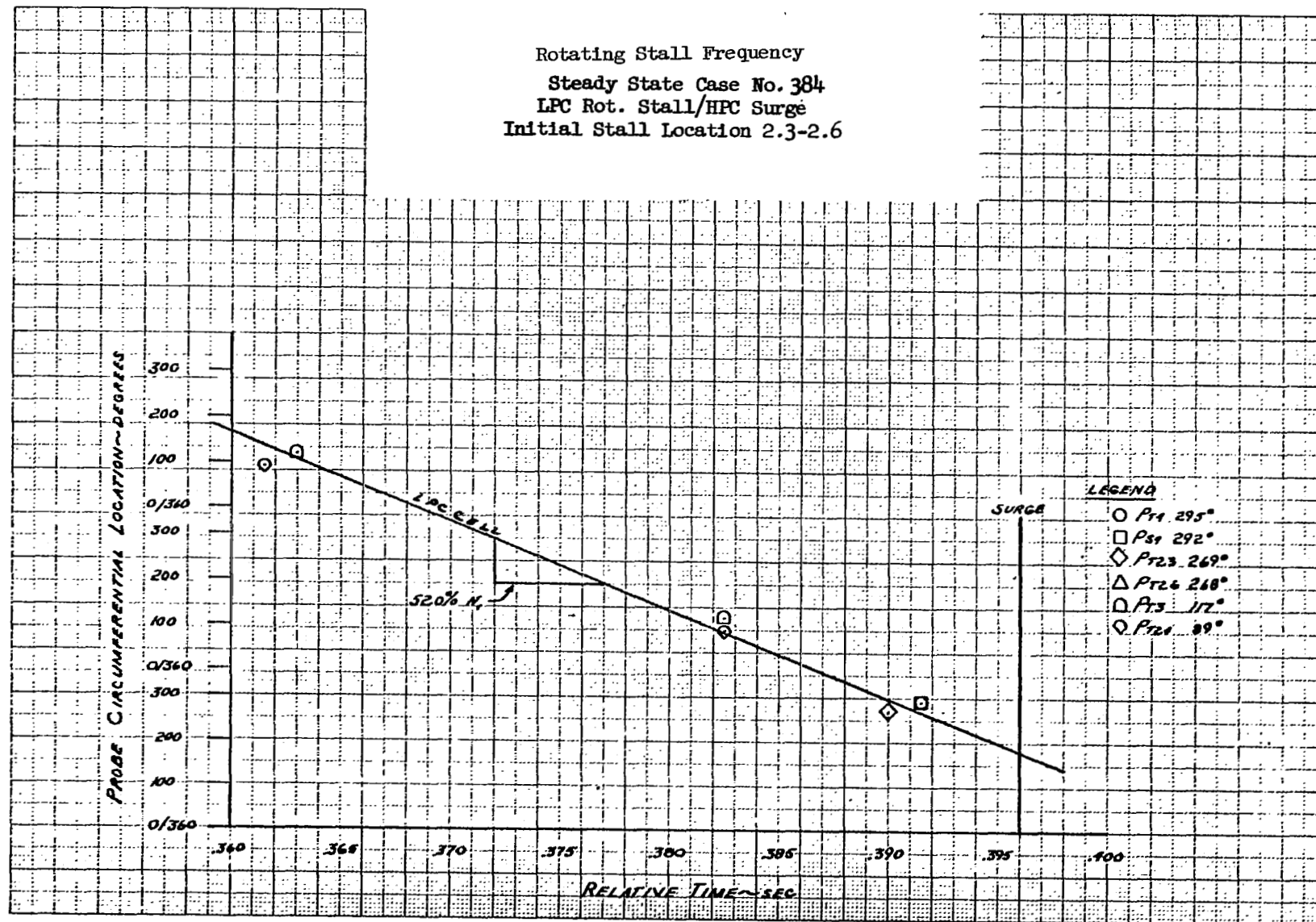
SURGE

.380   .385   .390   .395   .400

RELATIVE TIME ~ SEC.
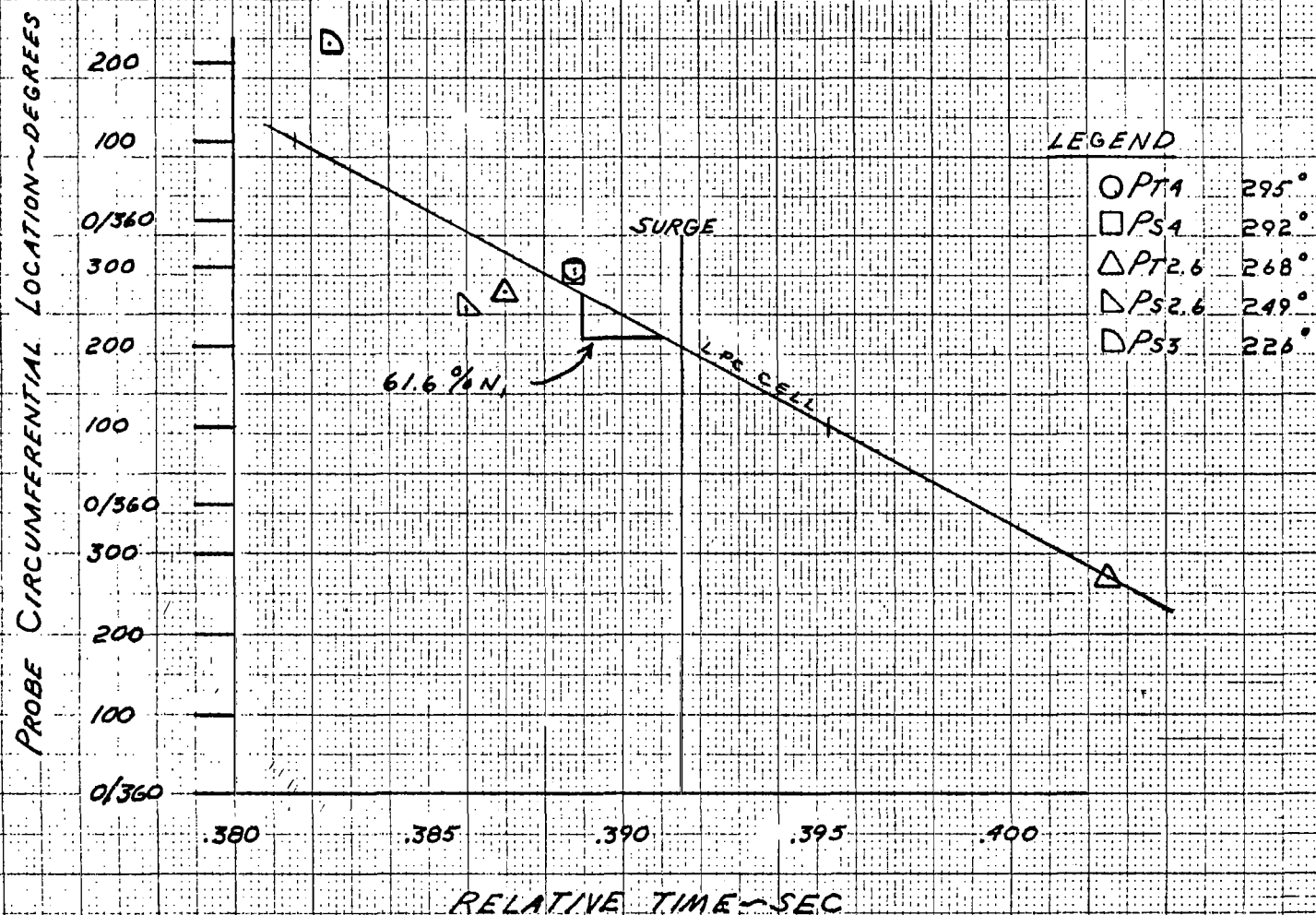
Rotating Stall Frequency
Steady State Case No. 408
LPC Rot. Stall/HPC Surge
Initial Stall Location 2.3-2.6

Rotating Stall Frequency
Steady State Case No. 421
LPC Rot. Stall/HPC Rot. Stall/HPC Surge
Initial Stall Location 2.3-2.6

Rotating Stall Frequency
Steady State Case No. 438
LPC Rot. Stall/HPC Surge
Initial Stall Location 2.6-3.0

Rotating Stall Frequency
Steady State Case No. 441
LPC Rot. Stall/HPC Surge
Initial Stall Location 2.3-2.6

Rotating Stall Frequency
Steady State Case No. 445
Fan Rot. Stall/LPC Rot. Stall/HPC Surge
Initial Stall Location 2.0-2.3

Rotating Stall Frequency
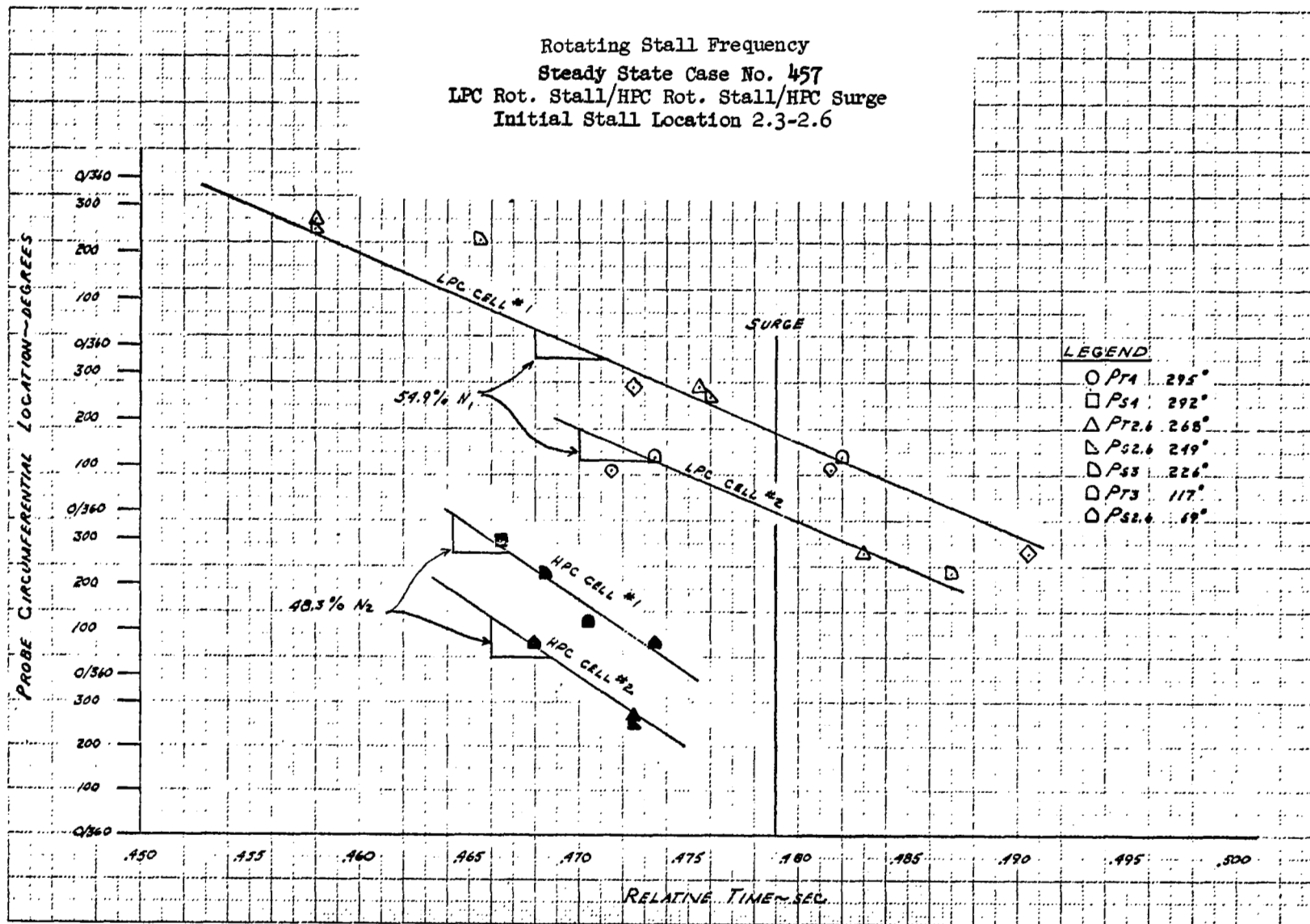**Steady State Case No. 457**
LPC Rot. Stall/HPC Rot. Stall/HPC Surge
Initial Stall Location 2.3-2.6

Rotating Stall Frequency
Steady State Case No. 464
LPC Rot. Stall/HPC Rot. Stall/HPC Surge
Initial Stall Location 2.3-2.6

Rotating Stall Frequency
Steady State Case No. 467
LPC Rot. Stall/HPC Surge
Initial Stall Location 2.3-2.6

LEGEND
◇ $P_{T2.3}$ 269°
△ $P_{T2.6}$ 268°
▷ $P_{S2.6}$ 249°
○ $P_{T2.6}$ 89°
⬠ $P_{S2.6}$ 69°

SURGE

LPC CELL

47.5% N_1

PROBE CIRCUMFERENTIAL LOCATION-DEGREES

0/360
300
200
100
0/360
300
200
100
0/360
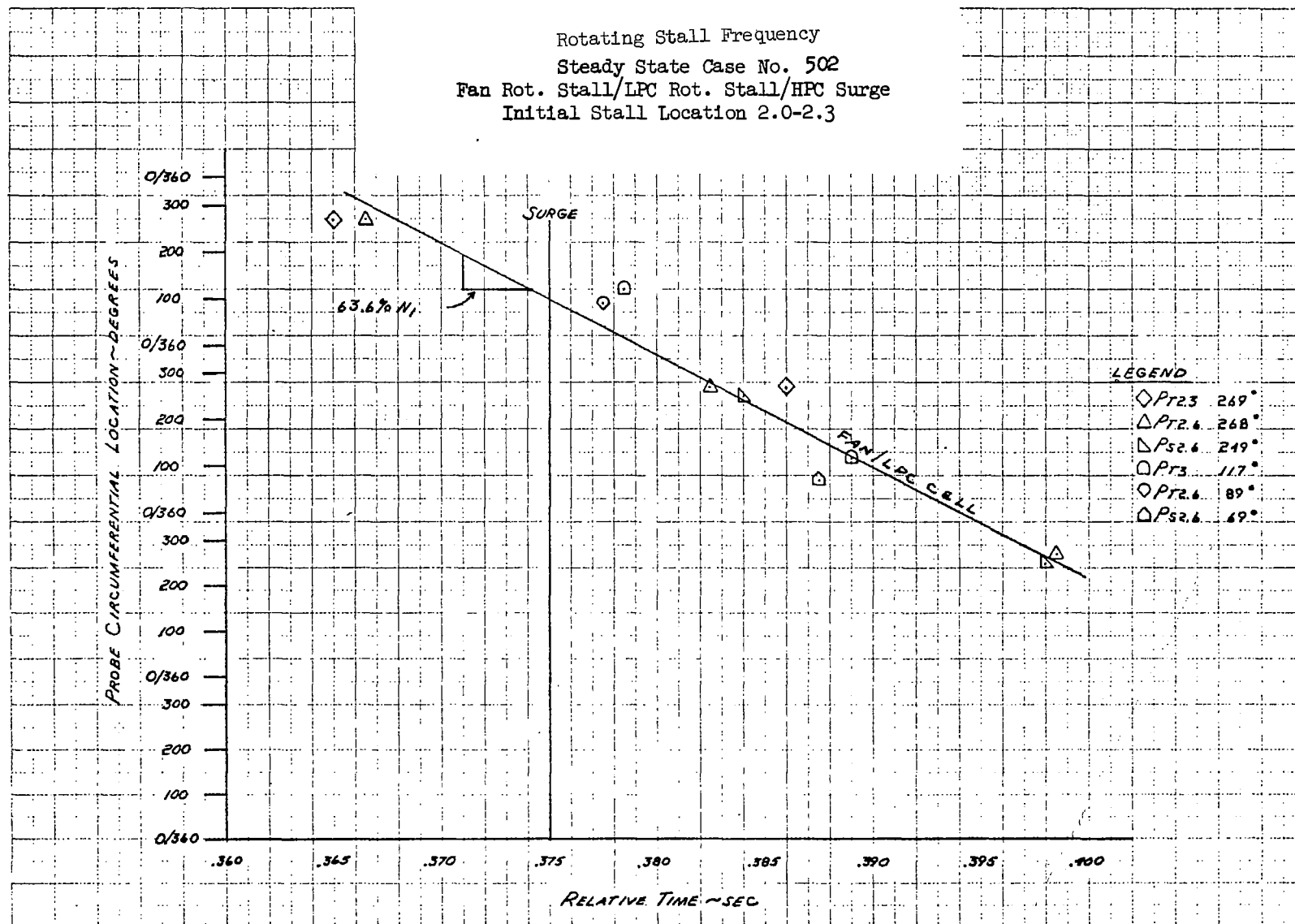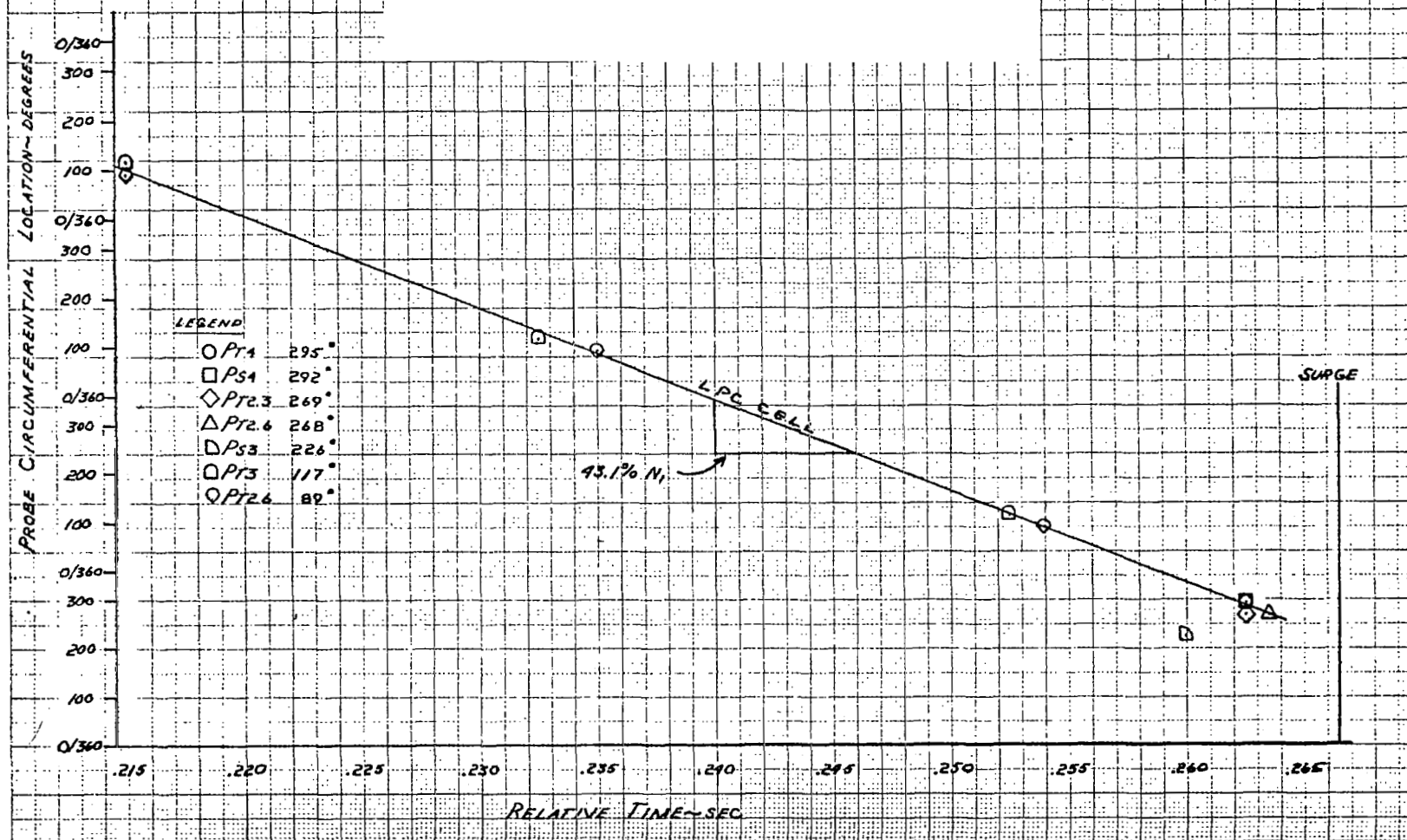
.390   .395   .400   .405   .410

RELATIVE TIME ~ SEC

120

Rotating Stall Frequency
Steady State Case No. 502
Fan Rot. Stall/LPC Rot. Stall/HPC Surge
Initial Stall Location 2.0-2.3

Rotating Stall Frequency
Steady State Case No. 528
LPC Rot. Stall/HPC Surge
Initial Stall Location 2.3-2.6

LEGEND

○ Pr4   295°
□ Ps4   292°
◇ Pr2.3 269°
△ Pr2.6 268°
⬠ Ps3   226°
⬡ Pr3   117°
⬠ Pr2.6 89°

43.1% N₁

LPC CELL

SURGE

PROBE CIRCUMFERENTIAL LOCATION~ DEGREES

RELATIVE TIME~SEC

122

Rotating Stall Frequency
Steady State Case No. 537
LPC Rot. Stall/HPC Surge
Initial Stall Location 2.3-2.6

LEGEND
◇ $P_{T2.3}$ 269°
△ $P_{T2.6}$ 268°
◺ $P_{S2.6}$ 249°
▱ P_{S3} 117°
◯ $P_{T2.6}$ 89°
△ $P_{S2.6}$ 89°

SURGE

57.2% N_1

LPC CELL

PROBE CIRCUMFERENTIAL LOCATION~DEGREES

0/360
300
200
100
0/360
300
200
100
0/360

.370   .375   .380   .385   .390

RELATIVE TIME ~SEC

123

Rotating Stall Frequency
Steady State Case No. 561
LPC Rot. Stall/HPC Surge
Initial Stall Location 2.3-2.6

LEGEND
$\triangle P_{T2.6}$ 268°
$\triangle P_{S2.6}$ 249°

SURGE

51.0% N_1

LPC CELL

PROBE CIRCUMFERENTIAL LOCATION~DEGREES

O/360
300
200
100
O/360
300
200
100
O/360

.330   .335   .340   .345   .350   .355   .360

RELATIVE TIME ~SEC

124

Rotating Stall Frequency
Steady State Case No. 451
LPC Rot. Stall/HPC Surge
Initial Stall Location 2.3-2.6

LEGEND

- ○ P_{T4} 295°
- □ P_{S4} 292°
- ◇ $P_{T2.3}$ 269°
- △ $P_{T2.6}$ 268°
- ▷ $P_{S2.6}$ 249°
- ▷ P_{S3} 226°
- ○ P_{T3} 117°
- ○ $P_{T2.6}$ 89°
- △ $P_{S2.6}$ 69°

PROBE CIRCUMFERENTIAL LOCATION—DEGREES

0/360
300
200
100
0/360
300
200
100
0/360

LPC CELL
53.8% N_r
SURGE

RELATIVE TIME — SEC

.370   .375   .380   .385   .390

JAS 1-22-75

125

Rotating Stall Frequency
Steady State Case No. 461
Fan Rot. Stall/LPC Rot. Stall/HPC Surge
Initial Stall Location 2.0-2.3

LEGEND
○ PT1   295°
□ PS1   292°
◇ PT2.3 269°
△ PT2.6 268°
◁ PS2.6 249°
⬠ PT3   117°
⬡ PT2.6 89°

SURGE

FAN/LPC CELL

60.7% N1

PROBE CIRCUMFERENTIAL LOCATION~DEGREES

RELATIVE TIME ~ SEC

.380 .385 .390 .395 .400

100
0/360
300
200
100
0/360
300
200
100
0/360

126

Rotating Stall Frequency

Steady State Case No. 471
LPC Rot. Stall/HPC Rot. Stall/HPC Surge
Initial Stall Location 2.3-2.6

Rotating Stall Frequency
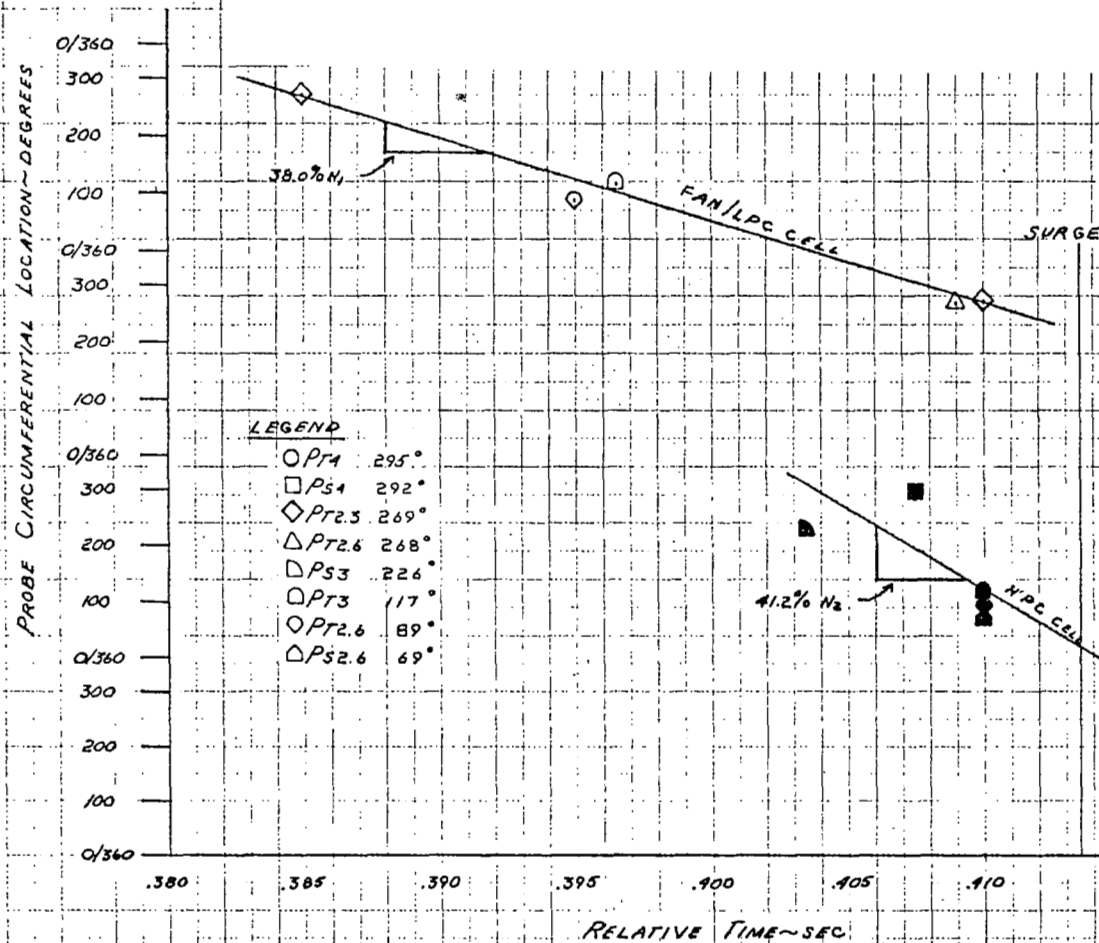Steady State Case No. 497
Fan Rot. Stall/LPC Rot. Stall/HPC Rot. Stall/HPC Surge
Initial Stall Location 2.0-2.3

LEGEND
○ Pr4   295°
□ Ps4   292°
◇ Pr2.5 269°
△ Pr2.6 268°
◻ Ps3   226°
○ Pr3   117°
◇ Pr2.6   89°
△ Ps2.6   69°

38.0% N1
FAN/LPC CELL
SURGE
41.2% N2
HPC CELL

PROBE CIRCUMFERENTIAL LOCATION~DEGREES

RELATIVE TIME~SEC

.380 .385 .390 .395 .400 .405 .410 .416 .420

0/360 300 200 100 0/360 300 200 100 0/360 300 200 100 0/360 300 200 100 0/360

Rotating Stall Frequency
Steady State Case No. 515
LPC Rot. Stall/HPC Surge
Initial Stall Location 2.3-2.6

LEGEND
◇ Pт2.3 269°
△ Pт2.6 268°
◁ Ps2.6 249°
⬠ Pт3   117°
◇ Pт2.6 89°
△ Ps2.6 69°

LPC CELL

SURGE

49.4% N₁

PROBE CIRCUMFERENTIAL LOCATION~DEGREES

0/360
300
200
100
0/360
300
.200
100
0/360

RELATIVE TIME~ SEC

.420 .425 .430 .435 .440 .445 .450

129

Rotating Stall Frequency
Steady State Case No. 540
LPC Rot. Stall/HPC Surge
Initial Stall Location 2.3-2.6

SURGE

LEGEND

◇ Pt 2.3   269°
△ Pt 2.6   268°
⬡ Pt 2.6   89°

LPC CELL

53.1% N₁

PROBE CIRCUMFERENTIAL LOCATION ~ DEGREES

0/360
300
200
100
0/360
300
200
100
0/360

.390   .395   .400   .405   .410

RELATIVE TIME ~ SEC

130

TABLE D1

NASA Lewis
TF30-P-3 60-40 Mixed Compression Inlet Testing
K_{D2} - ΔP_{t2} RMS

Pt. No.	Bleed		Steady State K_{D2}	Turbulence Unfiltered 0-1000 Hz	Turbulence % 0-150 Hz	WATC pps	A_j/Alpha	Comments
	7th	12th						
384	O	C	404	7.1	4.34	148.6	100%/0°	
389	O	C	385	7.29	4.29	159.7	100%/0°	
405	O	C	432	7.87	4.66	168.4	140%/0°	
408	O	C	267	5.23	3.26	144.7	83%/0°	
421	O	C	806	3.85	2.66	159.0	100%/2.3°	
438	O	C	899	3.97	2.39	171.8	140%/2.3°	
441	O	C	796	3.78	3.17	171.7	140%/2.73°	
445	O	C	859	3.26	2.19	146.9	83%/2.3°	
451	C	C	809	1.97	1.01	148.5	100%/3.8°	
457	O	C	1198	2.50	1.42	150.1	100%/5.6°	
461	C	C	570	2.17	1.15	145.9	100%/2.24°	
464	O	C	643	2.66	1.92	159.9	100%/2.88°	Non-stationary activity
467	O	C	799	2.70	1.02	159.4	100%/3.04°	Non-stationary activity
471	C	C	392	2.02	0.95	155.1	100%/1.91°	Non-stationary activity
497	C	C	734	2.31	1.53	142.6	83%/2.09°	
502	O	C	897	2.54	1.37	151.0	100%/3.53°	
515	C	C	702	2.60	1.50	149.0	100%/0°	
519	O	O	420	7.74	4.76	147.9	100%/0°	
528	O	C	432	8.17	4.34	171.4	120%/0°	
537	O	C	760	3.93	3.09	153.0	100%/1.55°	
540	C	C	641	3.12	2.18	149.4	100%/1.55°	
561	O	C	621	3.53	2.68	145.8	83%/1.55°	

POINT NUMBER   3830

ALPHA(DEGREES)   0.0
BETA(DEGREES)   0.0
MAP DISTORTION FACTOR(KD)   418.27
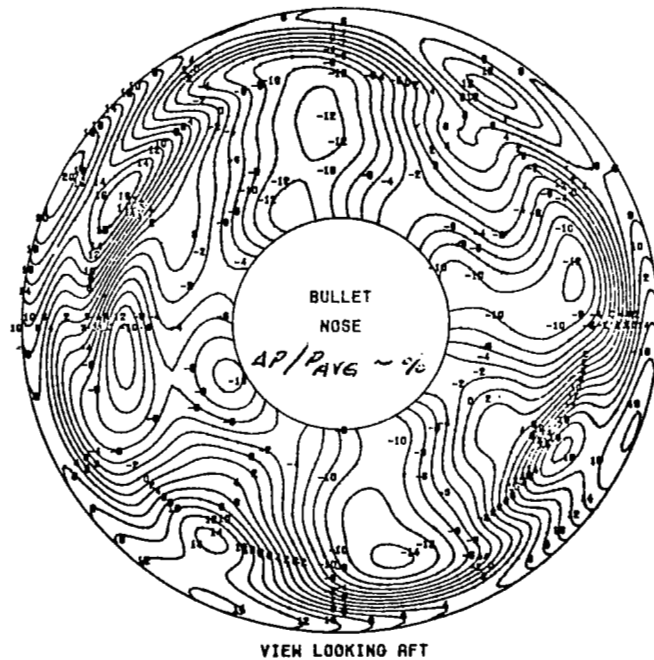
VIEW LOOKING AFT
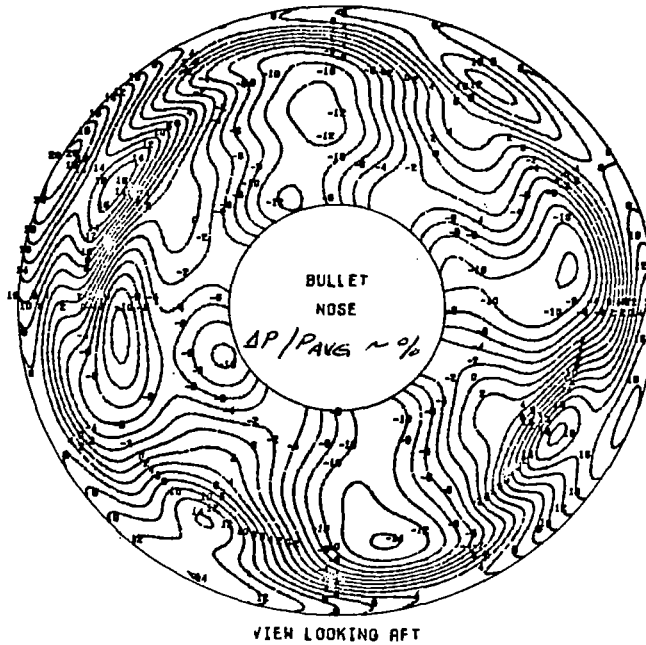
PRATT & WHITNEY AIRCRAFT

ENGINE TF30 TURBOFAN

TF30P3 10X10   NASA/LEWIS 60/40 INLET TEST TF30P-3 TURB.

POINT NUMBER   3830

TURBULENCE(AVERAGE)   7.1728
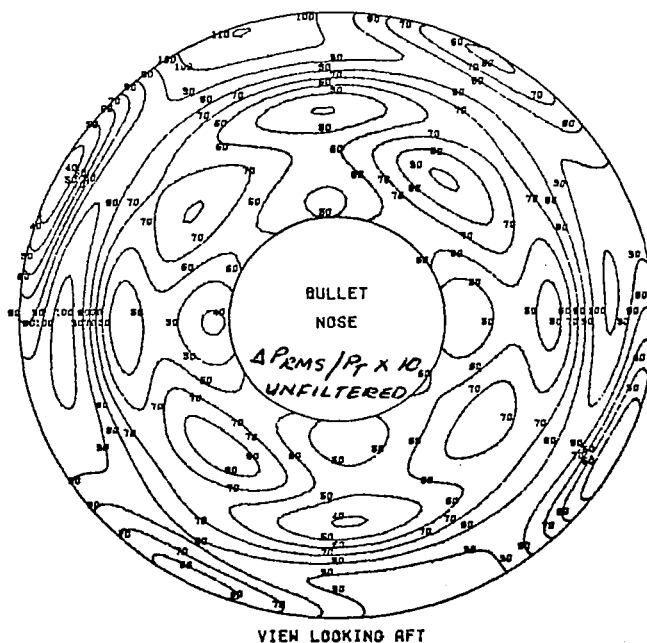TURBULENCE(HIGHEST QUADRANT)   8.6223
ISOBAR(10=1 O/O DELTA PRMS/PT)
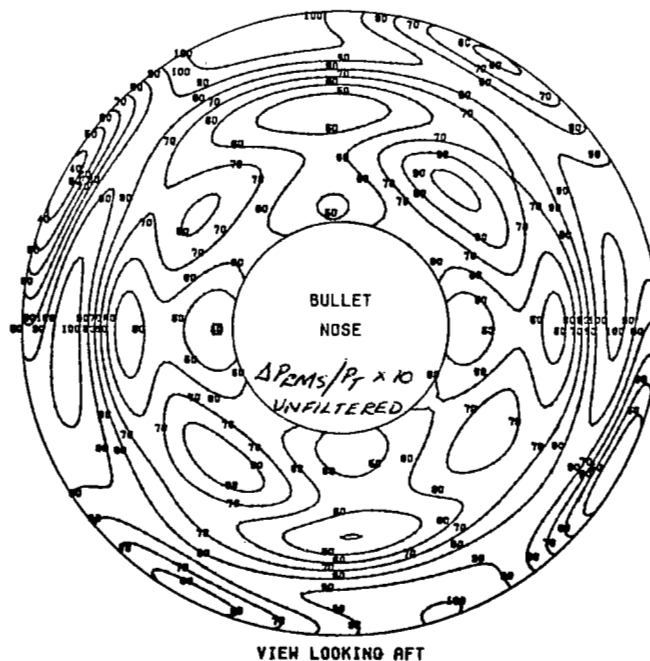
VIEW LOOKING AFT

132

POINT NUMBER   3840

WATC   148.60

ALPHA(DEGREES)   0.0

BETA(DEGREES)   0.0
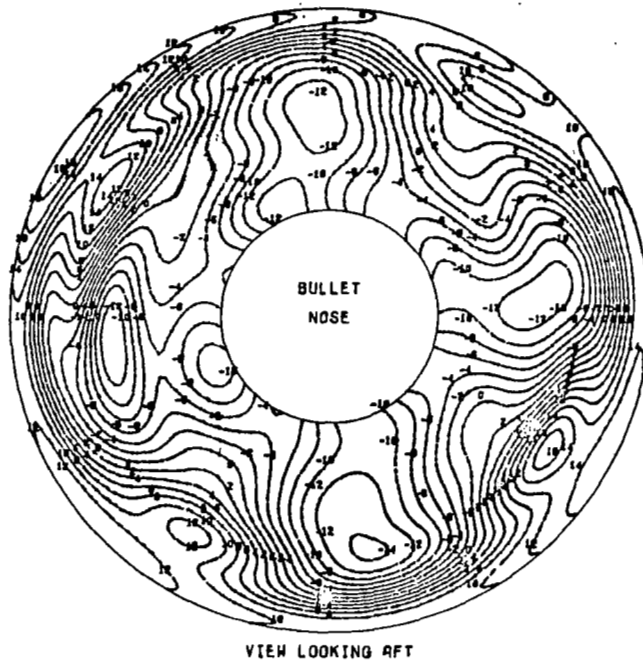
MAP DISTORTION FACTOR(KD)   401.15

BULLET
NOSE
$\Delta P / P_{AVG} \sim \%$

VIEW LOOKING AFT

PRATT & WHITNEY AIRCRAFT

ENGINE TF30 TURBOFAN

TF30P3 10X10   NASA/LEWIS 60/40 INLET TEST TF30P-3 TURB.

POINT NUMBER   3840

TURBULENCE(AVERAGE)   7.0921

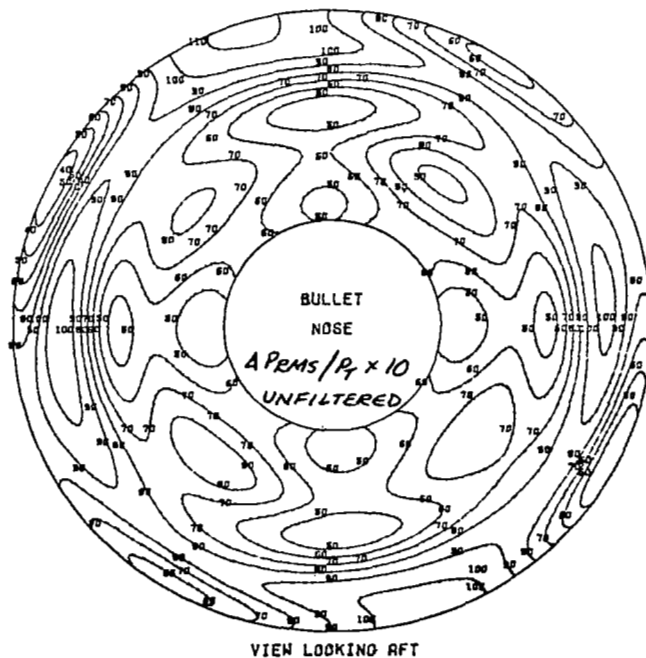TURBULENCE(HIGHEST QUADRANT)   8.5858

ISOBAR(10=1 0/0 DELTA PRMS/PT)

BULLET
NOSE
$\Delta P_{RMS} / P_T \times 10$
UNFILTERED

VIEW LOOKING AFT

PRATT & WHITNEY AIRCRAFT

ENGINE TF30 TURBOFAN

TF30P3 10X10 NASA/LEWIS 60/40 INLET TEST/TF30P-3 KD2

POINT NUMBER 3890

WATC 159.70

ALPHA(DEGREES) 0.0

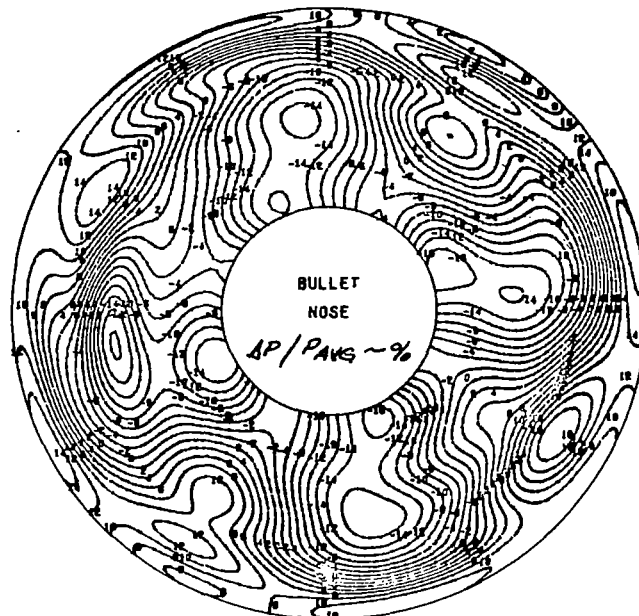BETA(DEGREES) 0.0

MAP DISTORTION FACTOR(KD) 384.26

BULLET
NOSE

VIEW LOOKING AFT

PRATT & WHITNEY AIRCRAFT

ENGINE TF30 TURBOFAN

TF30P3 10X10 NASA/LEWIS 60/40 INLET TEST TF30P-3 TURB.

POINT NUMBER 3890

TURBULENCE(AVERAGE) 7.2785

TURBULENCE(HIGHEST QUADRANT) 8.9130

ISOBAR(10=1 0/0 DELTA PRMS/PT)

BULLET
NOSE

$\Delta PRMS / P_T \times 10$
UNFILTERED

VIEW LOOKING AFT

134

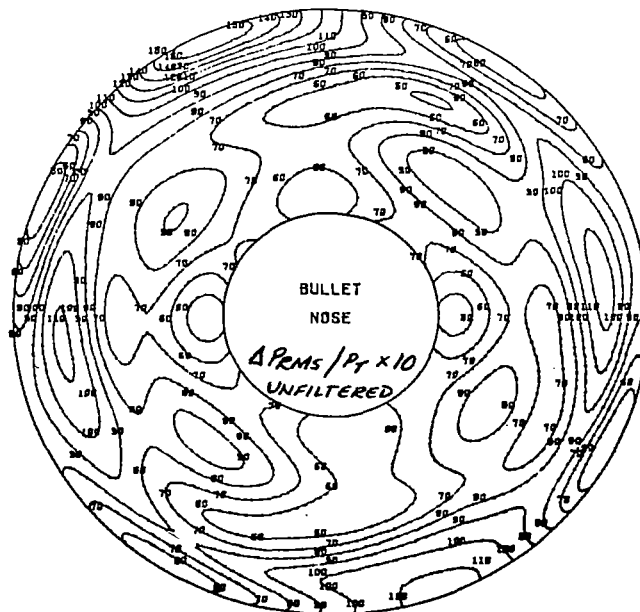POINT NUMBER   4050

WATC   168.40

ALPHA(DEGREES)   0.0

BETA(DEGREES)   0.0

MAP DISTORTION FACTOR(KD)   429.63

BULLET

NOSE

$\Delta P / P_{AVG} \sim \%$

VIEW LOOKING AFT

PRATT & WHITNEY AIRCRAFT

ENGINE TF30 TURBOFAN

TF30P3 10X10   NASA/LEWIS 60/40 INLET TEST TF30P-3 TURB.

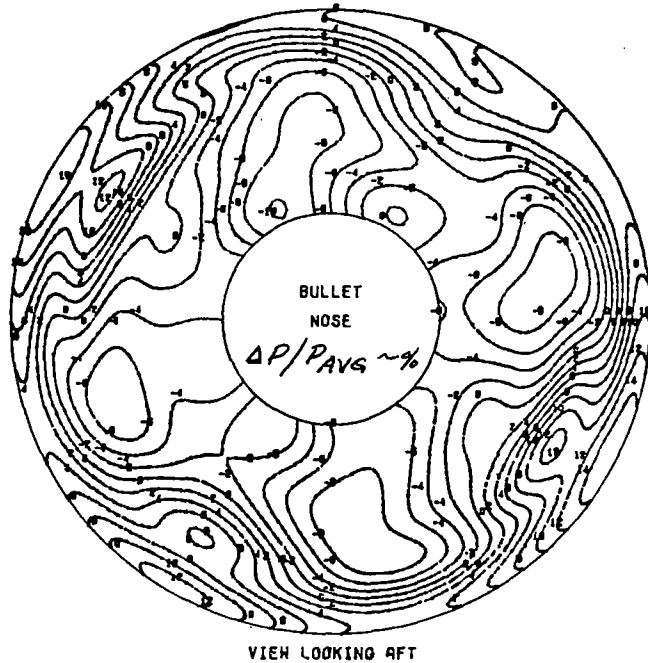POINT NUMBER   4050

TURBULENCE(AVERAGE)   7.8730

TURBULENCE(HIGHEST QUADRANT) 10.3847

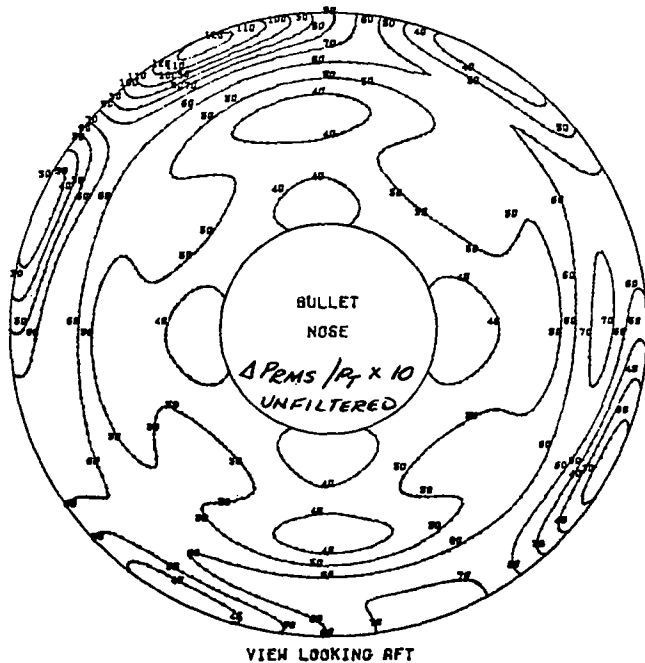ISOBAR(10=1 O/O DELTA PRMS/PT)

BULLET

NOSE

$\Delta P_{RMS} / P_T \times 10$

UNFILTERED

VIEW LOOKING AFT

135

POINT NUMBER   4080
WATC   144.70
ALPHA(DEGREES)   0.0
BETA(DEGREES)   0.0
MAP DISTORTION FACTOR(KD)   264.80

BULLET
NOSE
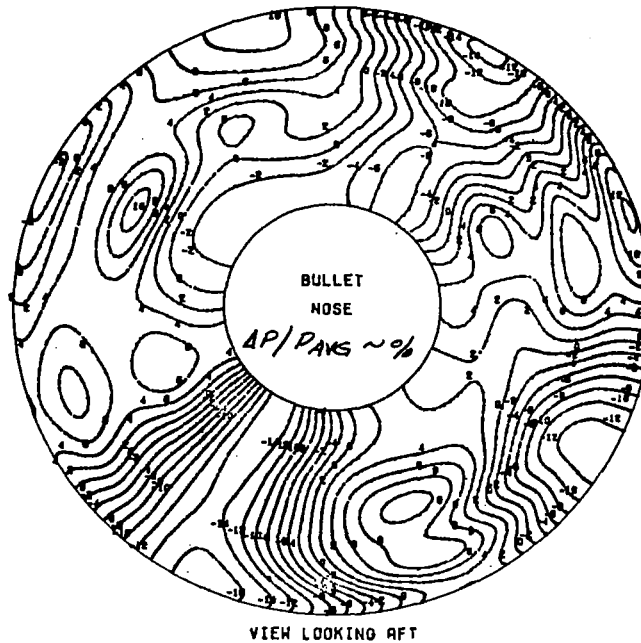$\Delta P / P_{AVG} \sim \%$

VIEW LOOKING AFT

POINT NUMBER   4080

TURBULENCE(AVERAGE)   5.2339
TURBULENCE(HIGHEST QUADRANT)   7.2508
ISOBAR(10=1 0/0 DELTA PRMS/PT)

BULLET
NOSE
$\Delta P_{RMS} / P_T \times 10$
UNFILTERED

VIEW LOOKING AFT

136

POINT NUMBER   4210
WATC   169.00
ALPHA(DEGREES)   2.36
BETA(DEGREES)   0.0
MAP DISTORTION FACTOR(KD)   805.33

BULLET
NOSE
$\Delta P / P_{AVG} \sim \%$

VIEW LOOKING AFT

POINT NUMBER   4210

TURBULENCE(AVERAGE)   3.8474
TURBULENCE(HIGHEST QUADRANT) 5.1416
ISOBAR(10=1 O/O DELTA PRMS/PT)
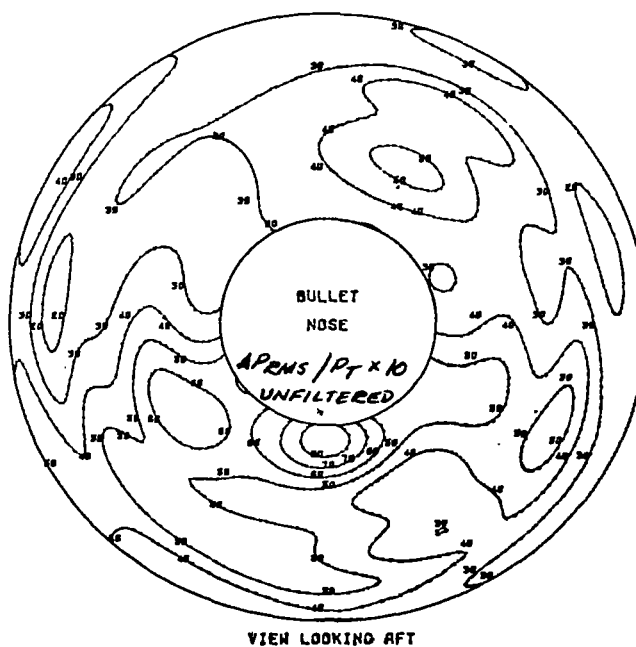
BULLET
NOSE
$\Delta P_{RMS} / P_T \times 10$
UNFILTERED

VIEW LOOKING AFT

137
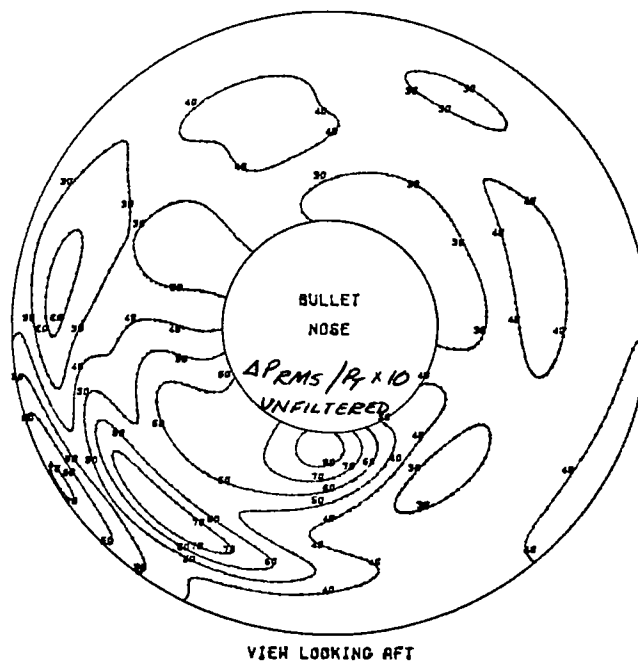
ENGINE TF30 TURBOFAN

TF30P3 10X10   NASA/LEWIS 60/40 INLET TEST/TF30P-3 K02

POINT NUMBER   4380

WATC   171.30

ALPHA(DEGREES)   2.37

BETA(DEGREES)   0.0

MAP DISTORTION FACTOR(KD)   899.56
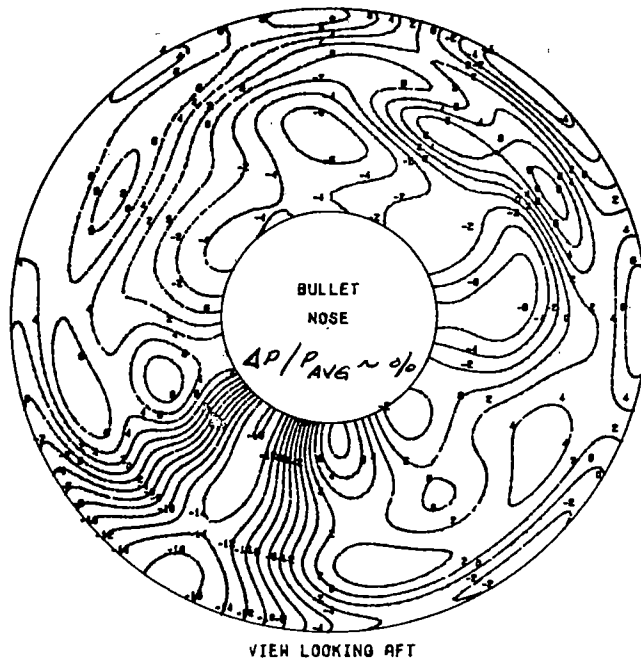
BULLET

NOSE

$\Delta P / P_{AVG} \sim \%$

VIEW LOOKING AFT
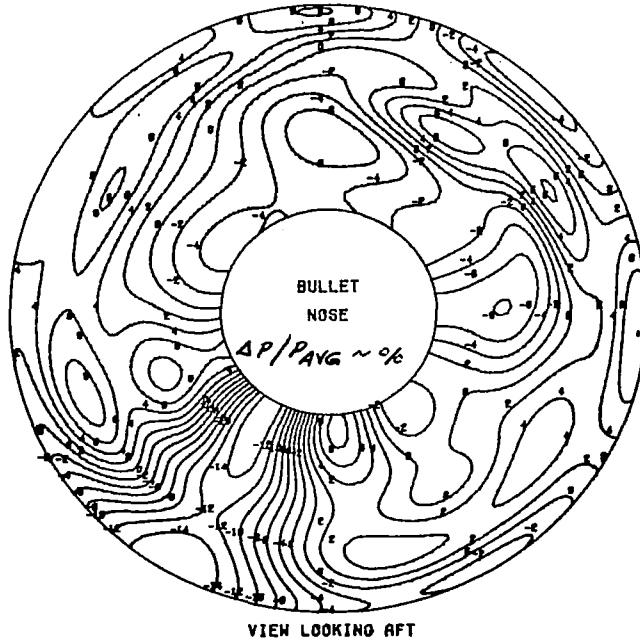
PRATT & WHITNEY AIRCRAFT

ENGINE TF30 TURBOFAN

TF30P3 10X10   NASA/LEWIS 60/40 INLET TEST TF30P-3 TURB.

POINT NUMBER   4380

TURBULENCE(AVERAGE)   3.9656

TURBULENCE(HIGHEST QUADRANT)   5.9223

ISOBAR(10=1 0/0 DELTA PRMS/PT)

BULLET

NOSE

$\Delta P_{RMS} / P_T \times 10$

UNFILTERED

VIEW LOOKING AFT

138

POINT NUMBER   4410

ALPHA(DEGREES)   2.37
BETA(DEGREES)   0.0
MAP DISTORTION FACTOR(KD)   796.12

BULLET
NOSE
$\Delta P / P_{AVG} \sim \%$

VIEW LOOKING AFT

PRATT & WHITNEY AIRCRAFT

ENGINE TF30 TURBOFAN

TF30P3 10X10 NASA/LEWIS 60/40 INLET TEST TF30P-3 TURB.

POINT NUMBER   4410

TURBULENCE(AVERAGE)   3.7760
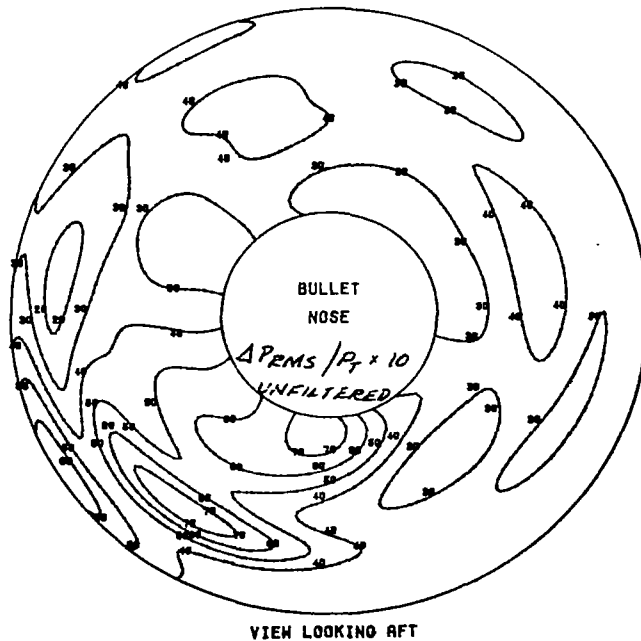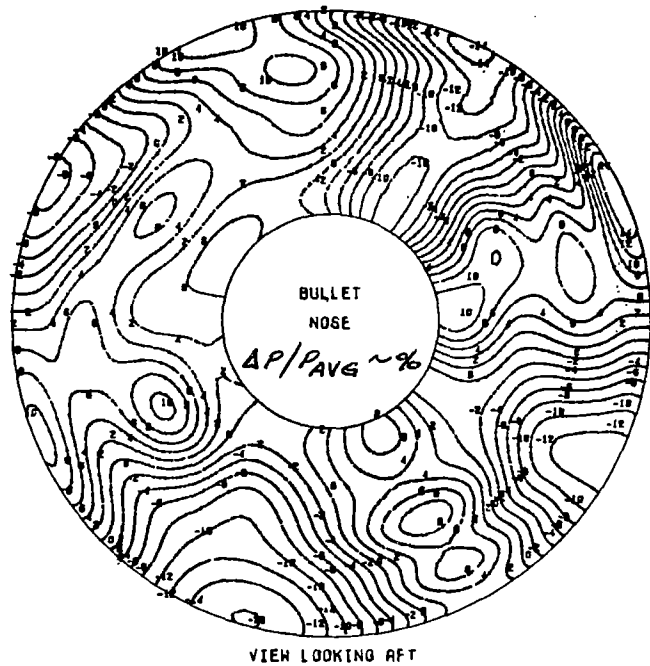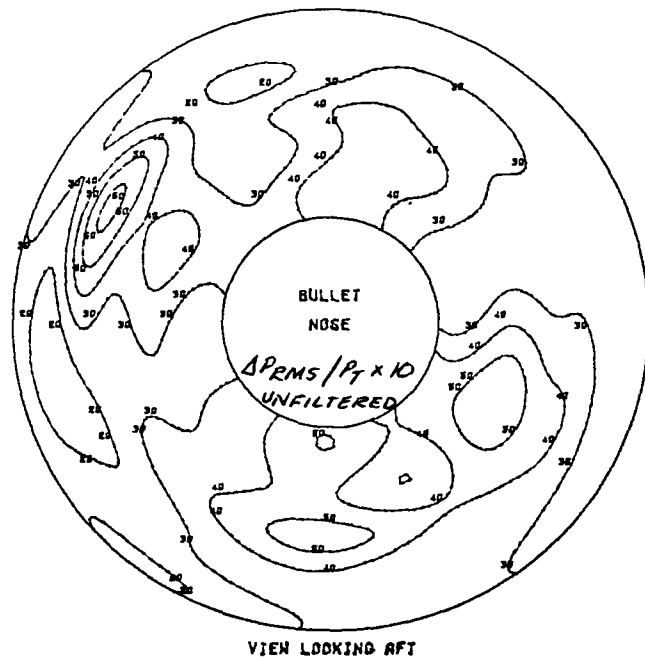TURBULENCE(HIGHEST QUADRANT)   5.4786
ISOBAR(10=1 0/0 DELTA PRMS/PT)

BULLET
NOSE
$\Delta P_{RMS} / P_T \times 10$
UNFILTERED

VIEW LOOKING AFT

POINT NUMBER   4450

WATC   146.90

ALPHA(DEGREES)   2.38

BETA(DEGREES)   0.0

MAP DISTORTION FACTOR(KD)   656.41

BULLET
NOSE
$\Delta P/P_{AVG} \sim \%$

VIEW LOOKING AFT

POINT NUMBER   4450

TURBULENCE(AVERAGE)   3.2550

TURBULENCE(HIGHEST QUADRANT)   3.8659

ISOBAR(10=1 O/O DELTA PRMS/PT)

BULLET
NOSE
$\Delta P_{RMS}/P_T \times 10$
UNFILTERED

VIEW LOOKING AFT

140

PRATT & WHITNEY AIRCRAFT

ENGINE TF30 TURBOFAN

TF30P3 10X10 NASA/LEWIS 60/40 INLET TEST/TF30P-3 K02

POINT NUMBER	451.0
WATC	148.50
ALPHA(DEGREES)	3.78
BETA(DEGREES)	0.0
MAP DISTORTION FACTOR(KD)	811.00

BULLET NOSE

$\Delta P/P_{AVG} \sim \%$

VIEW LOOKING AFT

PRATT & WHITNEY AIRCRAFT

ENGINE TF30 TURBOFAN

TF30P3 10X10 NASA/LEWIS 60/40 INLET TEST TF30P-3 TURB.
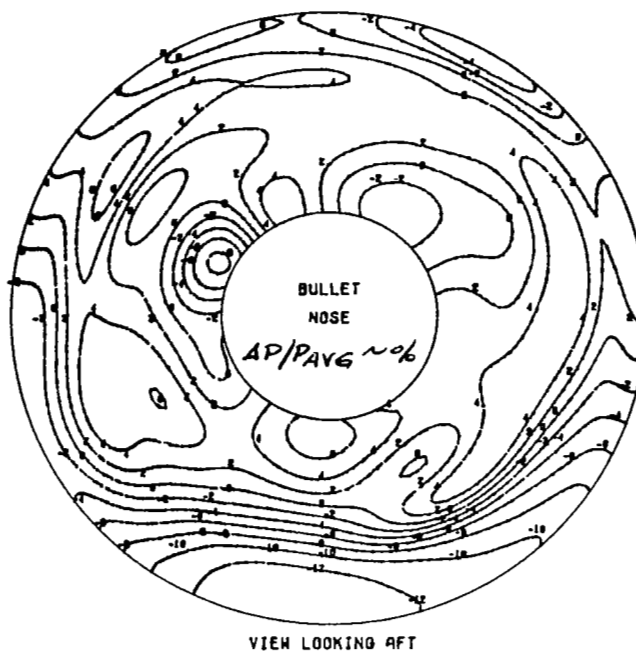
POINT NUMBER	451.0
TURBULENCE(AVERAGE)	1.9697
TURBULENCE(HIGHEST QUADRANT)	2.6426
ISOBAR(10=1 O/O DELTA PRMS/PT)	
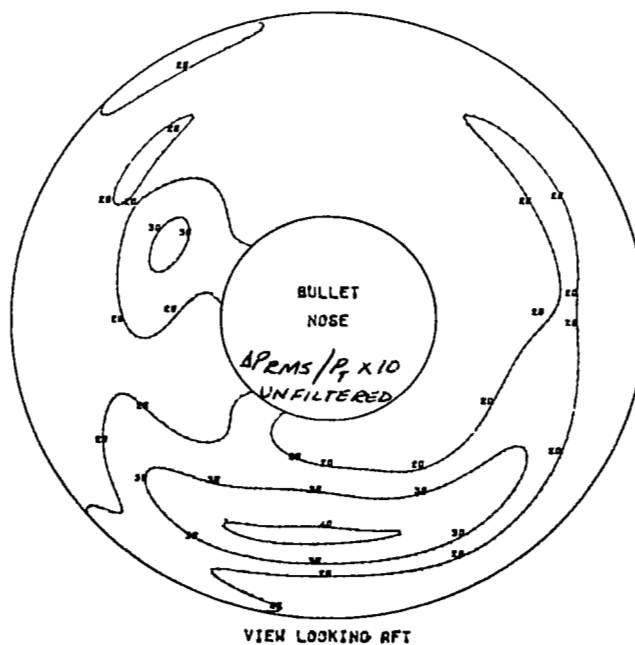
BULLET NOSE

$\Delta P_{RMS}/P_T \times 10$ (UNFILTERED)

VIEW LOOKING AFT

141

POINT NUMBER   457.0

WATC   150.10

ALPHA(DEGREES)   5.60

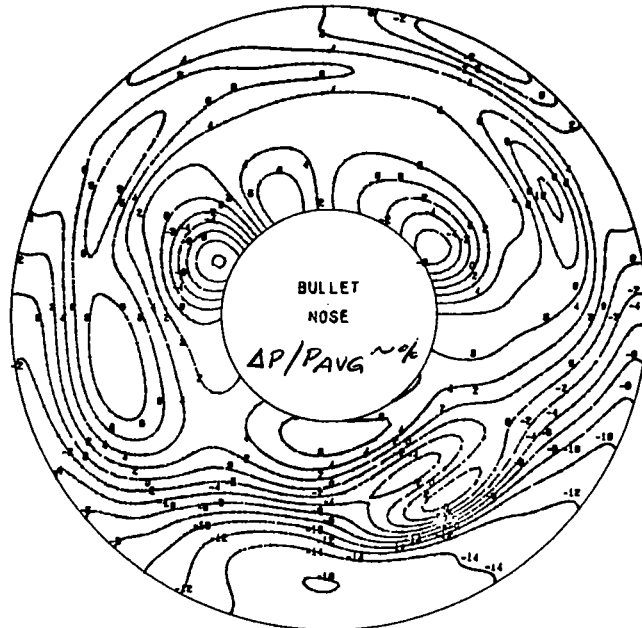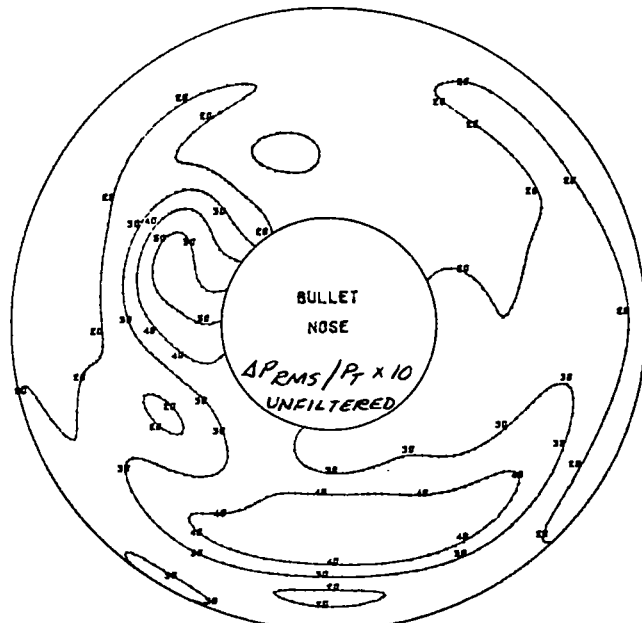BETA(DEGREES)   0.0

MAP DISTORTION FACTOR(KD)   1198.96

BULLET
NOSE

$\Delta P / P_{AVG} \sim \%$

VIEW LOOKING AFT

PRATT & WHITNEY AIRCRAFT

ENGINE TF30 TURBOFAN

TF30P3 10X10   NASA/LEWIS 60/40 INLET TEST TF30P-3 TURB.

POINT NUMBER   457.0

TURBULENCE(AVERAGE)   2.4986

TURBULENCE(HIGHEST QUADRANT)   3.3284

ISOBAR(10=1 O/O DELTA PRMS/PT)

BULLET
NOSE

$\Delta P_{RMS} / P_T \times 10$
UNFILTERED

VIEW LOOKING AFT

142

PRATT & WHITNEY AIRCRAFT

ENGINE TF30 TURBOFAN

TF30P3 10X10   NASA/LE+IS 60/40 INLET TEST TF30P-3 KD2

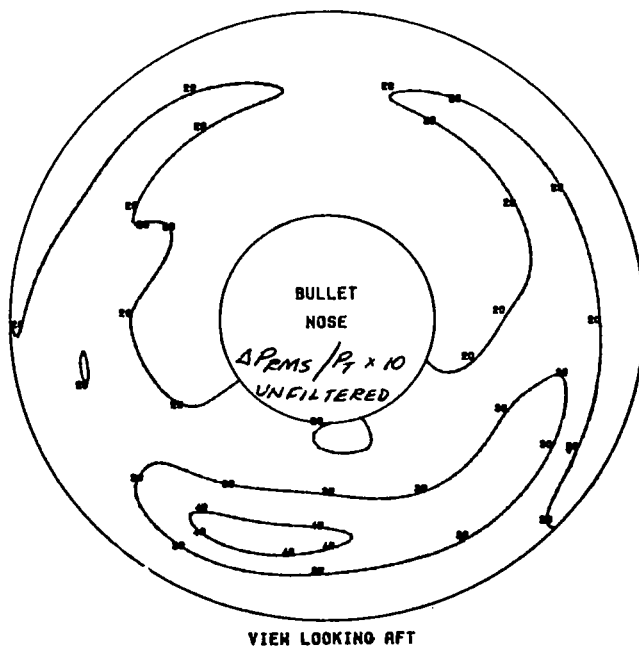POINT NUMBER   46 L0

ALPHA(DEGREES)   2.24
BETA(DEGREES)   0.0
MAP DISTORTION FACTOR(KD)   570.13
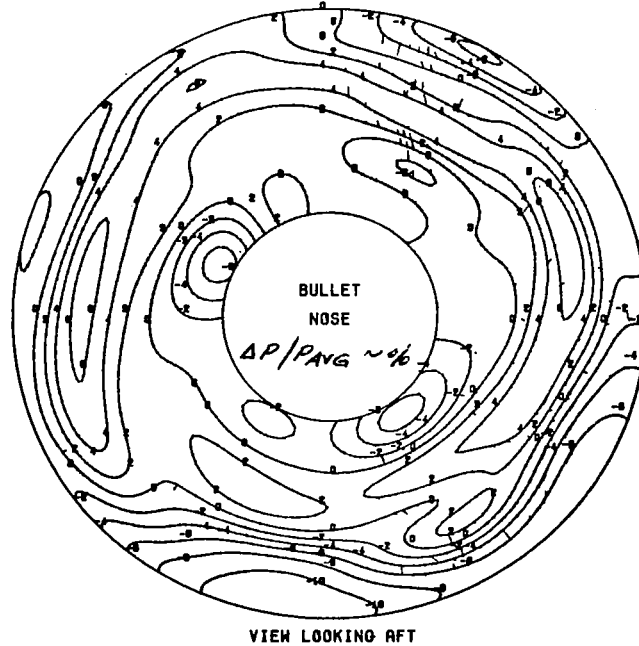
BULLET
NOSE
$\Delta P / P_{AVG} \sim \%$
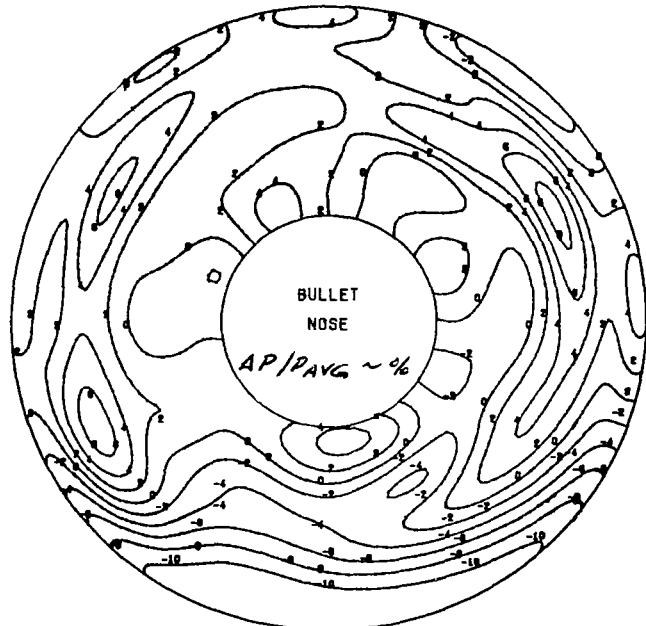
VIEW LOOKING AFT

PRATT & WHITNEY AIRCRAFT

ENGINE TF30 TURBOFAN

TF30P3 10X10   NASA/LEWIS 60/40 INLET TEST TF30P-3 TURB.

POINT NUMBER   46 L0

TURBULENCE(AVERAGE)   2.1736
TURBULENCE(HIGHEST QUADRANT)   3.0133
ISOBAR(10=1 O/O DELTA PRMS/PT)

BULLET
NOSE
$\Delta P_{RMS} / P_T \times 10$
UNFILTERED

VIEW LOOKING AFT

143

PRATT & WHITNEY AIRCRAFT

ENGINE TF30 TURBOFAN

TF30P3 10X10 NASA/LEWIS 60/40 INLET TEST TF30P-3 KD2

POINT NUMBER   4640

ALPHA(DEGREES)   2.28
BETA(DEGREES)   0.0
MAP DISTORTION FACTOR(KD)   643.44

BULLET
NOSE

$\Delta P/P_{AVG} \sim \%$

VIEW LOOKING AFT

PRATT & WHITNEY AIRCRAFT

ENGINE TF30 TURBOFAN

TF30P3 10X10 NASA/LEWIS 60/40 INLET TEST TF30P-3 TURB.

POINT NUMBER   4640

TURBULENCE(AVERAGE)   2.6625
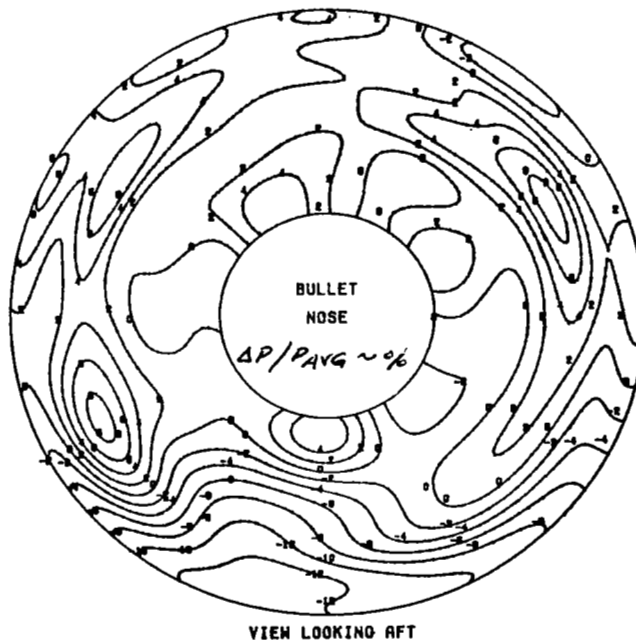TURBULENCE(HIGHEST QUADRANT)   4.7016
ISOBAR(10=1 0/0 DELTA PRMS/PT)
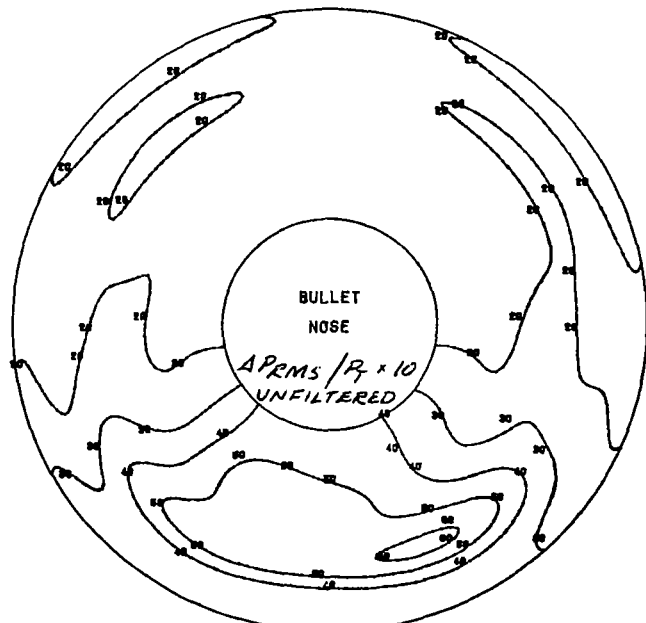
BULLET
NOSE

$\Delta P_{RMS}/P_{f} \times 10$
UNFILTERED

VIEW LOOKING AFT

144

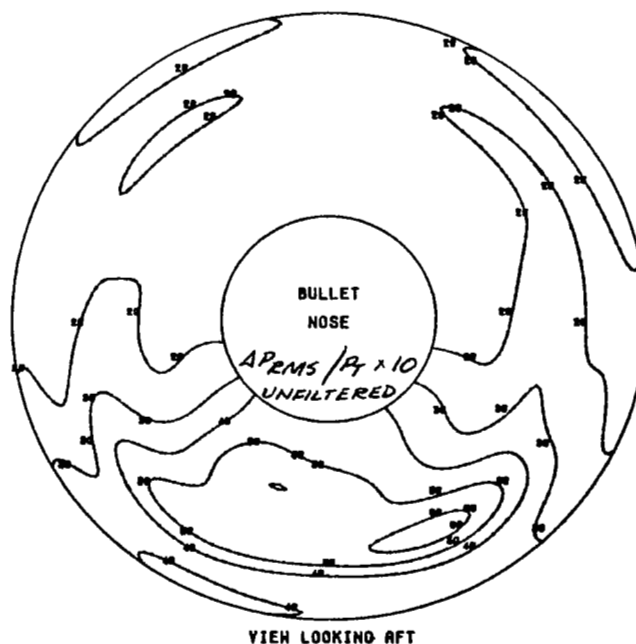PRATT & WHITNEY AIRCRAFT

ENGINE TF30 TURBOFAN

TF30P3 10X10   NASA/LE+IS 60/40 INLET TEST TF30P-3 KD2

POINT NUMBER   467.0

ALPHA(DEGREES)   3.04
BETA(DEGREES)   0.0
MAP DISTORTION FACTOR(KD)   799.99

BULLET
NOSE

$\Delta P / P_{AVG} \sim \%$

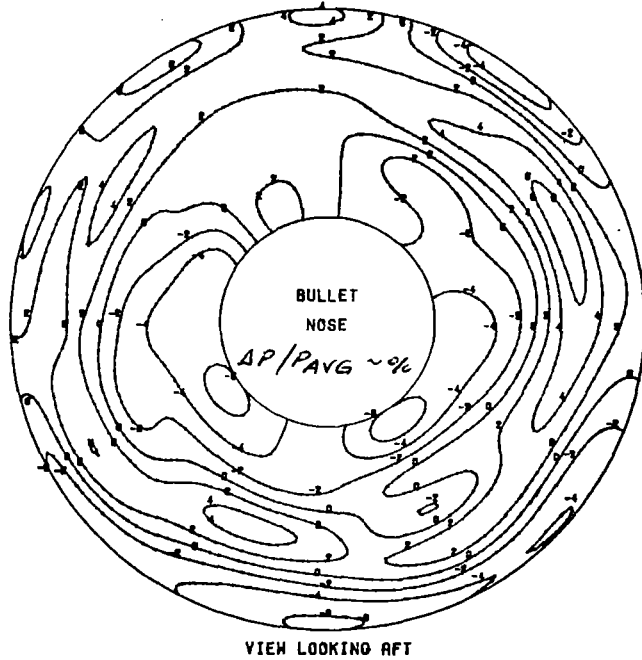VIEW LOOKING AFT

PRATT & WHITNEY AIRCRAFT

ENGINE TF30 TURBOFAN

TF30P3 10X10   NASA/LEWIS 60/40 INLET TEST TF30P-3 TURB.

POINT NUMBER   467.0

TURBULENCE(AVERAGE)   2.7029
TURBULENCE(HIGHEST QUADRANT)   4.8078
ISOBAR(10=1 O/O DELTA PRMS/PT)

BULLET
NOSE

$\Delta P_{RMS} / P_T \times 10$
UNFILTERED

VIEW LOOKING AFT

145

POINT NUMBER   471.0

ALPHA(DEGREES)   1.91
BETA(DEGREES)   0.0
MAP DISTORTION FACTOR(KD)   392.49

BULLET
NOSE

$\Delta P / P_{AVG} \sim \%$

VIEW LOOKING AFT

POINT NUMBER   471.0

TURBULENCE(AVERAGE)   2.0148
TURBULENCE(HIGHEST QUADRANT)   2.3004
ISOBAR(10=1 O/O DELTA PRMS/PT)

BULLET
NOSE

$\Delta P_{RMS} / P_T \times 10$
UNFILTERED

VIEW LOOKING AFT

146
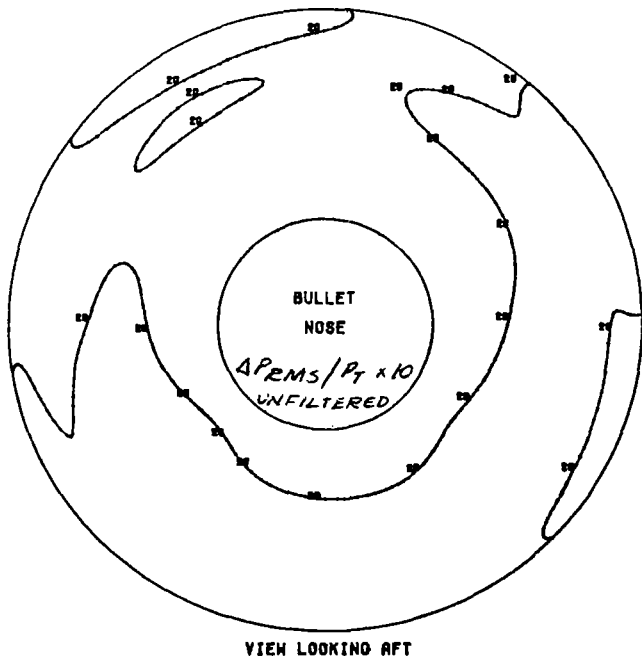
PRATT & WHITNEY AIRCRAFT

ENGINE TF30 TURBOFAN

TF30P3 10X10   NASA/LEWIS 60/40 INLET TEST TF30P-3 KD2

POINT NUMBER   4970

ALPHA(DEGREES)   2.09
BETA(DEGREES)   0.0
MAP DISTORTION FACTOR(KD)   734.69

BULLET
NOSE

$\Delta P/P_{AVG} \sim \%$
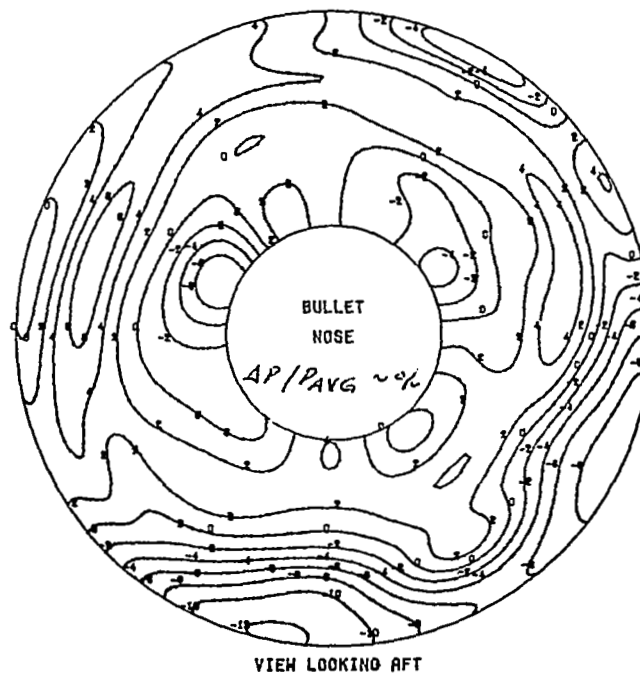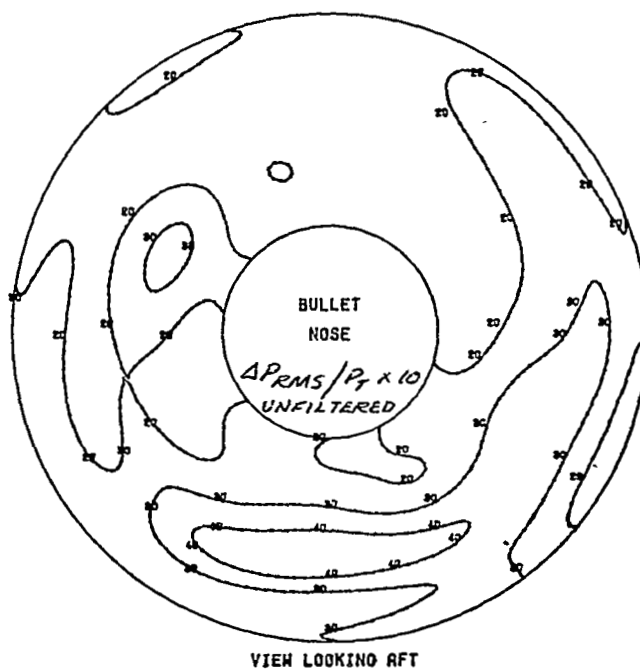
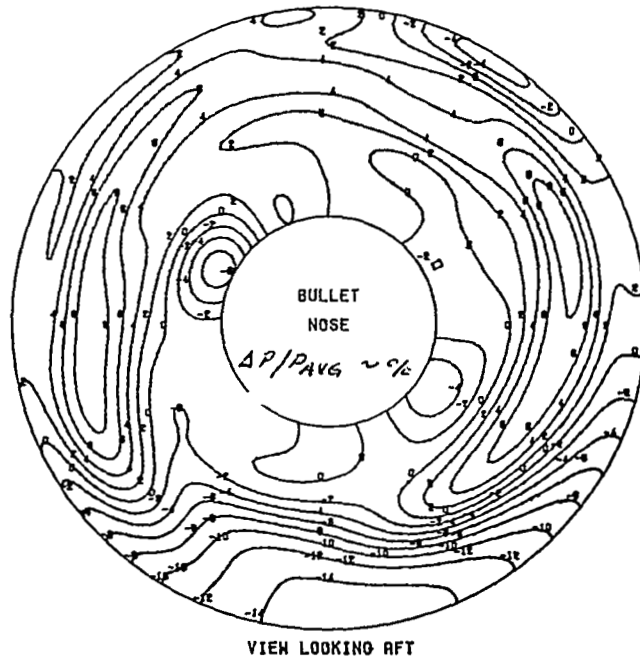VIEW LOOKING AFT

PRATT & WHITNEY AIRCRAFT

ENGINE TF30 TURBOFAN

TF30P3 10X10   NASA/LEWIS 60/40 INLET TEST TF30P-3 TURB.

POINT NUMBER   4970

TURBULENCE(AVERAGE)   2.3123
TURBULENCE(HIGHEST QUADRANT)   3.1240
ISOBAR(10=1 O/O DELTA PRMS/PT)

BULLET
NOSE

$\Delta P_{RMS}/P_T \times 10$
UNFILTERED

VIEW LOOKING AFT
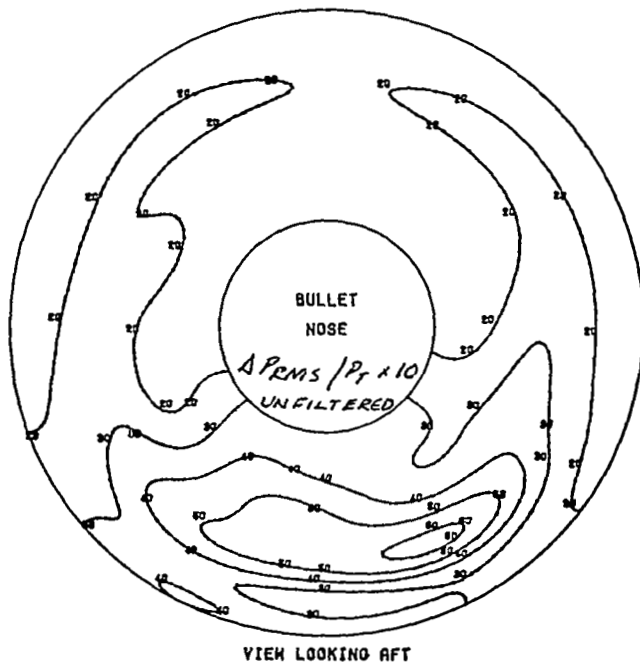
PRATT & WHITNEY AIRCRAFT

ENGINE TF30 TURBOFAN

TF30P3 10X10 NASA/LE+IS 60/40 INLET TEST TF30P-3 KD2

POINT NUMBER   5020

ALPHA(DEGREES)   3.53
BETA(DEGREES)   0.0
MAP DISTORTION FACTOR(KD)   896.99

BULLET
NOSE

$\Delta P / P_{AVG} \sim \%$

VIEW LOOKING AFT

PRATT & WHITNEY AIRCRAFT

ENGINE TF30 TURBOFAN

TF30P3 10X10 NASA/LEWIS 60/40 INLET TEST TF30P-3 TURB.

POINT NUMBER   5020

TURBULENCE(AVERAGE)   2.5406
TURBULENCE(HIGHEST QUADRANT)   4.1325
ISOBAR(10=1 O/O DELTA PRMS/PT)

BULLET
NOSE

$\Delta P_{RMS} / P_T \times 10$
UNFILTERED

VIEW LOOKING AFT

148

PRATT & WHITNEY AIRCRAFT
ENGINE TF30 TURBOFAN
TF30P3 10X10 NASA/LEWIS 60/40 INLET TEST/TF30P-3 K02

POINT NUMBER   5150
WATC   149.00
ALPHA(DEGREES)   0.0
BETA(DEGREES)   0.0
MAP DISTORTION FACTOR(KD) 700.92

BULLET
NOSE
$\Delta P/P_{AVG} \sim \%$
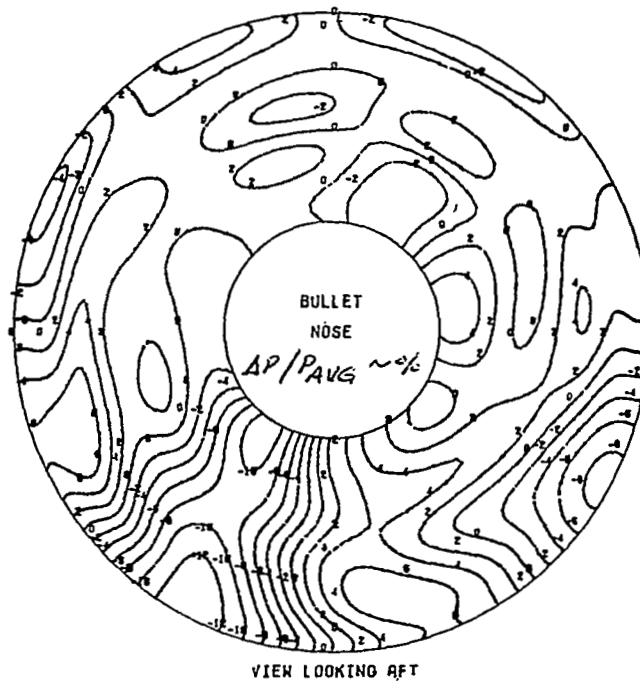
VIEW LOOKING AFT

PRATT & WHITNEY AIRCRAFT
ENGINE TF30 TURBOFAN
TF30P3 10X10 NASA/LEWIS 60/40 INLET TEST TF30P-3 TURB.

POINT NUMBER   5150

TURBULENCE(AVERAGE)   2.5560
TURBULENCE(HIGHEST QUADRANT)   3.5074
ISOBAR(10=1 O/O DELTA PRMS/PT)
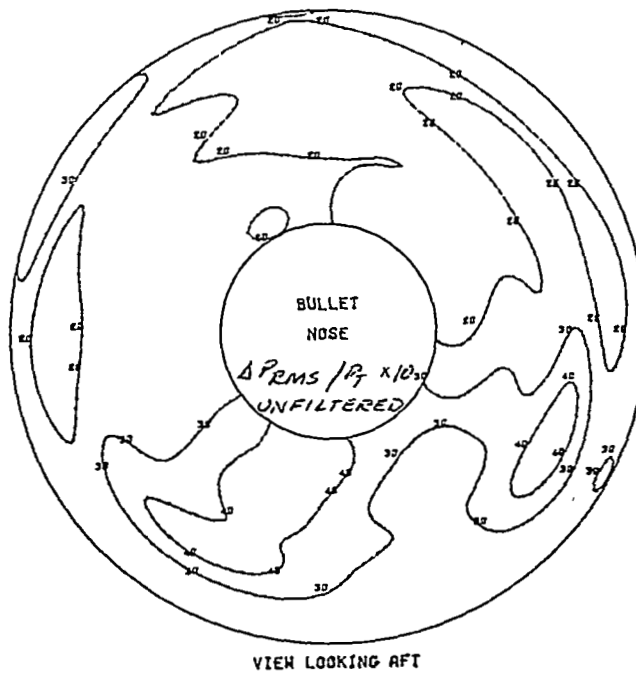
BULLET
NOSE
$\Delta P_{RMS}/P_T \times 10$
UNFILTERED

VIEW LOOKING AFT

149

PRATT & WHITNEY AIRCRAFT

ENGINE TF30 TURBOFAN

TF30P3 10X10 NASA/LE+IS 60/40 INLET TEST TF30P-3 KD2

POINT NUMBER   5190

ALPHA(DEGREES)   0.0
BETA(DEGREES)   0.0
MAP DISTORTION FACTOR(KD)   419.86
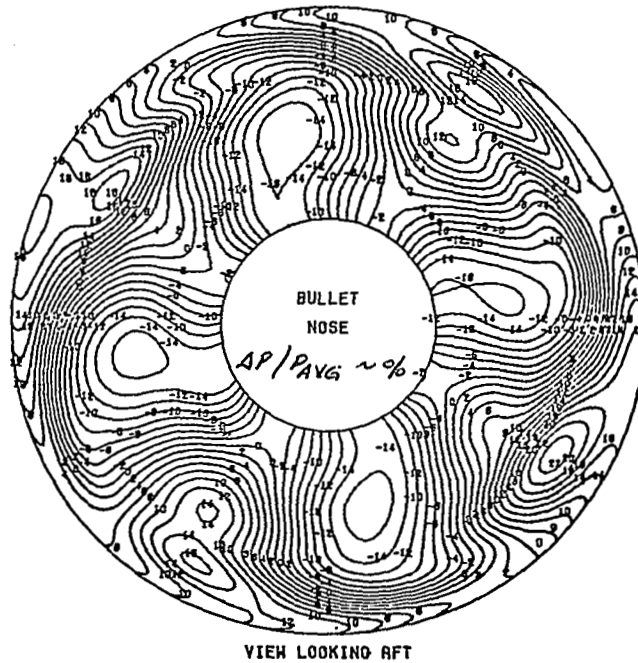
BULLET
NOSE
$\Delta P / P_{AVG} \sim \%$

VIEW LOOKING AFT

PRATT & WHITNEY AIRCRAFT

ENGINE TF30 TURBOFAN

TF30P3 10X10 NASA/LEWIS 60/40 INLET TEST TF30P-3 TURB.

POINT NUMBER   5190

TURBULENCE(AVERAGE)   7.7957
TURBULENCE(HIGHEST QUADRANT)   8.6859
ISOBAR(10=1 O/O DELTA PRMS/PT)

BULLET
NOSE
$\Delta P_{RMS} / P_T \times 10$
UNFILTERED

VIEW LOOKING AFT
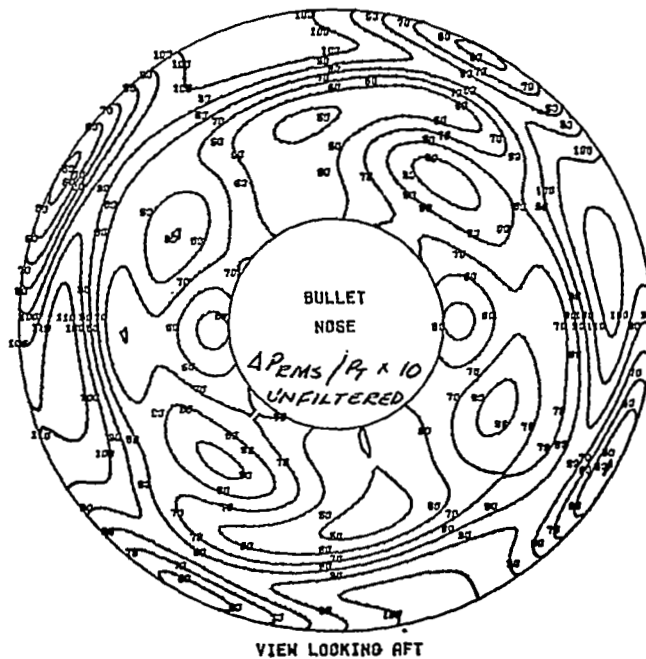
150

PRATT & WHITNEY AIRCRAFT

ENGINE TF30 TURBOFAN

TF30P3 10X10   NASA/LE+IS 60/40 INLET TEST TF30P-3 KD2

POINT NUMBER   5280

ALPHA(DEGREES)   0.0
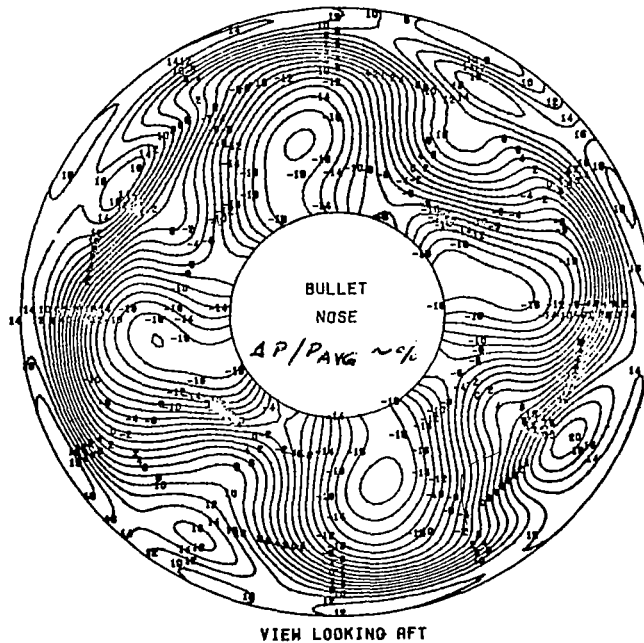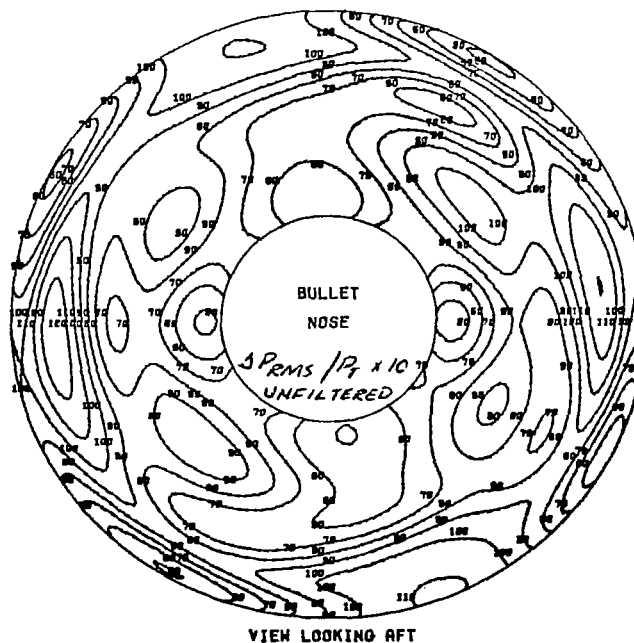BETA(DEGREES)   0.0
MAP DISTORTION FACTOR(KD)   432.30

BULLET
NOSE

$\Delta P / P_{AVG} \sim \%$

VIEW LOOKING AFT

PRATT & WHITNEY AIRCRAFT

ENGINE TF30 TURBOFAN

TF30P3 10X10   NASA/LEWIS 60/40 INLET TEST TF30P-3 TURB.

POINT NUMBER   5280

TURBULENCE(AVERAGE)   8.1744
TURBULENCE(HIGHEST QUADRANT)   9.0546
ISOBAR(10=1 0/0 DELTA PRMS/PT)

BULLET
NOSE

$\Delta P_{RMS} / P_T \times 10$
UNFILTERED

VIEW LOOKING AFT

PRATT & WHITNEY AIRCRAFT

ENGINE TF30 TURBOFAN

TF30P3 10X10   NASA/LEWIS 60/40 INLET TEST TF30P-3 K02

POINT NUMBER   537.0

ALPHA(DEGREES)   1.55
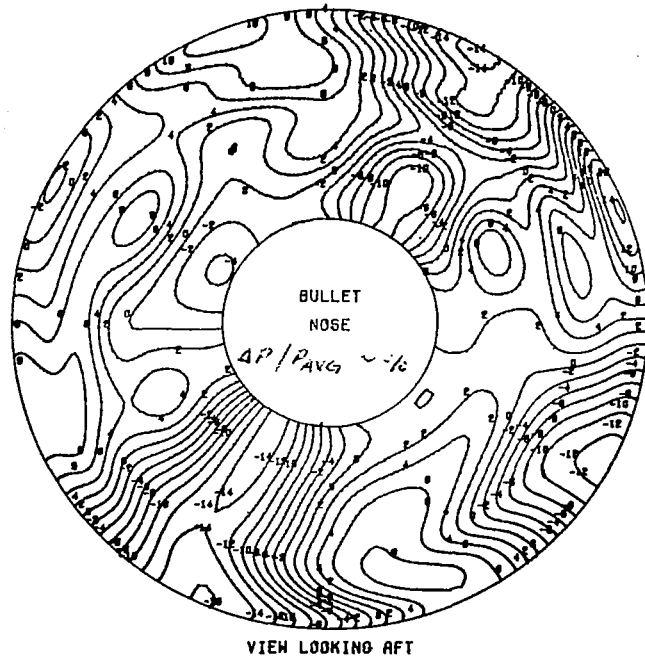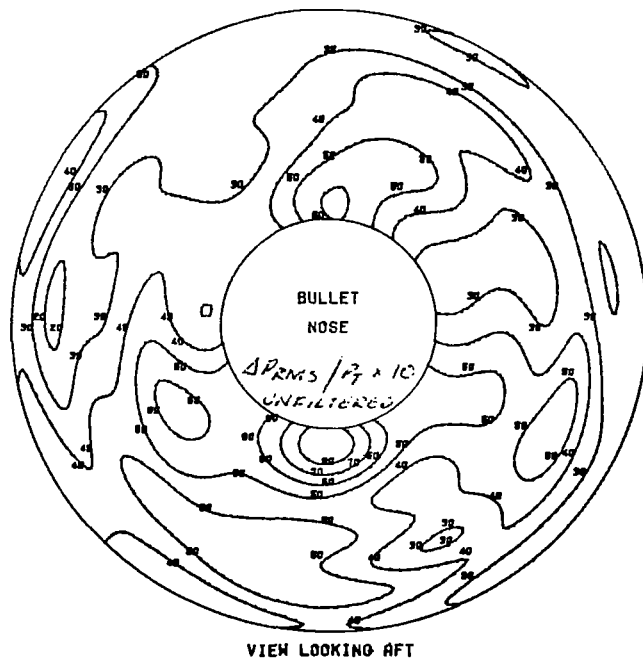BETA(DEGREES)   0.0
MAP DISTORTION FACTOR(KD)   760.52

VIEW LOOKING AFT

PRATT & WHITNEY AIRCRAFT

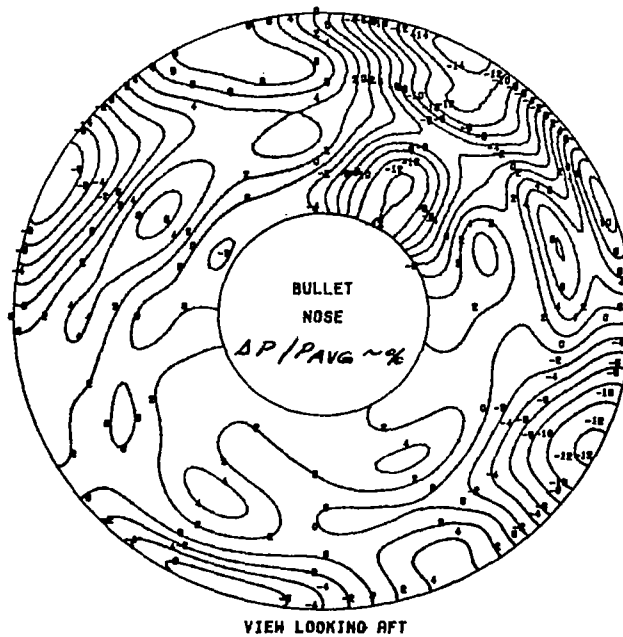ENGINE TF30 TURBOFAN

TF30P3 10X10   NASA/LEWIS 60/40 INLET TEST TF30P-3 TURB.

POINT NUMBER   537.0

TURBULENCE(AVERAGE)   3.9357
TURBULENCE(HIGHEST QUADRANT)   5.2015
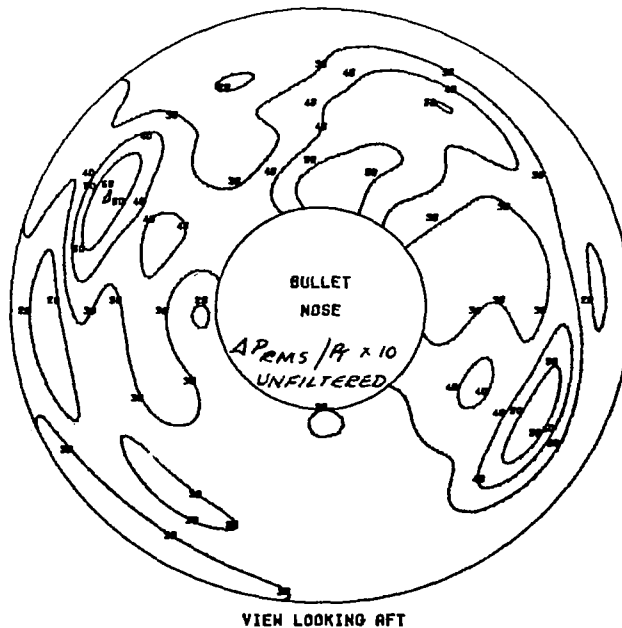ISOBAR(10=1 0/0 DELTA PRMS/PT)

VIEW LOOKING AFT

152

PRATT & WHITNEY AIRCRAFT

ENGINE TF30 TURBOFAN

TF30P3 10X10   NASA/LEWIS 60/40 INLET TEST TF30P-3 KD2

POINT NUMBER   5400

ALPHA(DEGREES)   1.55
BETA(DEGREES)   0.0
MAP DISTORTION FACTOR(KD)   641.14

BULLET
NOSE
$\Delta P / P_{AVG} \sim \%$

VIEW LOOKING AFT

PRATT & WHITNEY AIRCRAFT

ENGINE TF30 TURBOFAN

TF30P3 10X10   NASA/LEWIS 60/40 INLET TEST TF30P-3 TURB.

POINT NUMBER   5400

TURBULENCE(AVERAGE)   3.1220
TURBULENCE(HIGHEST QUADRANT)   3.4053
ISOBAR(10=1 O/O DELTA PRMS/PT)

BULLET
NOSE
$\Delta P_{RMS} / P \times 10$
UNFILTERED

VIEW LOOKING AFT

153

PRATT & WHITNEY AIRCRAFT

ENGINE TF30 TURBOFAN

TF30P3 10X10   NASA/LE↓IS 60/40 INLET TEST TF30P-3 KD2

POINT NUMBER   5610

ALPHA(DEGREES)   1.55
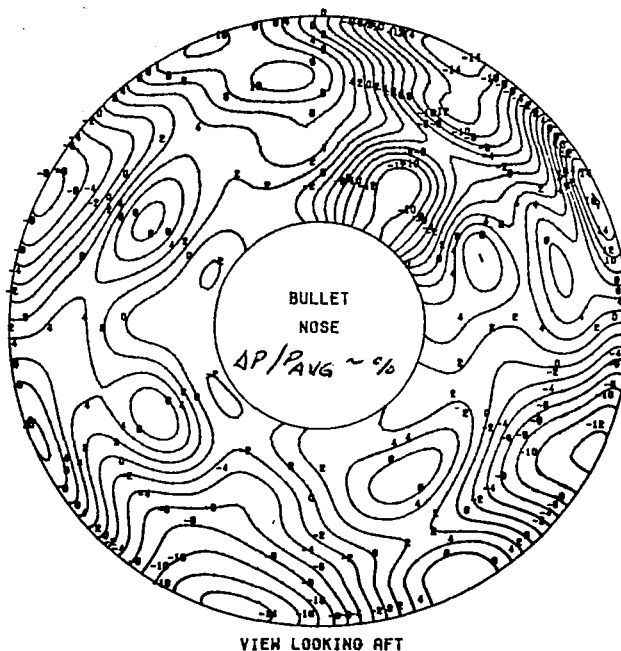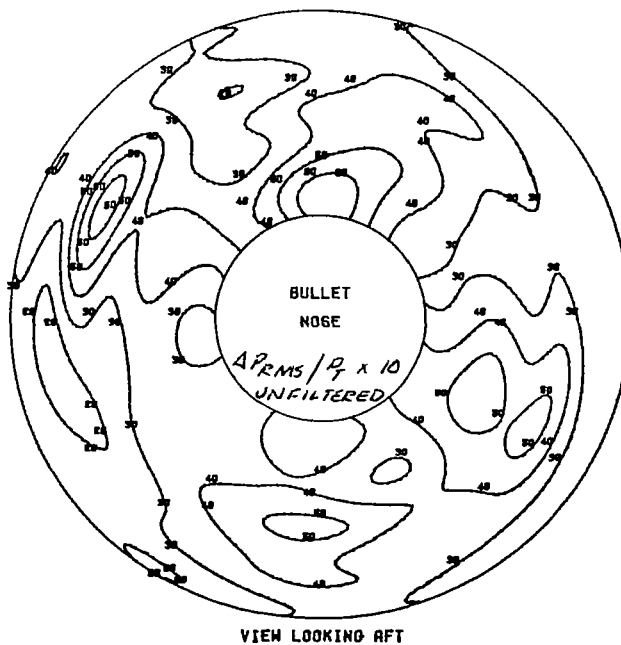BETA(DEGREES)   0.0
MAP DISTORTION FACTOR(KD)   620.66

$\Delta P / P_{AVG} \sim \%$

BULLET
NOSE

VIEW LOOKING AFT

PRATT & WHITNEY AIRCRAFT

ENGINE TF30 TURBOFAN

TF30P9 10X10   NASA/LEWIS 60/40 INLET TEST TF30P-3 TURB.

POINT NUMBER   5610

TURBULENCE(AVERAGE)   3.5284
TURBULENCE(HIGHEST QUADRANT)   3.8471
ISOBAR(10=1 0/0 DELTA PRMS/PT)

$\Delta P_{RMS} / P_T \times 10$
UNFILTERED

BULLET
NOSE

VIEW LOOKING AFT

154

APPENDIX E

Symbols

A Multiplying coefficient used to generate synthetic distortion patterns; flow area

K_{A2} Fan distortion factor

K_{C2} High compressor distortion factor

K_{D2} TF30 distortion factor

K_{RA2} Radial distortion factor

K_{θ} Circumferential distortion factor

N_1 Low compressor mechanical rotor speed (rpm)

$N_1/\sqrt{\theta_{t2}}$ Corrected low compressor rotor speed (rpm)

P Pressure

ΔP Pressure increment

R $T/.75$

T Return period (seconds)

W_a Mass flow rate

α Asymptote parameter

β Asymptote parameter

δ Pressure parameter P/P_{SL}

ν Asymptote parameter

σ Standard deviation

ϕ $\dfrac{W_a \; \theta_t}{t \; A} \quad \dfrac{(N_1/\sqrt{\theta_t})\,\text{Design}}{(N_1/\sqrt{\theta_t})}$

Symbols (Cont'd.)

ψ $\dfrac{\Delta P_s}{P_s}$ $\dfrac{(N_1/\sqrt{\theta_t})^2 \text{ Design}}{(N_1/\sqrt{\theta_t})^2}$

θ Temperature parameter, T/T_{SL}

Subscripts

rms   Root mean square value

t   Total condition

s   Static condition

SL   Standard sea level condition

REFERENCES

1. Plourde, G. A. and Brimlow, B., "Pressure Fluctuations Cause Compressor Instability," Proceedings of the Air Force Airframe-Propulsion Compatibility Symposium - 24-26 June, 1969, Technical Report AFAPL-TR-69-103, June, 1970.

2. Aeronautical Propulsion Conference, May 13-14, 1975, Lewis Research Center, Engine Systems Technology Session, Figure XII-48.

3. Farr, A. Pike, "Evaluation of F-15 Inlet Dynamic Distortion," AIAA Paper 73-784, St. Louis, 1973.

4. Kimsey, W. F. and McIlveen, M. W., "Analysis and Synthesis of Distorted and Unsteady Turbo Engine Inlet Flow Fields," AIAA 7th Propulsion Joint Specialist Conference, Salt Lake City, Utah, June 14-18, 1971.

5. Ellis, S. H. and Brownstein, B. J., "A Procedure for Estimating Maximum Time-Variant Distortion Levels with Limited Instrumentation," AIAA Paper 72-1099, New Orleans, La., 1972.

6. Jacocks, J. L., "Statistical Analysis of Distortion Factors," AIAA Paper No. 72-1100, New Orleans, La., 1972.

7. Jacocks, J. L. and Kneile, K. R., "Statistical Prediction of Maximum Time-Varient Inlet Distortion Levels," AEDC-TR-74-121, January, 1975.

8. Anders, E. B., et. al, "Digital Filters," NASA-CR-136.

9. Otnes, R. K. and Enochson, L., Digital Time Series Analysis, John Wiley & Sons, 1972.